AGU PUBLICATIONS

JGR

Journal of Geophysical Research: Solid Earth

RESEARCH ARTICLE
10.1002/2016JB012923

Key Points:
- Twenty-eight East Asia subducted slabs mapped from tomography and unfolded to constrain plate reconstructions
- Slab evidence for a subducted 8000 × 2500 km "East Asian Sea" that existed between the Pacific and Indian Oceans in the early Cenozoic
- Miocene arc-arc collision between the northern Philippine Sea plate and the Ryukyu-SW Japan Eurasian margin ~15–20 Ma

Supporting Information:
- Supporting Information S1
- Data Set S1
- Movie S1
- Movie S2
- Movie S3

Correspondence to:
J. Wu,
jonnywu_rhul@yahoo.co.uk

Citation:
Wu, J., J. Suppe, R. Lu, and R. Kanda (2016), Philippine Sea and East Asian plate tectonics since 52 Ma constrained by new subducted slab reconstruction methods, *J. Geophys. Res. Solid Earth*, *121*, doi:10.1002/2016JB012923.

Received 15 FEB 2016
Accepted 10 MAY 2016
Accepted article online 13 MAY 2016

©2016. The Authors.
This is an open access article under the terms of the Creative Commons Attribution-NonCommercial-NoDerivs License, which permits use and distribution in any medium, provided the original work is properly cited, the use is non-commercial and no modifications or adaptations are made.

Philippine Sea and East Asian plate tectonics since 52 Ma constrained by new subducted slab reconstruction methods

Jonny Wu[1], John Suppe[1], Renqi Lu[1,2], and Ravi Kanda[1,3]

[1]Department of Geosciences, National Taiwan University, Taipei, Taiwan, [2]Institute of Geology, China Earthquake Administration, Beijing, China, [3]Department of Geology, Utah State University, Logan, Utah, USA

Abstract We reconstructed Philippine Sea and East Asian plate tectonics since 52 Ma from 28 slabs mapped in 3-D from global tomography, with a subducted area of ~25% of present-day global oceanic lithosphere. Slab constraints include subducted parts of existing Pacific, Indian, and Philippine Sea oceans, plus wholly subducted proto-South China Sea and newly discovered "East Asian Sea." Mapped slabs were unfolded and restored to the Earth surface using three methodologies and input to globally consistent plate reconstructions. Important constraints include the following: (1) the Ryukyu slab is ~1000 km N-S, too short to account for ~20° Philippine Sea northward motion from paleolatitudes; (2) the Marianas-Pacific subduction zone was at its present location (±200 km) since 48 ± 10 Ma based on a >1000 km deep slab wall; (3) the 8000 × 2500 km East Asian Sea existed between the Pacific and Indian Oceans at 52 Ma based on lower mantle flat slabs; (4) the Caroline back-arc basin moved with the Pacific, based on the overlapping, coeval Caroline hot spot track. These new constraints allow two classes of Philippine Sea plate models, which we compared to paleomagnetic and geologic data. Our preferred model involves Philippine Sea nucleation above the Manus plume (0°/150°E) near the Pacific-East Asian Sea plate boundary. Large Philippine Sea westward motion and post-40 Ma maximum 80° clockwise rotation accompanied late Eocene-Oligocene collision with the Caroline/Pacific plate. The Philippine Sea moved northward post-25 Ma over the northern East Asian Sea, forming a northern Philippine Sea arc that collided with the SW Japan-Ryukyu margin in the Miocene (~20–14 Ma).

1. Introduction

We present new subducted-slab constraints from seismic tomography to reconstruct the past motions of the Philippine Sea plate and surrounding East Asia since the early Cenozoic ~52 Ma. The Philippine Sea plate is the largest of the collage of plates and marginal basins that occupy the complex boundary zone between the three major plates that converge in East Asia: the Pacific, Indo-Australian, and Eurasian/Sundaland plates (Figures 1 and 2). In contrast with the motions of these major plates, which are constrained by global plate circuits based on seafloor spreading and hot spot reference frames [e.g., *Seton et al.*, 2012], past Philippine Sea plate motions since its early Eocene inception have been uncertain and controversial for reasons discussed below. Strongly contrasting Philippine Sea plate reconstructions have been proposed for many years [e.g., *Hall*, 2002, 2012; *Hilde et al.*, 1977; *Seno and Maruyama*, 1984; *Uyeda and Ben-Avraham*, 1972; *Xu et al.*, 2014; *Zahirovic et al.*, 2014]. Continued work on Philippine Sea plate motions has been motivated by its importance for deciphering the tectonic histories of a vast swath of East Asia in the Cenozoic [e.g., *Hall*, 2002], including the Taiwan orogen, the Philippines, southwest Japan and the Ryukyus, the South China Sea, the western Pacific Izu-Bonin-Marianas arcs, the northern Australian margin, Sundaland, and other southeast Asian terranes and marginal seas. Furthermore, assumptions about Philippine Sea absolute motions underpin geodynamical models of subduction initiation, trench migration, back-arc basin formation, forearc deformation, and small-plate driving mechanisms [*Arculus et al.*, 2015; *Čížková and Bina*, 2015; *Gurnis et al.*, 2004; *Iaffaldano*, 2012; *Leng and Gurnis*, 2011].

Present-day MORVEL Philippine Sea motions are rapid (~6–11 cm/yr) to the WNW (~300°) relative to eastern Eurasia, similar to the adjacent Pacific and Caroline plate motions (9.5–11 cm/yr) [*Argus et al.*, 2011; *DeMets et al.*, 2010]. Current motions of the southernmost Philippine Sea plate are only slightly different in rate and azimuth to the Pacific and Caroline plate rates, whereas the rate near southwest Japan is about 60% of the Pacific rate (Figure 1b). Such rapid motion of the Philippine Sea plate requires strong coupling to

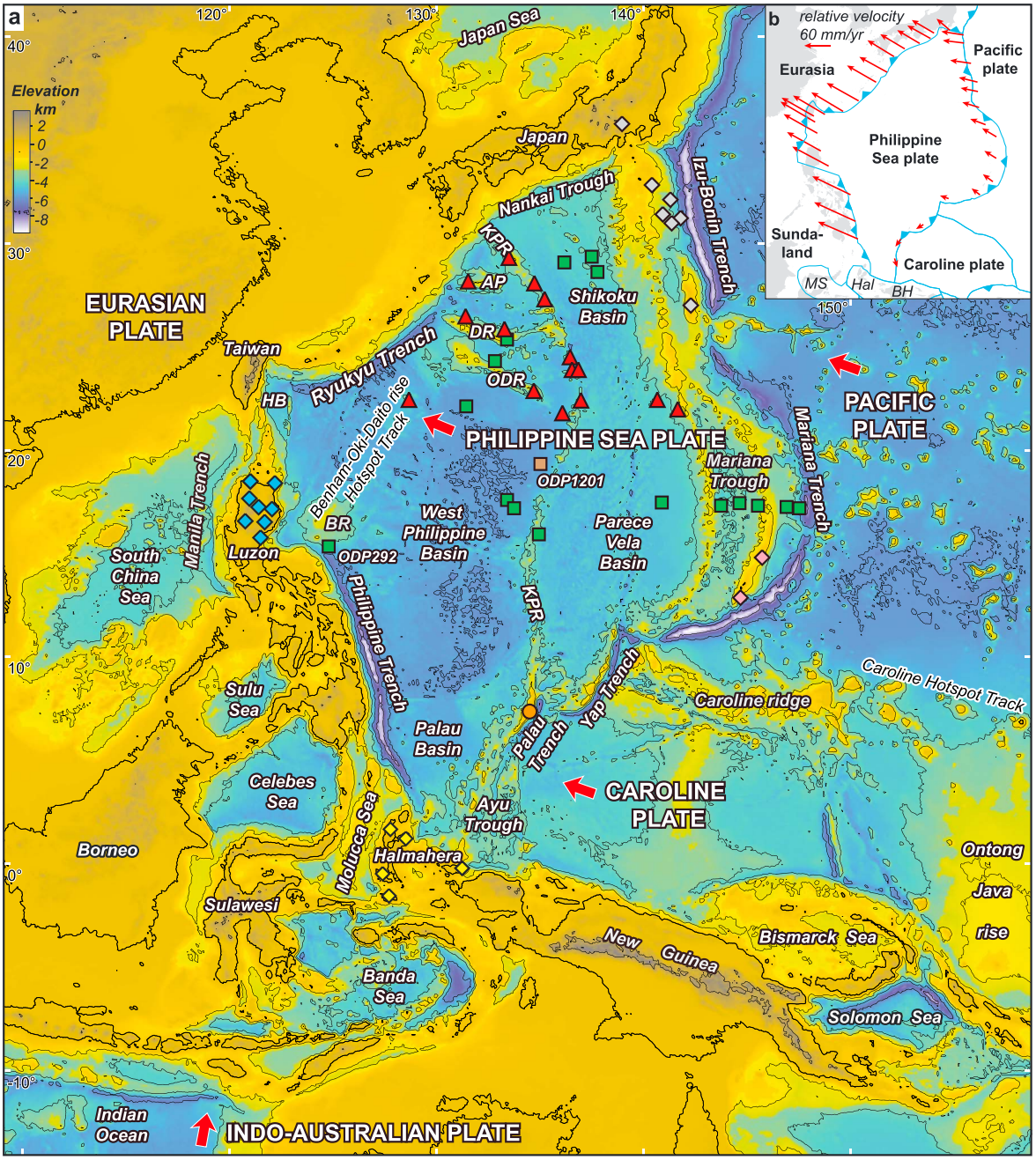

Figure 1. (a) Present-day Philippine Sea and East Asian tectonic setting. Plate motion azimuths in Figure 1a are shown relative to stable Eurasia from the MORVEL model [*deMets et al*., 2010]. Paleomagnetic sample locations in Figure 3 are shown by the colored symbols. (b) Present-day differential velocities across the Philippine Sea plate boundaries calculated from MORVEL. The southeast Philippine Sea plate is strongly edge coupled to the Pacific plate through the Caroline Sea, which has Pacific-like velocities. HB, Huatung Basin; AP, Amami Plateau; DR, Daito Ridge; ODR, Oki-Daito Ridge; BR, Benham Rise; KPR, Kyushu-Palau ridge; MS, Molucca Sea minor plate; BH, Bird's Head minor plate; Hal, Halmahera.

the Pacific, especially through the Caroline Sea, because the present-day rapid Philippine Sea plate motions cannot simply be explained by slab-pull forces alone [*Iaffaldano*, 2012].

A prime reason for uncertainty in the past Philippine Sea plate motions is that the plate has been isolated from seafloor spreading and hot spot-based global reconstruction circuits [e.g., *Seton et al*., 2012] due to its surrounding subduction zones (Figure 1b). Therefore, Philippine Sea motion histories are largely guided by paleomagnetic studies (Figure 3), which are reviewed in more detail in section 1.2. Published paleomagnetic

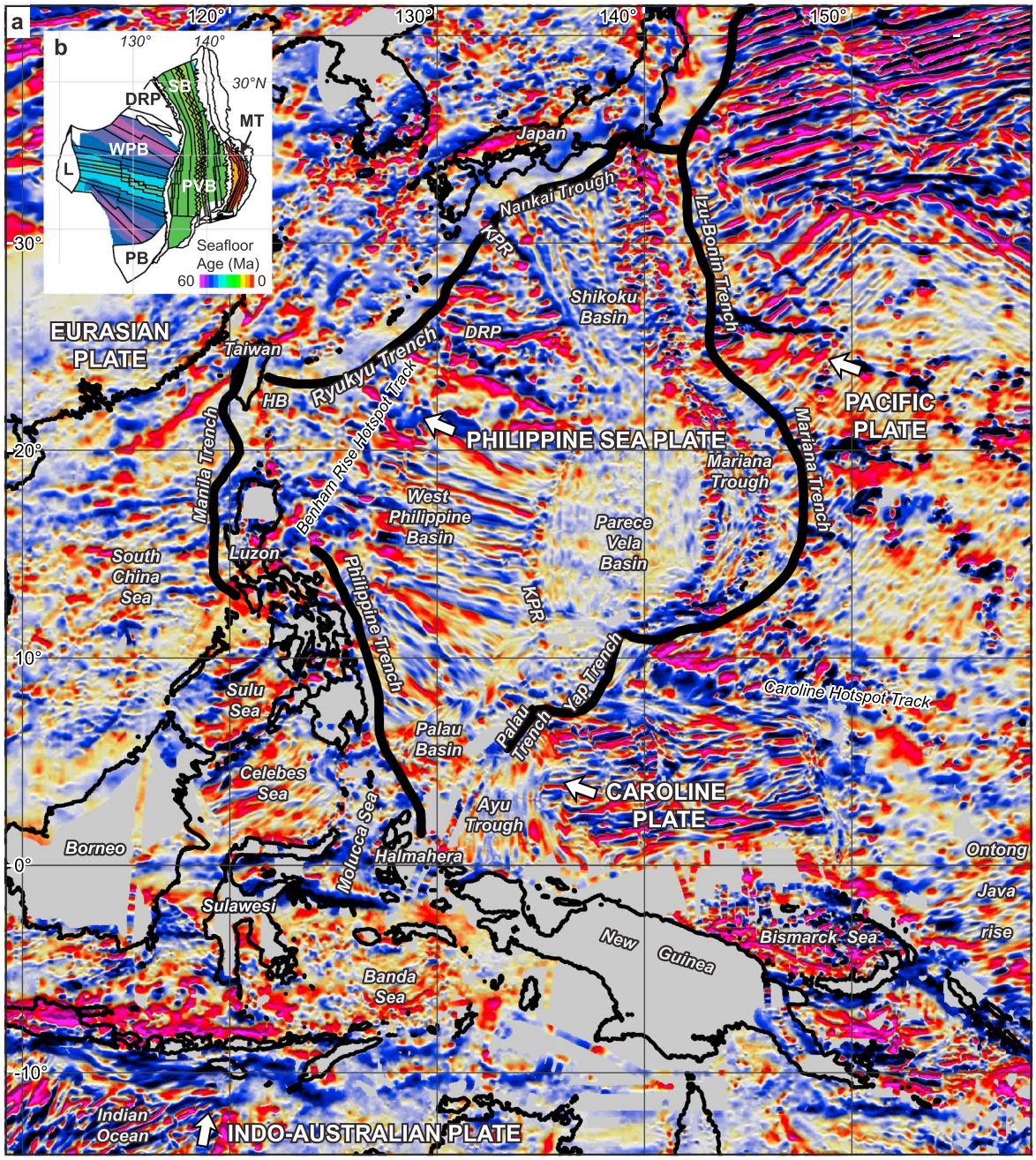

Figure 2. (a) EMAG2 gridded magnetic anomalies for the Philippine Sea and East Asia [*Maus et al*., 2009]. Plate motion azimuths as in Figure 1. (b) Philippine Sea gridded seafloor spreading model used in this study (modified from *Müller et al*. [2008] and *Seton et al*. [2012]). WPB, West Philippine Basin; SB, Shikoku Basin; PVB, Parece Vela Basin; MT, Mariana Trough; DRP, Daito ridges province; PB, Palau Basin; L, Luzon; KPR, Kyushu-Palau ridge; HB, Huatung Basin.

data generally agree that the Philippine Sea is far traveled and has moved ~20° northward from a near-equatorial position since the Eocene (~40 Ma, Figure 3a) [e.g., *Hall et al*., 1995c; *Haston and Fuller*, 1991; *Queano et al*., 2007; *Yamazaki et al*., 2010]. The ~6 cm/yr mean northward component of Philippine Sea plate motion since ~40 Ma from published paleolatitudes shows similarities to Indo-Australian plate motions (Figure 3a). In contrast, the present Philippine Sea motions are similar to the current and past WNW Pacific motions, with a ~3 cm/yr northward component that is only half of its past northward rate from paleomagnetism. Therefore, it is required that the past Philippine Sea plate motions were substantially different from present-day motions, and this has added to the uncertainties in reconstructing its past motions.

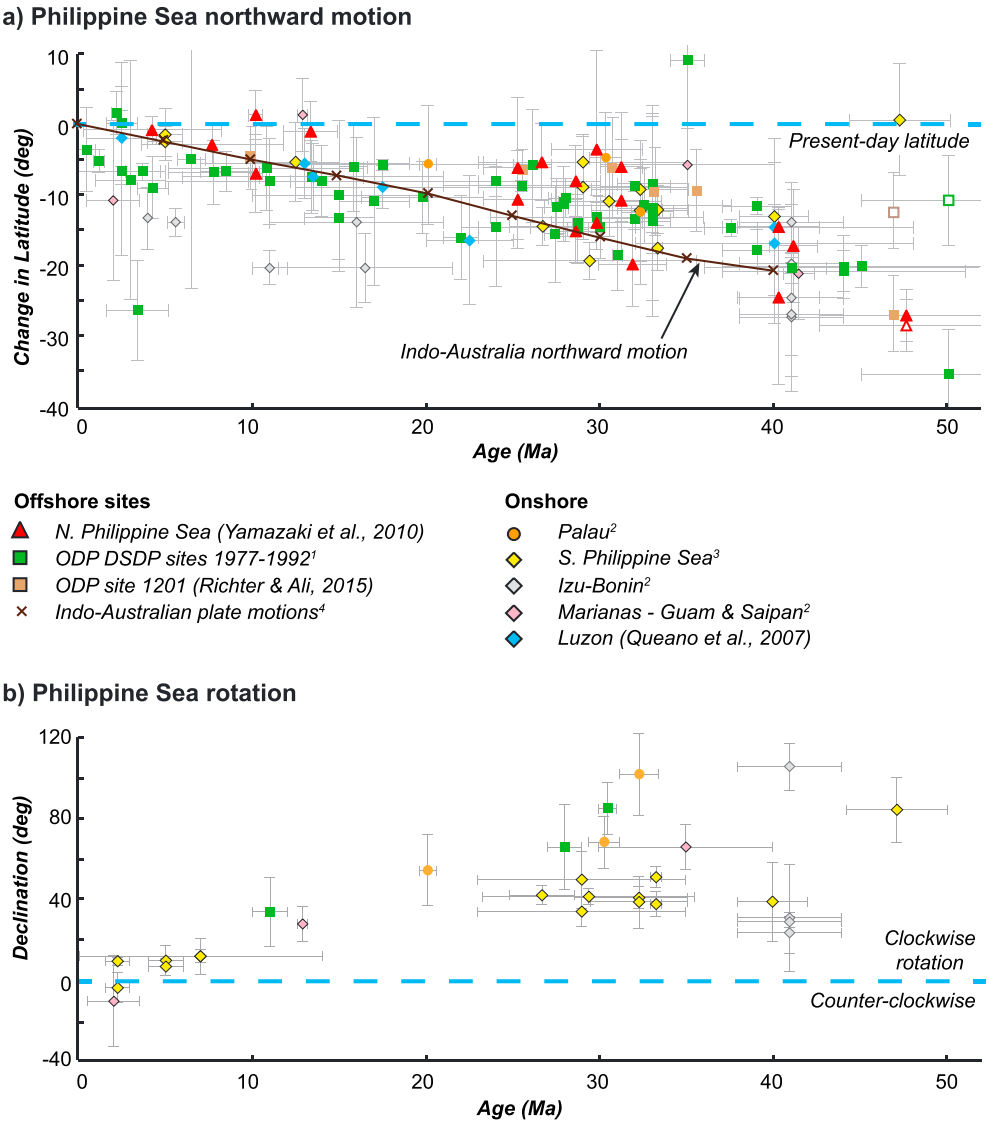

Figure 3. (a) Philippine Sea plate change in latitude versus age plot compiled from published studies. It is generally agreed that the Philippine Sea plate has moved northward ~20° since the Eocene. Hollow dots show the equatorial ambiguity within paleolatitudes from the earliest plate history. (b) Philippine Sea declinations versus age plot compiled from published studies. The declination data show up to 120° clockwise rotations, but it is controversial to what extent the rotations indicate whole plate as opposed to local block rotations at the plate margin only. Sampling locations are shown in Figure 1. Additional references: 1 = ODP DSDP sites 6, 31, 58, 59, 60, 125, and 126 [*Louden*, 1977; *Kinoshita*, 1980; *Keating and Herrero*, 1980; *Keating*, 1980; *Bleil*, 1982; *Haston et al*., 1992; *Koyama et al*., 1992]; 2 = *Haston and Fuller* [1991]. 3 = *Ali and Hall* [1995] and *Hall et al*. [1995a]; 4 = Northern Philippine Sea plate reference location (23°N, 137°E) moved with *Seton et al*. [2012] Indo-Australia motions.

Paleomagnetic declinations further indicate up to 110° clockwise rotation (Figure 3b) [cf. *Hall et al*., 1995c], but it has been difficult to deconvolve rotations of the entire Philippine Sea plate from local block rotations since the declinations come almost exclusively from the plate margins, where local block rotations are likely and in some cases well documented (see section 1.2). Finally, surrounding East Asia has numerous complex subduction and collisional plate boundaries that contribute additional reconstruction uncertainties to the problem of Philippine Sea plate reconstruction.

Here we present major new constraints on Philippine Sea plate motions based on mapping and unfolding 28 subducted lithospheric slabs imaged in seismic tomography (Table 1). To accomplish this, we have had to develop a set of methodologies for 3-D mapping and unfolding imaged slabs, which are then incorporated

Table 1. List of Mapped and Unfolded Slabs Included in the Plate Reconstructions in This Study

	Slab Name	Present-Day or Past Associated Plate	Slab Type	Subduction Zone	Unfolded Area (km^2)	Slab Depth (km) Minimum	Slab Depth (km) Maximum	Slab Age (Ma) Base	Slab Age (Ma) Top
1	Celebes Sea south	Celebes Sea	attached	North Sulawesi trench	1.68×10^5	0	370	10	0
2	Celebes Sea east	Celebes Sea	attached	Cotabato trench	6.00×10^4	0	250	5	0
3	Eurasia	Eurasia (including South China Sea)	attached	Manila trench	7.85×10^5	0	480	20	0
4	Banda	Indo-Australia	attached	Timor and Seram trough	included with Sunda	0	550	15	0
5	New Guinea	Indo-Australia	attached	New Guinea	3.01×10^5	0	500	5	0
6	New Hebrides	Indo-Australia	attached	New Hebrides trench	9.74×10^5	0	820	15	0
7	Solomon Sea east	Indo-Australia	attached	San Cristobal trench	7.90×10^5	0	770	15	0
8	Solomon Sea west	Indo-Australia	attached	New Britain trench	7.55×10^5	0	900	15	0
9	Sunda	Indo-Australia	attached	Sunda trench	1.08×10^7	0	1250	50	0
10	Molucca Sea east	Molucca Sea	attached	Halmahera thrust	1.76×105	0	510	15	0
11	Molucca Sea west	Molucca Sea	attached	Sangihe thrust	1.15×10^6	0	900	30	0
12	north and central Marianas	Pacific	attached	central Marianas	5.73×10^6 [a]	0	1200	50	0
13	Izu-Bonin-Japan-Kuril	Pacific	attached	Izu-Bonin-Japan-Kurile	1.60×10^7 [a]	0	1160	50	0
14	Ontong Java	Pacific	attached	North Solomon trench	2.61×10^5	0	170	20	0
15	Tonga-Kermadec	Pacific	attached	Tonga-Kermadec	9.28×10^6 [a]	0	1300	50	0
16	Philippine Trench	Philippine Sea	attached	Philippine trench	3.53×10^5	0	400	5	0
17	Ryukyu-Shikoku	Philippine Sea	attached	Ryukyu and Nankai trenches	1.75×10^6	0	450	15	0
18	Sulu Sea	Sulu Sea	attached	Negros trench	1.40×10^5	0	390	10	0
19	East Asia Sea north	East Asia Sea?	detached	unnamed	2.82×10^6	500	1040	40	20
20	East Asia Sea south	East Asia Sea?	detached	unnamed	1.12×10^7	510	1290	50	20
21	East Asia Sea west	East Asia Sea?	detached	unnamed	2.44×10^6	660	1300	50	20
22	proto-South China Sea north	Eurasia or Sundaland?	detached	unnamed	1.91×10^6	460	950	35	15
23	proto-South China Sea south	Eurasia or Sundaland?	detached	unnamed	1.19×10^6	860	950	45	35
24	New Guinea offshore	Indo-Australia?	detached	Caroline Sea?	4.02×10^5	380	700	25	10
25	Solomon Sea south	Indo-Australia?	detached	Aure-Pocklington trough?	7.79×10^5	0	600	25	5
26	Southern Marianas	Pacific or Caroline Sea?	detached	southern Marianas	4.39×10^5	290	780	15	5
27	Ontong Java deep	Pacific?	detached	unnamed	6.22×10^5	1150	1260	35	30
28	Ayu Trough deep	Pacific or Philippine Sea plate?	detached	unnamed	2.76×10^5	510	680	15	5
				Total	7.16×10^7				
				Present-day Philippine Sea plate	6.05×10^6				

[a] Unfolded using cross-sectional area method.

into GPlates plate-tectonic software [*Boyden et al.*, 2011] for quantitative plate reconstructions in a global context. In this paper we illustrate these new methodologies and strategies in the course of our presentation of new results for the Philippine Sea plate. This paper is organized as follows: (1) We review existing constraints on Philippine Sea reconstructions from its subducted slabs, paleomagnetism, Philippine Sea seafloor spreading models, and globally constrained motions of adjacent plates. (2) We introduce the slab unfolding and plate reconstruction methods that we have developed for this study. (3) We show our mapped and unfolded slab results for the circum-Philippine Sea plate slabs, the western Pacific slabs, and other key regional slabs including the South China Sea, the Molucca Sea, and the disappeared East Asian Sea. (4) We incorporate these slab constraints to show two possible classes of Philippine Sea and East Asian plate reconstructions since ~52 Ma, corresponding to two possible starting positions constrained by slabs and showing different internal rotations, given current paleomagnetic ambiguities. (5) Finally, we discuss robust conclusions, including evidence for predicted arc-continent and arc-arc collisions within the context of our new slab-constrained plate reconstruction.

1.1. Philippine Sea Slab Predictions From Published Plate Reconstructions

Additional uncertainty in Philippine Sea plate reconstruction arises from the already subducted parts of the plate that now reside in the mantle associated with the Ryukyu-Nankai and Philippine trench subduction zones. Lack of precise constraints on the full presubduction size and shape of the plate at each stage in its history has contributed to strongly contrasting plate tectonic models. Published models show Philippine Sea plate sizes for the Eocene that differ by thousands of kilometers (combined green, orange and yellow areas in Figure 4). The variety of Philippine Sea plate reconstructions is too numerous to

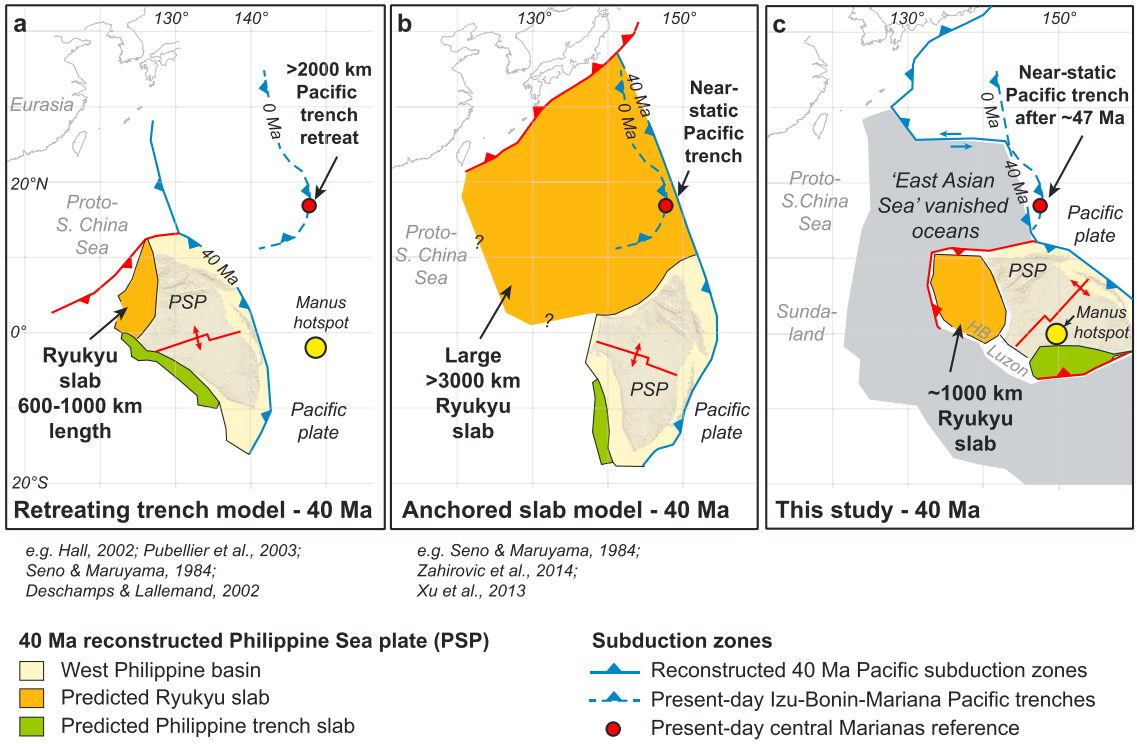

Figure 4. Comparison between (a and b) published Philippine Sea plate reconstructions and (c) the preferred plate reconstruction from this study at 40 Ma. The published plate reconstructions differ on the total Philippine Sea plate size at 40 Ma (orange, yellow, and green areas) by thousands of kilometers. Furthermore, retreating trench models in Figure 4a predict >2000 km trench retreat relative to the present-day central Marianas (red dot) whereas anchored slab models in Figure 4b predict a long-lived, near-stationary subduction zone near the central Marianas. (c) Our slab constraints support the short 1000 km length Ryukyu slab in Figure 4a and the near-stationary central Marianas Pacific trench in Figure 4b. In this study, we use subducted slab constraints to show the Philippine Sea originated above the Manus plume near coordinates 0°/150°E. As the Philippine Sea was driven to the north and west, it overran and subducted the East Asian Sea, which are vanished oceans preserved as flat slabs under East Asia at 500 to 1300 km depths today. HB, Huatung basin.

individually review here but can be illustrated in simplified form as two distinct groups emphasizing: (1) their predicted Philippine Sea slab sizes and (2) their predicted western Pacific paleotrench locations at 40 Ma. We call these two groups the "retreating trench" and "anchored slab" models, following *Seno and Maruyama* [1984] (Figures 4a and 4b).

Retreating trench models infer that the Philippine Sea plate was a relatively small plate that moved northeastward concurrent with up to 2000 km of Pacific trench retreat toward the east (Figure 4a) [e.g., *Byrne and DiTullio*, 1992; *Deschamps and Lallemand*, 2002; *Hall*, 2002, 2012; *Pubellier et al.*, 2003; *Seno and Maruyama*, 1984]. Some models show in addition up to 90° Philippine Sea clockwise rotation [*Hall*, 2002]. These models typically predict a relatively short 600–1000 km slab that is subducted at the Ryukyu trench. The observed large northward motion of the Philippine Sea plate is accommodated by large northeastward motion of the Pacific trench. For example, the model of *Hall* [2002] predicts that the central Marianas Pacific trench has retreated >2000 km since 40 Ma (Figure 4a).

In contrast, anchored slab models infer a near-stationary Pacific subduction zone near the central Marianas that has been anchored in the lower mantle since at least 40 Ma (Figure 4b). These models also have inferred long-lived, northward subduction of a much larger Philippine Sea plate under Eurasia (Figure 4b) [e.g., *Seno and Maruyama*, 1984; *Uyeda and Ben-Avraham*, 1972; *Xu et al.*, 2014; *Zahirovic et al.*, 2014]. They predict a very long (~3000 km) Ryukyu slab, a difference of more than 2000 km compared to the retreating trench models. The obvious incompatibilities between these models lead to conflicting implications for how the Eurasian margin and the oceans surrounding East Asia are reconstructed since the Eocene (Figures 4a and 4b).

1.1.1. Slab Constraints From Previous Seismic Tomographic Studies

Seismic tomographic images can show the locations and geometries of subducted slabs and thus offer a way to test the proposed Philippine Sea plate reconstruction models. Tomography generally shows that the slabs

attached to the Philippine Sea plate are confined to the upper mantle [e.g., *Cao et al*., 2014; *Hasegawa et al*., 2013; *Huang et al*., 2013; *Lallemand et al*., 2001; *Miller et al*., 2006; *Zhao*, 2015]. *Lallemand et al*. [2001] illustrated the western Ryukyu slab from global tomography and interpreted a ~500–1000 km length that was consistent with their retreating trench model [*Deschamps and Lallemand*, 2002]. Regional tomography suggests that the Shikoku slab (i.e., the subducted Shikoku Basin at the Nankai Trough) has a length of ~500–600 km under southwest Japan [*Huang et al*., 2013; *Zhao et al*., 2012]. These observations have suggested that the Ryukyu slab may be on the order of 500–1000 km length, similar to the retreating trench model of Figure 4a.

In contrast, images of the Pacific slabs under the central Marianas show a near-vertical "slab wall" of subducted slab remnants down to at least 1000 km depths in the lower mantle [e.g., *Jaxybulatov et al*., 2013; *Miller et al*., 2006; *van der Hilst and Seno*, 1993]. The most straightforward explanation for the slab wall is that subducted lithosphere accumulated within a laterally restricted area below a near-stationary Pacific trench, followed by lower mantle penetration and lower mantle slab anchoring [*van der Hilst and Seno*, 1993]. Complex upper mantle subducted slab dynamics could allow for some Pacific trench retreat or advance prior to lower mantle slab anchoring [*Jaxybulatov et al*., 2013; *Miller et al*., 2006; *van der Hilst and Seno*, 1993] but appears to be incompatible with the large-scale (~2000 km) Pacific trench retreat inferred by the retreating trench models (Figure 4a). In contrast, plate reconstructions using the tomographic constraints have suggested that a Pacific subduction zone existed within ±150 km of the present-day central Marianas back to at least the mid-Miocene [*Jaxybulatov et al*., 2013; *Miller et al*., 2006; *van der Hilst and Seno*, 1993] and as early as 40 Ma [*Zahirovic et al*., 2014]. These tomographic observations are consistent with the anchored slab Philippine Sea plate reconstruction of Figure 4b.

The preferred plate model presented in this paper contains both a short ~1000 km N-S Ryukyu slab and a near-stationary central Marianas Pacific trench since the Eocene (Figure 4c). We will show that these seemingly incompatible elements can be reconciled by our plate model, in part by showing the existence of a regionally extensive set of flat slabs in the upper part of the lower mantle between the northern Philippine Sea and the eastern Australian plate. These slabs are consistent with a regionally extensive vanished ocean that we call the "East Asian Sea," which once existed between the Pacific and the Indo-Australian oceans (e.g., Figure 4c).

1.2. Philippine Sea Paleomagnetic Constraints

1.2.1. Paleolatitudes

The locations of Philippine Sea paleomagnetic sites are concentrated at the northern half of the plate and along the plate margins (Figure 1a). Paleomagnetic inclinations show that the plate is far traveled, originating far to the south of its present-day location (Figure 3a). Paleomagnetic studies generally agree on the first-order interpretation that the Philippine Sea plate moved approximately 20° (i.e., ~2000 km) northward since the Eocene (Figure 3a) [*Hall et al*., 1995c, and references therein; *Haston and Fuller*, 1991; *Queano et al*., 2007; *Yamazaki et al*., 2010]. Since 40 Ma Indo-Australian and Philippine Sea rates of northward motion are similar within the error bounds (Figure 3a). Prior to 40 Ma, the early Cenozoic paleolatitudes apparently show larger northward motions ($>$25°), but lower values are also possible (hollow dots in Figure 3a) due to well-known limitations in the paleomagnetic method that make it difficult to determine whether near-equatorial paleolatitudes were formed in the Northern or Southern Hemisphere (i.e., equatorial paleomagnetic ambiguity).

A study of northern Philippine Sea paleolatitudes (north of the West Philippine basin spreading center, Figures 1 and 2b), suggests that the majority of Philippine Sea northward motion occurred before 25 Ma, with smaller northward motion after 15 Ma (Figure 3a) [*Yamazaki et al*., 2010]. This result is supported by a recent paleomagnetic study of Ocean Drilling Program (ODP) Site 1201 (Figure 1) that also showed deceleration of Philippine Sea northward motions around 20 Ma and renewal of northward motions after 10 Ma (Figure 3a) [*Richter and Ali*, 2015]. The ODP Site 1201 study provides a new and important, relatively continuous Eocene to present-day paleomagnetic record at a single location within the West Philippine basin. We will later compare the ODP 1201 record with our proposed Philippine Sea plate reconstructions in section 5.1.

ODP Site 292 on the Benham Rise is also an important Philippine Sea plate paleomagnetic site because it provides a relatively long paleolatitude record from 10 to 36 Ma starting from the top of the basalt section

[*Hickey-Vargas*, 1998; *Louden*, 1977]; it is one of the few paleomagnetic sites located south of the West Philippine basin spreading center [*Karig et al*., 1973; *Louden*, 1977] and is also part of the proposed Oki-Daito/Benham-Rise hot spot track [*Ishizuka et al*., 2013] (Figures 1 and 2). The ODP 292 paleolatitude at the end of hot spot volcanism is near-equatorial 0±3° (see Figure 26c), which is similar to the Manus hot spot at the north edge of the Bismarck Sea, as imaged in global tomography. One of our two plate models has the Philippine Sea plate nucleate as a small back-arc basin adjacent to the Manus hot spot, analogous to the Bismarck Sea (Figure 1).

The latitudinal motions of the southern West Philippine basin have been less certain than the northern because of limited paleomagnetic sampling (Figure 1), limited constraints on seafloor age in the south, and paleomagnetic equatorial ambiguity. However, paleolatitudes from Luzon are consistent with the nearby Benham Rise ODP Site 292 and provides an important time series for the southern West Philippine basin that we can compare with the ODP 1201 northern West Philippine basin time series in the discussion of our plate reconstructions. Note, however, that some plate models [e.g., *Hall*, 2002] have Luzon detached from the Philippine Sea plate until very recently, as discussed in the next section.

1.2.2. Rotations

Philippine Sea plate paleomagnetic declinations indicate up to 110° clockwise rotations with considerable scatter (Figure 3b). Declination data have been obtained primarily from the plate margins (Figure 1a), with two main tectonic interpretations: (1) clockwise rotation of the entire Philippine Sea plate [e.g., *Hall et al*., 1995c; *Haston et al*., 1992; *Keating and Helsley*, 1985; *Koyama et al*., 1992; *Yamazaki et al*., 2010] or (2) clockwise rotation of local blocks at the Philippine Sea plate margins [e.g., *Kodama et al*., 1983; *Zahirovic et al*., 2014]. Local small block rotations have been documented at several sites around the Philippine Sea plate and surrounding areas, showing rotations of 15°–90° in 1–3 Ma [e.g., *Ali et al*., 1996; *Lee et al*., 1991; *Weiler and Coe*, 1997, 2000]. Furthermore, some sites may not have been part of the Philippine Sea plate at the time of magnetization. Given the large scatter in declination in Figure 3b relative to uncertainties, it seems that local block rotations may exist and need to be deconvolved from any whole-plate rotations. Given the present uncertainties, we consider both rotational and nonrotational plate models in this paper, with our preferred model having large clockwise rotation, but less than the maximum values derived from paleomagnetic declinations.

Proponents of entire-plate rotation have argued that Philippine Sea declinations show a relatively smooth incremental increase with time, a trend that might not be expected for local block rotations [*Hall et al*., 1995c; *Haston et al*., 1992; *Keating and Helsley*, 1985; *Koyama et al*., 1992]. Recently published Luzon declinations do not fit neatly with the published Philippine Sea declination trends, but these Luzon declinations could have been affected by local faulting due to the nearby Philippine Fault or Philippine Sea plate margin [*Queano et al*., 2007]. Alternatively, Luzon could have been decoupled from the Philippine Sea plate until recently [*Hall*, 2012], and therefore, its declinations would not be representative of Philippine Sea motions, as discussed below. At ODP Site 1201 extraction of the present-day field overprints indicate clockwise rotation of the Philippine Sea plate [*Richter and Ali*, 2015], but this method is often highly unreliable due to drilling-induced magnetic overprints. It has been argued that clockwise Philippine Sea plate rotations are consistent with Parece Vela and Shikoku basin seafloor spreading rate and direction changes [*Sdrolias et al*., 2004]; however, a link between changes in relative motion and absolute plate rotation is not yet well established. On the other hand, Philippine Sea seamount magnetization vectors are not consistent with Philippine Sea clockwise rotations but instead suggest possible counterclockwise plate rotations [*Ueda*, 2004].

1.2.3. Problematic Paleomagnetic Sites

Some important paleomagnetic sites near the margins of the Philippine Sea plate have been controversial because they may not have been part of the plate during their entire history, including Luzon and Halmahera. At present, Luzon Island is considered part of the Philippine Sea plate, but its earlier affiliations have been disputed [*Hall*, 2012; *Queano et al*., 2007]. A number of paleomagnetic studies have shown that Luzon moved north from low latitudes, but conflicting timings have been proposed due to lack of detailed geological ages for sampled units [*Fuller et al*., 1983; *McCabe et al*., 1987; *Queano et al*., 2007]. The most recent study by *Queano et al*. [2007] showed that north Luzon paleolatitudes fit within the overall Philippine Sea plate trend (blue dots in Figure 3a). This motivated a plate reconstruction in which north Luzon moved together with the Philippine Sea plate after 40 Ma [*Queano et al*., 2007], which was disputed by *Hall* [2012]

based on its fit within a regional reconstruction and equatorial paleomagnetic ambiguity. Instead, the reconstruction of *Hall* [2002, 2012] prefers Luzon to be separate from the Philippine Sea plate until 5 Ma, although it allows for Luzon to move nonrigidly with the Philippine Sea plate after 40 Ma. However, it should be noted that Luzon paleolatitudes are in agreement with the Benham Rise ODP Site 262 time series within the adjacent southern west Philippine basin (see Figures 26c and 26d), as discussed above.

It is also controversial whether paleomagnetic sites on Halmahera and adjacent islands of Kasiruta, Waigeo, Halmahera, and Obi in eastern Indonesia are representative of the Philippine Sea plate motions (yellow dots in Figure 1) [e.g., *Yamazaki et al*., 2010]. Data from Halmahera are important because they play a key role in constraining a widely used Philippine Sea rotational plate model [*Ali and Hall*, 1995; *Hall et al*., 1995a, 1995b, 1995c]. Present-day global plate boundary models do not include Halmahera and adjacent islands with the present-day Philippine Sea plate, but rather within the Bird's Head subplate of Australia [*Bird*, 2003]. This is consistent with Halmahera's present obducted position onto fragments of the Australian continent (Figure 1). However, it has been argued that Halmahera data fit well with earlier Philippine Sea paleomagnetic trends [*Ali and Hall*, 1995; *Hall et al*., 1995c]. Their reconstruction proposes that Halmahera was part of a rotating Philippine Sea plate until 25 Ma, at which time they interpret it to have collided with northern Australia and shuffled WNW along the Sorong Fault, attached to the southern Philippine Sea margin [*Ali and Hall*, 1995].

Additional ambiguities have arisen from the use of Halmahara paleomagnetic data because of divergent models of the relationships between the Caroline and Philippine Sea plates. *Ali and Hall* [1995] and *Hall et al*. [1995a, 1995b] presented evidence for important geologic links between Halmahera and arcs of apparent Caroline Sea origin that collided with New Guinea ~25 Ma. Accordingly, Halmahara was kinematically linked to both the Caroline Sea/northern New Guinea and the Philippine Sea Plate in the *Hall* [2002] plate model. More recent plate models followed *Hall* [2002] in coupling the Caroline Sea to the Philippine Sea for much of its life, with large convergence (~1000–2000 km) between the Pacific and Caroline plates [*Deschamps and Lallemand*, 2002; *Gaina and Müller*, 2007; *Hall*, 2002; *Zahirovic et al*., 2014]. In contrast, older interpretations of *Hegarty et al*. [1983] and *Yan and Kroenke* [1993] have the Caroline Sea move with the Pacific plate with very minor relative motion, which would be incompatible with the Caroline Sea-Philippine Sea reconstruction models [e.g., *Hall*, 2002]. Other studies have also inferred that the Caroline plate moved with the Pacific since at least the Miocene based on bending of the southern Mariana arc, Sorol Trough opening, and upper mantle and transition zone tomographic anomalies [*Altis*, 1999; *McCabe and Uyeda*, 1983; *Miller et al*., 2006]. In a later section 1.4, we will argue that the Caroline plate was tied to the Pacific plate by the overlapping Caroline ridge large igneous province (LIPs) and associated Caroline hot spot track. This further suggests that Halmahera paleomagnetism may not be representative of Philippine Sea plate motions as argued by *Ali and Hall* [1995] and *Hall et al*. [1995a, 1995b].

It also appears that changes in paleolatitude of sites from Halmahera and adjacent islands are distinct from the ~20° northward motion of the Philippine Sea plate. The Halmahera sites move southward by ~10° from a position at the equator at 110–45 Ma to a location ~10°S at 30–25 Ma, followed by northward motion back to the equator [*Hall et al*., 1995c]. These latitudinal motions are similar to the prediction for an arc at the southern edge of the Caroline plate, tied to the Pacific plate (see Model 1 in Movie S1). Therefore, we provisionally exclude Halmahera and adjacent islands as a constraint from Philippine Sea plate analysis; nevertheless, keeping open the possibility that links between Halmahera and the Philippine Sea plate may emerge from slab constrained models. The remaining declination data from the eastern margin of the Philippine Sea plate are largely consistent with large clockwise rotation of ~50–90° between 40 Ma and 5 Ma (Figure 3b) [*Yamazaki et al*., 2010]. This is consistent with our subducted slab constraints that strongly limit the maximum possible rotations since ~30 to 20 Ma, based on the combination of plate size and maximum available space in which it must fit, discussed later (section 5).

1.3. Philippine Sea Plate Seafloor Spreading History

The Philippine Sea plate is composed of a number of Cenozoic subbasins including the West Philippine basin, the Shikoku and Parece Vela basins, and the Mariana basin (Figures 1 and 2). The plate also includes a Mesozoic core of rifted Cretaceous island arcs that include the Amami Plateau, Daito ridges, and Oki-Daito ridges (Figure 1). Seafloor spreading began at the West Philippine basin in the early Cenozoic and estimates for spreading initiation include 58 Ma [*Hilde and Lee*, 1984], 55 Ma [*Deschamps and Lallemand*, 2002], or 52–51 Ma [*Ishizuka et al*., 2013]. Initial seafloor spreading was highly disorganized [*Deschamps and*

Lallemand, 2002]. West Philippine basin spreading appears to have been contemporaneous with the so-called Oki-Daito/Benham-Rise hot spot track (Figure 1a), a chain of age-progressive oceanic plateaus astride the spreading center [e.g., *Hickey-Vargas*, 1998; *Ishizuka et al*., 2013]. West Philippine Basin spreading ended sometime between 34 and 36 Ma [cf. *Sasaki et al*., 2014] or 33 and 30 Ma [*Deschamps and Lallemand*, 2002]. Very slow spreading or dextral shear continued at the West Philippine basin spreading center (i.e., the Central Basin rift) until 26–28 Ma [*Deschamps et al*., 1999; *Fujioka et al*., 1999].

Recent results suggest that the Palau subbasin, a little-studied Philippine Sea subbasin to the south, formed during the mid-Eocene to late Eocene and has N-S magnetic anomalies unlike the E-W anomalies of the adjacent West Philippine basin [*Sasaki et al*., 2014]. These observations agree with the EMAG2 magnetic map, which shows a magnetic pattern for the Palau subbasin that is distinct from the adjacent West Philippine basin (Figure 2a). The younger Shikoku and Parece Vela basins at the eastern Philippine Sea began to spread at ~30 Ma and continued until ~15 Ma (Figure 2b) [e.g., *Kobayashi and Nakada*, 1978; *Mrozowski and Hayes*, 1979; *Okino et al*., 1999; *Sdrolias et al*., 2004; *Watts and Weissel*, 1975]. Detachment-mode seafloor spreading [e.g., *Escartín and Canales*, 2011] occurred at a system of oceanic core complexes within the Parece Vela Basin until 7.9 Ma [*Tani et al*., 2011]. Finally, the Mariana basin was produced by seafloor spreading at the Mariana Trough that began in the latest Miocene around 7 Ma and continues to the present day (Figure 2b) [e.g., *Hussong and Uyeda*, 1982; *Yamazaki et al*., 2003].

Seafloor ages and spreading patterns determined from Philippine Sea plate magnetic lineations allow past plate geometries to be partially reconstructed within a range of uncertainty [*Deschamps and Lallemand*, 2002; *Hilde and Lee*, 1984; *Watts and Weissel*, 1975]. Figure 5 illustrates the predicted Philippine Sea plate sizes, excluding subducted slabs, at 6, 15, 40, and 52 Ma from a published Philippine Sea age grid model [*Müller et al*., 2008; *Seton et al*., 2012] based on *Hilde and Lee* [1984] that we use later in this study. Differences between published Philippine Sea age models are relatively minor for more recent Oligocene to present-day Philippine Sea spreading. However, there is significant variation in the interpreted ages of the oldest West Philippine basin anomalies [e.g., *Deschamps and Lallemand*, 2002; *Sasaki et al*., 2014]. These differences in spreading models result in a relatively wide range of predicted Philippine Sea plate sizes during the early Cenozoic, which has significant implications for fitting our reconstructed Philippine Sea plate and its unfolded slabs between surrounding lithosphere in a plate reconstruction. Hence, we briefly review the range of predicted early Cenozoic Philippine Sea plate sizes.

The *Hilde and Lee* [1984] age model has been used in many plate reconstructions [e.g., *Hall*, 2002, 2012; *Seton et al*., 2012] and suggests that West Philippine basin spreading began by 59 to 56 Ma. At 52 Ma the model predicts that the Philippine Sea plate has already reached a relatively large size of ~1300 × 1300 km [*Hilde and Lee*, 1984]. In contrast, recently published models interpret that the West Philippine basin initiated later from ~54 to 50 Ma based in part on new radiometric ages and the recognition of the age-progressive, oceanic plateau Oki-Daito hot spot track on either side of the West Philippine basin spreading center [*Deschamps and Lallemand*, 2002; *Ishizuka et al*., 2013; *Sasaki et al*., 2014]. This new model predicts a much smaller ~600 × 700 km Philippine Sea plate at 52 Ma (i.e., approximately the present-day size of the Oki-Daito province), which is about 25% of the size of the *Hilde and Lee* [1984] model. These differences in predicted size at 52 Ma contribute to uncertainties in the exact fit of the Philippine Sea at nucleation within our plate reconstructions (section 4).

1.4. Constraints of Surrounding Major Tectonic Plates and the Caroline Sea

The reconstructed past positions of the major surrounding Pacific, Indo-Australian, and Eurasian plates effectively limits the outer bounds of possible Philippine Sea plate positions at any given period. Further significant constraint comes from clarification of a Pacific origin for the Caroline plate. Figure 5 shows absolute positions of these major plates at 52, 40, 15, and 6 Ma reconstructions based on a modified global plate model of *Seton et al*. [2012] and its associated moving hot spot mantle reference [*O'Neill et al*., 2005].

1.4.1. Pacific and Indo-Australia

Of the three major surrounding plates, the Pacific and Indo-Australian plate motions are best constrained based on well-studied seafloor magnetic anomalies reconstructed within a global plate circuit [e.g., *Cande et al*., 1995; *Jacob et al*., 2014]. These plates show stable convergence toward Eurasia since at least 40 Ma (Figure 5), which leads to the obvious conclusion that Philippine Sea paleopositions are progressively better constrained near the present day (i.e., 15 and 6 Ma) relative to earlier periods (40 and 52 Ma) (Figure 5).

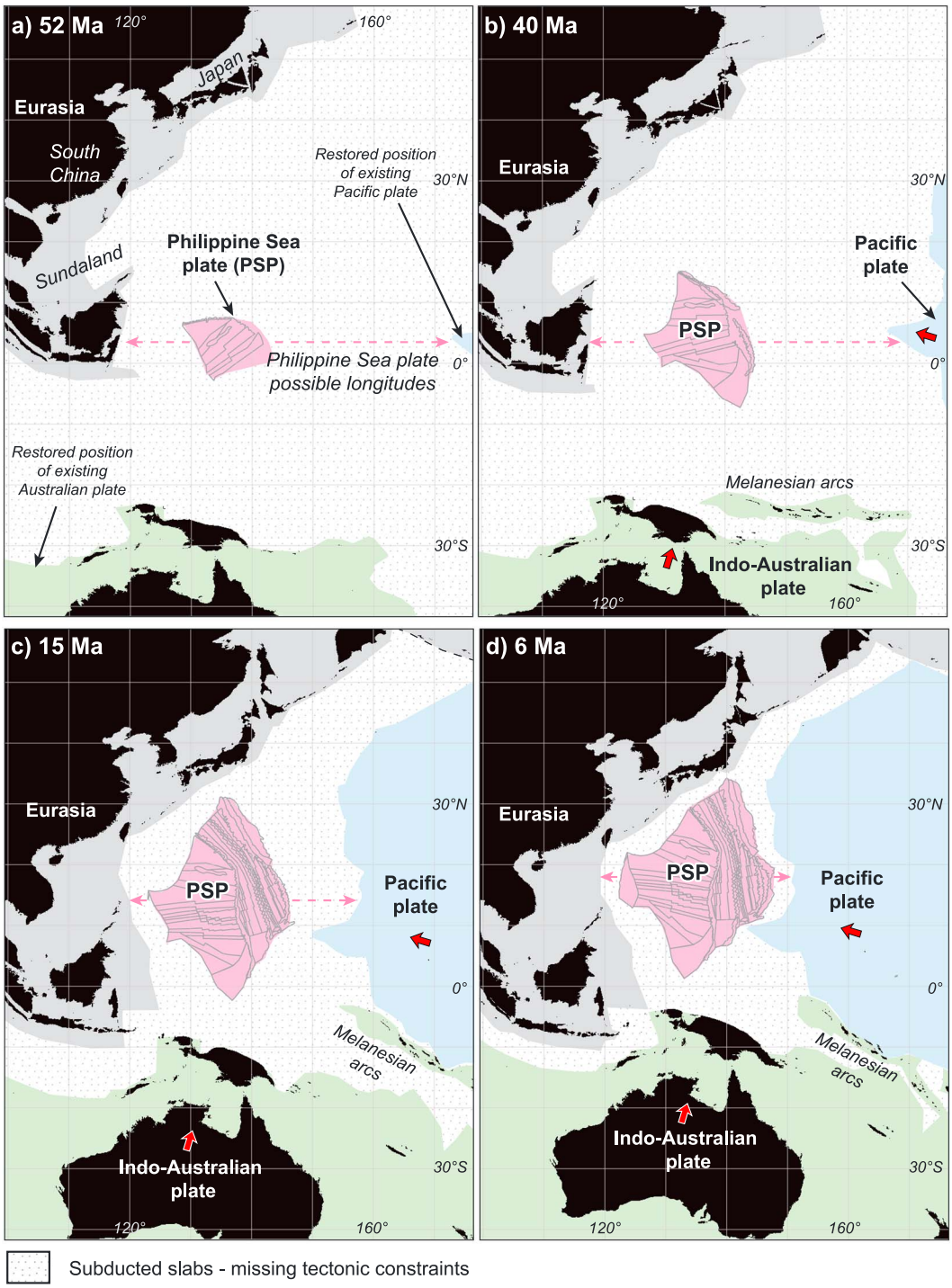

Figure 5. Possible Philippine Sea plate positions constrained by reconstructed positions of existing Pacific, Indo-Australian, and Eurasian plates at (a) 52 Ma, (b) 40 Ma, (c) 15 Ma, and (d) 6 Ma from *Seton et al.* [2012]. The Philippine Sea fits within the paleomagnetic constraints from Figure 3 but still cannot be uniquely positioned at any time period due to missing tectonic constraints (subducted slabs shown by the grey stippled areas). Red arrows show mean major plate motion since 40 Ma. Small microplates and terranes have been omitted for simplicity.

1.4.2. Eurasia and Sundaland

Eurasian plate motions in East Asia are less well constrained by the global plate circuit in the Cenozoic relative to the Pacific and Indo-Australian plates. Eurasian motions are primarily derived from distant North Atlantic and Arctic Ocean seafloor spreading histories [*Gaina et al*., 2002]. The application of these distant constraints to East Asia is somewhat uncertain because rigid motions must be assumed across the Eurasian continent, which undoubtedly has undergone some Cenozoic intracontinental deformation [*De Grave et al*., 2014; *Gaina et al*., 2002]. Eurasian paleomagnetic data also indicate probable Cenozoic intra-Eurasian deformation east of the Urals [*Cogné et al*., 2013].

The eastern Sundaland margin plays an important role by limiting Philippine Sea positions to the west. However, reconstructing the absolute eastern Sundaland margin position has many challenges due to subduction and loss of parts of the South China Sea, Celebes Sea, Molucca Sea, and other marginal seas. In addition, some parts of Sundaland (i.e., Indochina) may have been extruded between 200 and 1200 km in the Cenozoic [e.g., *Hall*, 2002; *Molnar and Tapponnier*, 1975]. Global plate reconstructions have placed the Eurasian and Sundaland plate paleopositions within a global self-consistent framework (Figure 4) [*Seton et al*., 2012] and suggest that the eastern Eurasian margin near Sundaland was at 120° ± 10°E longitude in the Cenozoic. Other reconstructions place the eastern Eurasian margin and Sundaland in similar locations within 200–300 km [e.g., *Hall*, 2002].

In this study we will use a slightly modified Eurasian plate motion model from *Seton et al*. [2012] with a small eastward shift (i.e., a constant ~200 km offset between 52 and 23 Ma, followed by a smooth interpolation between the 23 to 0 Ma positions). This choice was based on an assumption that the NS eastern edge of the South China Sea would have coincided with the NS eastern edge of the underlying proto-South China Sea flat slab during South China Sea NS opening prior to 23 Ma, assuming vertical sinking (see section 3.4.3). In comparison to other published plate models, our ~200 km adjustment in absolute Eurasia positioning at 23 Ma is smaller than the 350 km difference in 23 Ma Eurasia positions between *Seton et al*. [2012] and *Zahirovic et al*. [2014] produced by their choice of an alternate mantle reference frame. In turn, the 23 Ma position of Eurasia in these two models differ from *Hall* [2002] by ~200 km.

1.4.3. Caroline Plate

The Caroline plate (Figure 6) is important to this study because of its position adjacent to the Philippine Sea plate and because its motions have been closely linked to the Philippine Sea plate in widely accepted plate reconstructions. A number of plate models followed *Hall* [2002] in having the Caroline Sea move with the Philippine Sea for much of its life, with large convergence (~1000–2000 km) between the Pacific and the Caroline plates [e.g., *Deschamps and Lallemand*, 2002; *Gaina and Müller*, 2007; *Zahirovic et al*., 2014]. In contrast, other studies argue the Caroline Sea has moved with the Pacific for all or part of its existence [*Altis*, 1999; *Hegarty et al*., 1983; *McCabe and Uyeda*, 1983; *Miller et al*., 2006; *Yan and Kroenke*, 1993]. We argue here that the Caroline Sea has been tied to the Pacific plate since its inception, with only minor relative motion. However, there also is evidence that the Caroline Sea is more recently linked to the Philippine Sea plate through Ayu trough spreading. Nevertheless, the full history of Caroline-Philippine Sea interactions is not well constrained.

At present the Caroline plate is moving with Pacific-like motions, as is the southern Philippine Sea plate (Figures 1a and 1b), which is inconsistent with the long-term Philippine Sea motions from paleomagnetism (Figure 3) [*Argus et al*., 2011; *Bird*, 2003; *DeMets et al*., 2010]. Analysis of plate boundary seafloor morphologies suggests little total displacement between the Pacific and the Caroline plates [*Altis*, 1999; *Hegarty et al*., 1983; *Weissel and Anderson*, 1978]. No earthquake or tomographic evidence exists for a substantial subducted slab along the Mussau trench, which forms the eastern boundary of the Caroline Sea and shows decreasing morphologic expression northward (Figure 6). The Sorol trough within the Caroline ridge forms the northern boundary of the Caroline Sea and shows decreasing morphologic expression eastward. *Weissel and Anderson* [1978] interpreted the Sorol trough as a transtensional rift. It has been modeled as a rift with flanking uplifts, with $<$100 km of extension within the larger Caroline ridge [*Altis*, 1999]. These morphologic boundaries are consistent with only minor counterclockwise net rotation of the Caroline Sea relative to the Pacific.

The Caroline Sea formed in the late Eocene to Oligocene (36 to 25 Ma) with north-south spreading [*Gaina and Müller*, 2007], apparently as a back-arc basin that opened N-S with a trench to the south [*Weissel and Anderson*, 1978]. The bathymetrically shallow Caroline ridge large igneous province (LIPs) straddles the

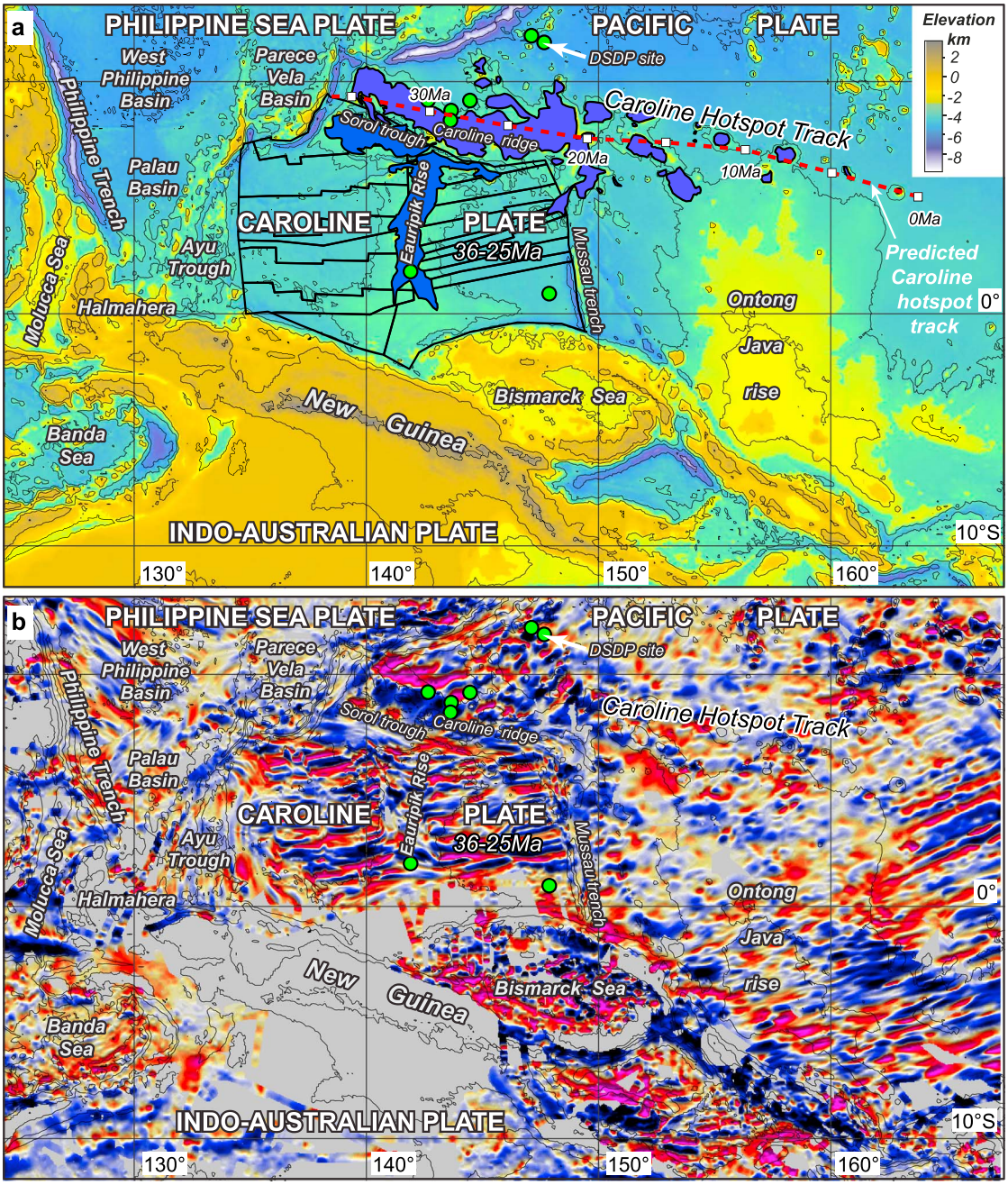

Figure 6. (a) Digital elevation model (DEM) bathymetry of the Caroline plate and surrounding areas. The modeled Caroline hot spot track (red dashed line) plotted using the moving Indo-Atlantic hot spot of *O'Neill et al.* [2005] overlaps and is coeval to the Caroline LIPs (large igneous province) shown by blue and purple polygons. (b) East-west trending magnetic anomalies within the Caroline Sea shown by EMAG2 gridded magnetic anomalies [*Maus et al.*, 2009]. Caroline LIPs in Figure 6a from the UTIG (University of Texas Institute for Geophysics) LIPs database [*Coffin*, 2011].

northern boundary Caroline plate with the adjacent late Mesozoic Pacific plate, providing evidence that they were connected (Figure 6). The Eauripik rise forms a N-S arm to the LIPs that has been interpreted as a leaky transform fed by an adjacent hot spot [*Altis*, 1999; *Gaina and Müller*, 2007]. The Caroline hot spot track extends eastward from the Caroline ridge LIPs, with decreasing age and decreasing magmatic activity [*Hegarty et al.*, 1983; *Keating et al.*, 1984; *Rehman et al.*, 2013]. The overlying postmagmatic stratigraphy is similar in age and composition on both the Caroline Sea and Pacific parts of the LIPs, composed of Oligocene and younger chalks based on DSDP drilling [*Fischer et al.*, 1971; *Winterer et al.*, 1971].

Predicted tracks of the Caroline hot spot traverse the northern boundary of the Caroline plate at the time of Caroline Sea spreading [e.g., *Harada and Hamano*, 2000; *Wessel and Kroenke*, 2008; *Wessel and Müller*, 2015] (Figure 6; see also Movies S1–S3 in the supporting information). The proximity of the Caroline hot spot at the time of formation of the Caroline plate is consistent with its abnormally thick crust, which is typical of ridge-hot spot interaction [*Whittaker et al*., 2015]. Crustal thicknesses are 10 to 25 km estimated from gravity, bathymetry, and seismic refraction, in contrast with the basins of the Philippine Sea plate of similar age which are deeper and have estimated crustal thicknesses of ~5 km [*Altis*, 1999; *Den et al*., 1971; *Yen et al*., 2015]. The only basinal areas of similar crustal thickness in the Philippine Sea Plate are parts of the Benham Rise hot spot track and the region NE of the Palau basin (Figures 1 and 6). Therefore, we conclude that the Caroline Sea and Pacific plates have been closely tied by the Caroline hot spot and overlapping large igneous province LIPs since its formation. This has the important implication that $>$2000 km of westward Pacific/Caroline Sea motion since ~25 to 35 Ma therefore must be accounted for west of the Caroline plate at equatorial latitudes (Figure 6). We further test this interpretation using subducted slab constraints.

The tectonic history of the western boundary of the Caroline plate with the Philippine Sea plate is not fully understood but is presently composed of the Yap and Palau trenches in the north and the northward narrowing extensional Ayu trough in the south, which has been considered a very slow-spreading ridge (Figures 1, 2, and 6) [*Fujiwara et al*., 1995; *Weissel and Anderson*, 1978]. Furthermore, little is known of the age or origin of the adjacent bathymetrically complex Palau basin to the west, but it appears to have a pattern of magnetic anomalies distinct from the West Philippine basin to the north, as shown by EMAG2 data (Figures 2 and 6). *Sasaki et al*. [2014] present bathymetric and magnetic evidence for EW spreading at ~39–35 Ma for the deepest part of the southern Palau basin. At present there is little relative motion between the Caroline, Philippine Sea, and Pacific plates [*Argus et al*., 2011; *DeMets et al*., 2010] (Figure 1b).

An extended history of Eocene to Miocene (~40–20 Ma) arc volcanism is recorded on Palau [*Cosca et al*., 1998; *Haston and Fuller*, 1991; *Meijer et al*., 1983]. These observations suggest significant subduction along this boundary at the southern end of the Kyushu-Palau ridge. The bathymetry and magnetic data (Figure 6) [*Sasaki et al*., 2014] suggest a possible southward continuation of a former arc to the west of the Ayu trough at the edge of the Palau basin. The possibility has been suggested that the Ayu trough was a site of subduction prior to its more recent spreading, based on dredge samples of arc affinities near both margins of the trough with dates of 20–25 Ma on the eastern margin [*Fornari et al*., 1979; *Kumagai et al*., 1996]. The trough itself shows morphological similarities to very slow-spreading ocean ridges with systematic decrease in overlying sediment thickness toward the axis [*Fujiwara et al*., 1995; *Weissel and Anderson*, 1978]. Well-defined seafloor spreading anomalies are missing in the trough [*Lee and Kim*, 2004]. The history of spreading is poorly constrained to $<$20–25 Ma; substantial sediment thicknesses in the axial zone suggests very little current activity; however, mid-Quaternary MORB basalts have been dredged [*Kumagai et al*., 1996; *Park et al*., 2006]. The northward narrowing has suggested that the Ayu trough provides a record of young rotation of the Philippine Sea plate relative to the Caroline plate [*Fujiwara et al*., 1995; *Weissel and Anderson*, 1978]. The magnetic map of the western Caroline Sea suggests a pattern of progressively rotated NS anomalies between the NS eastern bathymetric boundary of the Ayu trough and the region of well-defined EW anomalies of the Caroline Sea (Figure 6), with possible progressive Caroline Sea spreading ridge propagation toward the west. These unstudied anomalies may perhaps provide a record of substantial early rotational EW spreading of the Ayu trough coeval with NS Caroline Sea spreading, with the latter bathymetrically expressed Ayu trough representing a later magma poor and slow-spreading ridge. Nevertheless, the nature and history of plate interactions between the Caroline and Philippine Sea plates remain poorly constrained because of insufficient knowledge of each intervening element of the boundary zone, including the westernmost Caroline Sea, the Ayu trough, and the Palau basin and its contact with the West Philippine basin (Figure 6).

In summary, the Caroline back-arc basin and Pacific plates have been closely tied by the Caroline hot spot and overlapping large igneous province LIPs since its formation (36–25 Ma). The Caroline plate also appears to have been adjacent to the poorly studied Palau basin of the southern Philippine Sea plate based on Ayu trough spreading since sometime after 25 to 20 Ma, but the full history of Caroline-Philippine Sea interactions is not well constrained.

2. Data and Methods

2.1. Global Tomographic Models and Seismological Data

Subducted slabs in the mantle under East Asia were mapped from MITP08 *P* wave global seismic tomography [*Li et al*., 2008]. The MITP08 tomographic model included travel-time data from the Chinese Seismographic Network in addition to global bulletins and other regional arrays and is generally well regarded for resolving slabs under the circum-Asian subduction zones [*Li and van der Hilst*, 2010]. Resolution tests indicated that the inclusion of the Chinese stations produced a significant increase in resolution of upper mantle structure beneath our East Asian study area [*Li et al*., 2008].

The best-imaged areas within the MITP08 model have approximately 100 km effective resolution [*Li et al*., 2008]. However, as for most seismic tomographic models, the exact resolution at any given location is difficult to assess and dependent of station coverage and earthquake densities. Qualitative resolution estimates from MITP08 checkerboard tests generally indicate sufficient resolution under East Asia at the relevant depths (i.e., to 1350 km) of this study [*Li et al*., 2008]. We used the LLNL-G3Dv3 *P* wave and TX2011 *S* wave global tomography models [*Grand*, 2002; *Simmons et al*., 2012] for comparison to MITP08 for our lower mantle Pacific slab analysis in section 3.3. In particular, the *S* wave model may provide alternative sampling of the mantle in oceanic and Southern Hemisphere regions. We used Benioff zone seismicity from the U.S. Geological Survey Centennial earthquake catalogue [*Engdahl and Villaseñor*, 2002].

2.2. Slab Mapping Methodology and Workflow

Seismic tomographic images of subducted slabs at convergent plate boundaries provide a potentially decipherable tectonic record. Slabs are typically imaged in seismic tomography as relatively fast seismic velocity anomalies, which in the MITP08 tomography are the positive *P* wave perturbation (dV_p) anomalies. The most easily identified slabs are accompanied by both a fast tomographic anomaly and Benioff zone seismicity. In many other cases, however, slab-like tomographic anomalies are aseismic. Seismic tomography is independent of classical plate tectonic input and in recent decades has played an increasing role in either augmenting or testing plate tectonic reconstructions [e.g., *Hall and Spakman*, 2002; *Zahirovic et al*., 2014].

We designed a new slab reconstruction workflow for this study consisting of the following steps: (1) 3-D slab mapping and slab model building using Gocad software, (2) slab unfolding within a spherical Earth model in Gocad, and (3) input of unfolded slabs into a quantitative plate reconstruction using GPlates software [*Boyden et al*., 2011]. Three-dimensional slab mapping within Gocad software allowed us to develop and maintain a self-consistent 3-D Earth model of our mapped slabs. This had advantages for the East Asian study area, where many slabs have apparently subducted within close proximity of each other. Because slab mapping is necessarily interpretative, input of the unfolded slabs into a quantitative plate reconstruction allowed the tectonic viability of each mapped slab to be tested, both individually and in concert with other slab constraints. These parts of the workflow are described in more detail below in sections 2.3 and 2.4.

2.3. Slab Unfolding Methods and Constraints

If we can unfold subducted slabs from their current 3-D deformed shapes and sizes to obtain estimates of their presubduction geometries, we can place major constraints on plate reconstructions, especially for slabs that are much larger than their nominal imaging uncertainty of ~100 km. Most of the 28 unfolded slabs of this study have surface areas that range between 1×10^5 and 1×10^7 km^2, which may be compared to the current surface area of the Philippine Sea plate of 6.05×10^6 km^2 (Table 1). These large slabs fill substantial space and thereby place major constraints on possible plate reconstructions. Even small slabs provide evidence of locations of transient subducting boundaries. Furthermore, slab edges indicate boundaries that must play well-defined roles in plate models, including locations of trench initiation sites, lithosphere tearing STEP faults [*Govers and Wortel*, 2005], transform faults, edges of slab windows, and slab breakoffs. Finally, at each time step in the reconstruction sequence, we have the constraint that the surface of the Earth must be covered by lithosphere composed of a combination of (1) unfolded slabs and (2) lithosphere that still exists at the surface of the present-day Earth, without voids or overlaps within the uncertainty of the data (e.g., Figure 4c).

In this paper we used three methods to unfold slabs mapped in seismic tomography to constrain plate tectonic reconstructions. Each method is based on simple conservation assumptions to arrive at estimates of the presubduction size and shape of the slab: (1) *flexural unfolding* of the midslab surface of upper mantle slabs

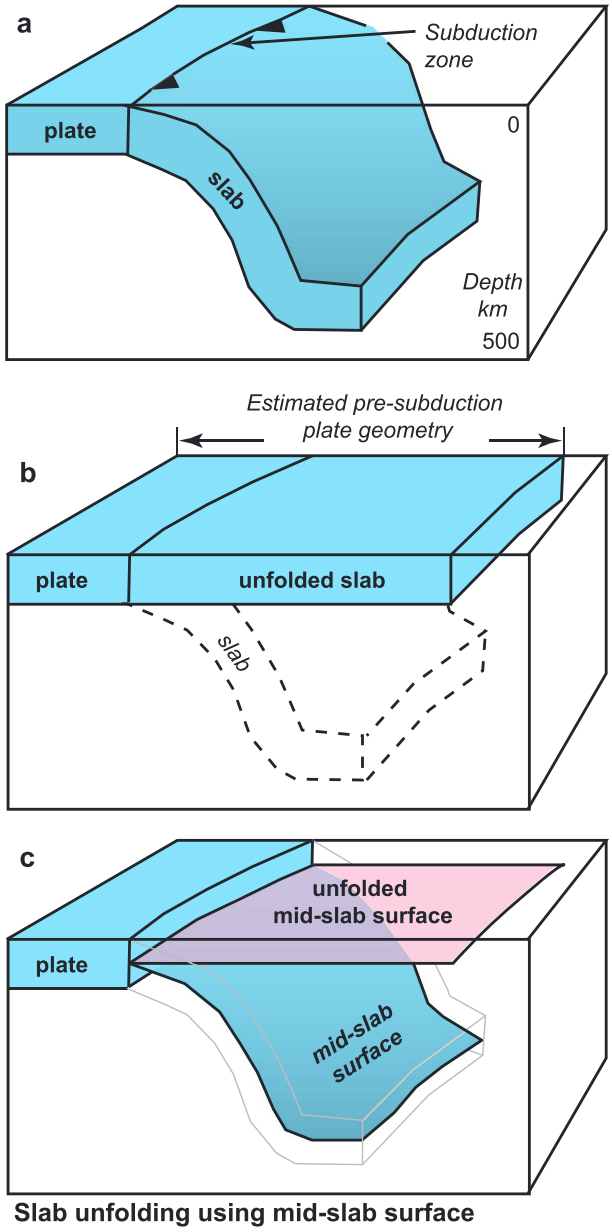

Figure 7. Conceptual cartoon showing slab unfolding. (a) The presubduction geometry of the slab can be estimated by unfolding it (b) back to the Earth surface, if the slab is relatively undeformed compared to its length. (c) In this study we flexurally unfolding a mapped midslab surface (blue) to estimate the unfolded slab geometry (pink).

by minimization of distortion and changes in surface area; (2) *constant-area unfolding* of cross sections through highly deformed slab walls, with corrections for volume changes; and (3) *radial unfolding* of flat lower mantle slabs based on an assumption that they sank vertically by radially convergent flow below the transition zone. In some cases we use multiple unfolding methods to evaluate uncertainties.

2.3.1. Flexural Unfolding of Midslab Surface

In flexural unfolding, we estimated the presubduction size and shape of a slab by flattening a midslab triangulated surface to the spherical Earth surface, minimizing changes in area and distortion (Figure 7). This method is most appropriate for upper mantle slabs that are relatively undeformed. This approach is similar to widely used algorithms that exist in structural geology for unfolding and unfaulting of deformed stratigraphic surfaces whose 3-D shapes are well constrained, for example, mapped seismic horizons in 3-D reflection data [e.g., *Rouby et al*., 2000]. Generally, these methods make use of conservation and minimization constraints to transform 3-D mapped surfaces to their flat equivalents within a local orthogonal Earth model. In our case we have modified these methods to unfold to the spherical Earth surface, which is essential for large slabs to be incorporated into a globally consistent plate tectonic framework. Such algorithms have been applied only to a limited extent to unfold of individual subducted slabs [*Chatelain et al*., 1993; *Heine et al*., 2012; *Lister et al*., 2012]. Ours is apparently the first attempt to systematically unfold 3-D slabs using conservation assumptions and incorporate them into quantitative globally consistent plate reconstructions. Advanced mapping of 3-D slab geometry in tomography has been done in a few cases [*Richards et al*., 2007].

Given the low resolution of global seismic tomography relative to the nominal initial thickness of oceanic lithosphere (~100 km), we have adopted a strategy of mapping 3-D midslab surfaces in seismic tomography, to which we then apply a flexural unfolding algorithm that minimizes changes in area and distortion [*Bennis et al*., 1991; *Gratier and Guillier*, 1993; *Mallet*, 2002]. This unfolding method is particularly suited to slabs with shapes that approximate developable surfaces, for example, the Sunda slab (Figure S1), which changes area by $<$0.4% on flexural unfolding. We have used 3-D mapping tools within Gocad software to create a midslab triangulated surface within a local orthogonal projection of the global mantle tomography. We then import this 3-D triangulated surface with any associated data such as seismic velocities and present depth into a

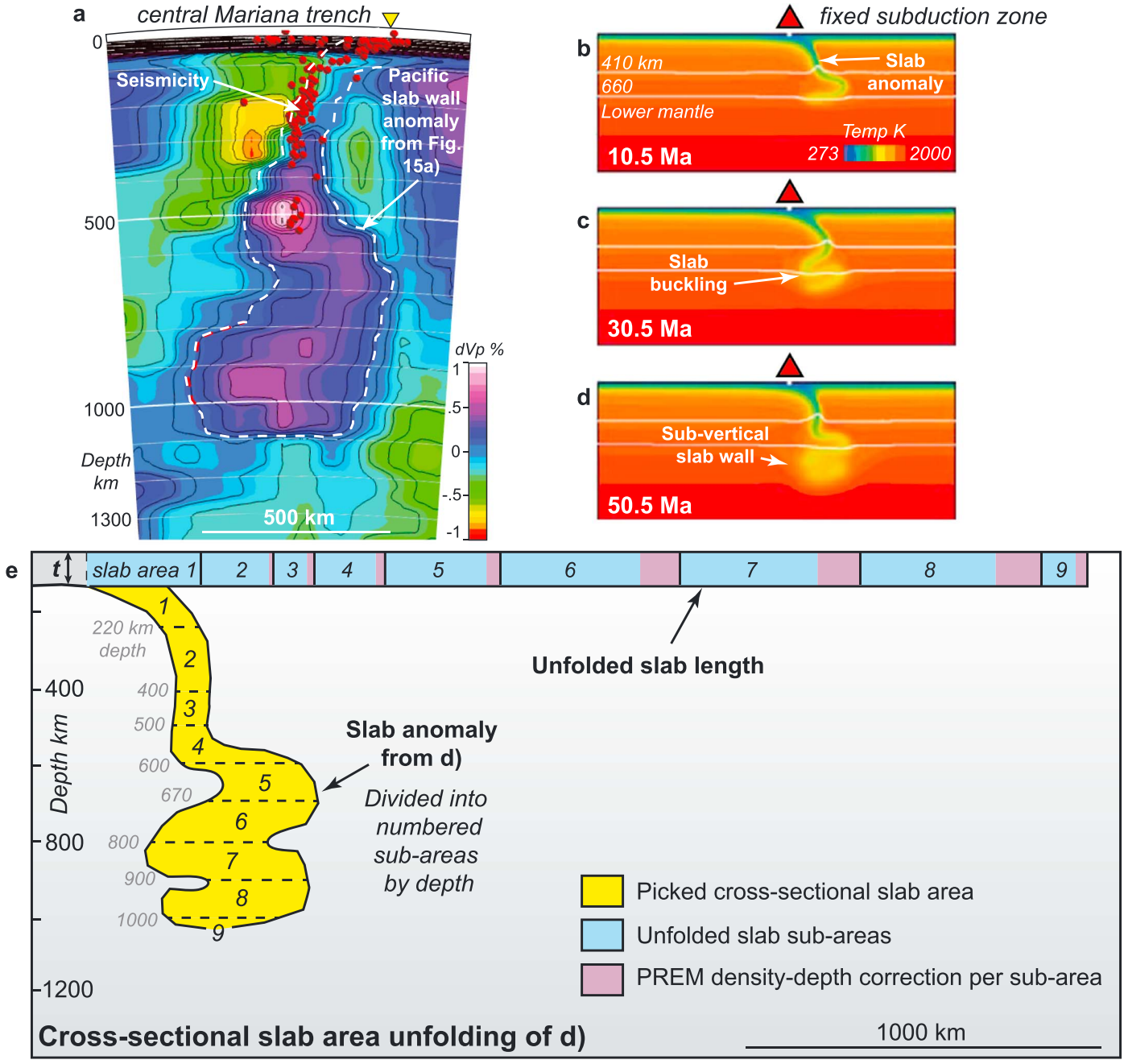

Figure 8. Illustration of cross-sectional area unfolding method for highly deformed slab walls. Examples of highly deformed slabs shown by (a) MITP08 seismic tomographic section and Benioff zone seismicity under the central Marianas and (b to d) progressive evolution of a subducted slab wall from a numerical model after 10.5, 30.5, and 50.5 Ma, respectively (adapted from *Čížková and Bina* [2013] with permission from Elsevier). (e) Cross-sectional area unfolding of the slab wall anomaly from Figure 8d using the following steps. First, a picked total slab area was subdivided into subareas 1 to 9 using depth increments from the PREM Earth model [*Dziewonski and Anderson*, 1981]. Second, the cross-sectional areas of 1 to 9 were assessed. Each subarea was divided by a notional incoming slab thickness "t" of 100 km to calculate an unfolded slab length for each subarea (numbered blue areas). Slab density change with depth was corrected according to the PREM model (purple areas). Finally, the corrected slab lengths were summed to assess a total unfolded subducted slab length.

spherical Earth model, which gives us the true 3-D shape of the surface, ready for unfolding (Figure S1). We use the flexural unfolding algorithm implemented within Gocad [*Bennis et al.*, 1991] to unfold the deformed slab to a flat tangent surface (Figure S1). We commonly place the tangent point above the barycenter of the folded surface. This tangent unfolded surface is then projected to the spherical Earth surface using a Lambert

azimuthal equal-area projection (the pole of which is the tangent point), which produces little distortion relative to tomographic resolution within 10–20° of the tangent point. We give a more complete illustration of our mapping and flexural unfolding in a later section, using the Ryukyu slab (see Figure 13).

2.3.2. Cross-Sectional Area Unfolding of Highly Deformed Slabs

In cross-sectional area unfolding, the presubduction length of a highly deformed slab is estimated from the cross-sectional area of its tomographic anomaly (Figure 8). This approach was first used by *Hafkenscheid et al*. [2006] to assess the amount of subducted lithosphere represented by lower mantle Tethyan slabs within the Alpine-Himalayan belt. In our method slab areas were manually interpreted on undistorted vertical spherical Earth tomographic cross sections. Our picked slab edges were guided by a dV_p cutoff value similar to *Hafkenscheid et al*. [2006]. However, because we are primarily concerned with slab geometry rather than any specific magnitude of velocity contrast within tomographies of heterogeneous resolution, we considered steeper velocity gradients to be a key indicator of slab edges, particularly for slabs showing heterogeneous velocities, such as the Eurasian slab of the South China Sea (section 3.4). This is one way our nonautomated approach allowed us the flexibility to adjust for regional differences within tomographic models if necessary. Our manual picking approach also permitted us to use our 3-D regional slab model to identify and exclude slab tomographic areas associated with other slabs in close proximity or in contact and to ignore obvious tomographic artifacts (see Figure 11).

The picked slab tomographic area was then divided into a set of prescribed subareas corresponding to depth increments in the preliminary reference Earth model (PREM) (Figure 8e) [*Dziewonski and Anderson*, 1981]. Each slab subarea was first measured using freely available structural area balancing software [*Judge and Allmendinger*, 2011] and then divided by an assumed slab initial thickness to calculate an unfolded length, not yet corrected for density changes. This initial thickness can be estimated from its presumed age [e.g., *Parker and Oldenburg*, 1973]; we used a nominal 100 km initial thickness for the western Pacific slabs. An Earth density-depth correction was then applied to each slab subarea according to the PREM model (Figure 8e). Finally, the total subducted slab length was given as the sum of the density corrected sublengths (Figure 8c). We give an illustration of the application to the central Marianas Pacific slab wall in section 3.3.

A secondary output from cross-sectional slab area unfolding is a top-down *cumulative unfolded slab length with depth* function. We can use this function to derive a slab subduction age versus depth relationship for a subvertical slab wall, if plate convergence rates are known relative to a mantle reference. We use this method to estimate slab sinking rates and regional slab ages for the central Marianas Pacific slab wall (section 3.3).

2.3.3. Radial Unfolding of Flat Lower Mantle Slabs

We assume that flat slabs within the lower mantle sank vertically by a radially convergent flow below the transition zone. Therefore, we reverse this assumed deformation by a radial unfolding of a mapped midslab surface within the lower mantle. This assumption is motivated the observed widespread vertical sinking over much of the lower mantle seen in global geodynamical models [e.g., *Steinberger et al*., 2012]. In the present paper radial unfolding is only applied as a minor correction to the East Asian Sea and Proto-South China Sea flat slabs, which are at relatively shallow depths in the upper part of the lower mantle (~700–1000 km). Radial unfolding is more important for restoration of deep lower mantle flat slabs.

2.4. Method for Plate Reconstruction With Unfolded Slab Constraints

2.4.1. Approach

In this paper we will attempt to build a Philippine Sea plate model primarily from East Asian slab constraints within the framework of a seafloor spreading-based, global plate reconstruction. In other words, we will determine the Philippine Sea plate motion history from slabs, using only minimal regional geologic or paleomagnetic constraints. Afterward, we will compare and discuss our slab-constrained model predictions against regional geology, paleomagnetism, and published plate models derived from these constraints [e.g., *Hall*, 2002; *Seno and Maruyama*, 1984]. This approach allows us to test whether relatively independent geological constraints could be reconciled with our interpreted mantle structure.

Our choice to prioritize slab constraints means that our plate models are appropriate for regional-scale insights but will have limited resolution for areas that include eastern Indonesia, Philippines, New Guinea, and parts of the Melanesian arcs, where small slabs are surrounded by complex arrangements of transient marginal seas and microplates, fragments, blocks, or terranes. In these areas our plate models permit us to estimate some boundary conditions, such as the maximum presubducted extent of these margins but at smaller scales will show obvious incompatibilities (i.e., gaps and overlaps). Here we will make only limited

plate motion modifications to ensure the plate model shows a reasonable visual fit relative to the slabs. Areas dominated by many smaller plate fragments will be largely unmodified from the global plate model with a view to update these areas in later plate model versions.

2.4.2. Selected Global Plate Model, Mantle Reference, and Plate Motion Inputs

We began our plate reconstructions at 52 Ma (early Eocene), which is considered the initiation of the Philippine Sea plate and Izu-Bonin Marianas arcs [*Cosca et al*., 1998; *Ishizuka et al*., 2013]. We used the global plate reconstruction model of *Seton et al*. [2012] with some modifications noted below and the associated moving hot spot mantle reference [*O'Neill et al*., 2005]. The choice of mantle reference has some effect on absolute plate positions, and key results were considered against an alternate global moving hot spot mantle reference from *Torsvik et al*. [2008].

We reconstructed West Philippine basin spreading following the GPlates plate polygons of *Seton et al*. [2012] with slight timing modifications to allow initiate spreading at 52 Ma [*Cosca et al*., 1998; *Ishizuka et al*., 2013] and proceed smoothly thereafter. The Oki Daito rise-Benham rise oceanic plateaus were digitized and reconstructed to appear on the West Philippine basin plate polygons following age dates in *Ishizuka et al*. [2013]. It was beyond the scope of this paper to synthesize West Philippine basin spreading with the Oki Daito rise-Benham rise oceanic plateau timings as proposed by the sketch models of *Ishizuka et al*. [2013]. Furthermore, our existing GPlates West Philippine basin spreading model does not currently reproduce the sheer complexity of rift propagations and ridge jumps during the early spreading phases [*Deschamps et al*., 2008]. Therefore, our plate models will show some discrepancies in the appearance of the conjugate Oki Daito rise-Benham rise plateaus relative to the actively spreading West Philippine basin.

We reconstructed the Caroline plate as a back-arc basin moving with the Pacific plate, similar to the *Yan and Kroenke* [1993] plate model, based on the overlapping Caroline LIPs and hot spot track (Figure 6) as discussed in section 1.4. The *Yan and Kroenke* [1993] model was straightforward to test in this study because it did not attempt to link Caroline Sea motions with the Philippine Sea, which was our main unknown parameter. We also noted early in the plate reconstruction process that Pacific-like Caroline Sea motions produced satisfactory results relative to our unfolded slabs. However, the implications of this choice will be explored in the discussion (section 5.6) relative to the alternative Philippine Sea-Caroline sea linked model [e.g., *Hall*, 2002] (see review in section 1.4) and our new slab constraints.

We adopted the globally consistent plate motion for Eurasia of *Seton et al*. [2012], modified by a slight eastward shift (maximum ~200 km at 23 Ma) based on the assumption that the observed NS the eastern edge of the South China Sea would have coincided with the NS eastern edge of the underlying Proto South China Sea flat slab during the NS opening of the South China Sea, based on the assumption of vertical sinking (for further explanation, see "Eurasia and Sundaland" in section 1.4). Japan Sea magnetic anomalies are not well defined; therefore, we followed the Japan Sea opening model of *Otofuji et al*. [1985] preferred by many Miocene to present-day reconstructions of the SW Japan margin [*Kimura et al*., 2005*,* 2014]. Borneo motions were updated from the oroclinal bending model of *Zahirovic et al*. [2014]. Sulu Sea extension spreading was modeled between 20 and 15 Ma following *Hall* [2013]. We fixed the Huatung basin and Luzon together based on their probable early Cretaceous age [*Deschamps et al*., 2000]. We simplified Luzon motions by moving it rigidly with the Philippine Sea plate after 40 Ma similar to *Queano et al*. [2007]. Our choice was motivated by similarities between Luzon and Philippine Sea paleolatitudes including the adjacent Benham Rise ODP292 borehole (Figures 1a and 3a). We acknowledge that fully rigid motion between Luzon and the Philippine Sea since the Eocene is a likely oversimplification [e.g., *Hall*, 2012] but appropriate for the regional scale of this study. The history of Molucca Sea motions is poorly constrained and therefore is a model output inferred from its spatial and kinematic position in each reconstruction relative to adjacent reconstructed slabs, such as the Sunda, Central East Asian Sea, Celebes Sea, and Philippine trench slabs (see below).

As discussed earlier (see section 1.2), we do not use Halmahera to constrain our Philippine Sea plate model. However, we placed Halmahera at the eastern margin of our unfolded east Molucca Sea slab at 20 Ma. After 20 Ma, Halmahera was moved loosely westward with the southern Philippine Sea plate to override the east Molucca Sea slab, consistent with age dating of the Halmahera arc [*Baker and Malaihollo*, 1996]. We did not fully reconstruct the tectonically complex Philippine archipelago due to our regional-scale scope. Following evidence for Mesozoic ophiolites concentrated within the eastern Philippines and Paleogene ophiolites to the west [*Tani et al*., 2015; *Yumul*, 2007], we arbitrarily chose to place the eastern Philippines

within a western Philippine Sea accretionary margin. The western Philippines were moved northward at the eastern Molucca Sea margin. We will discuss these predictions for the Philippines from our slab-based reconstructions (section 5.2).

2.4.3. Selected Philippine Sea Plate Motion Criteria

At ~15–20 Ma we invoked the arrival of the northern Philippine Sea Nankai/Ryukyu slab edge at the SW Japan margin based on ages of vigorous Nankai fore-arc magmatism and continental Asian-derived sediments deposited in the northernmost Shikoku basin [*Clift et al*., 2013; *Hibbard and Karig*, 1990; *Kimura et al*., 2005, 2014; *Pickering et al*., 2013]. We chose our main model (i.e., Model 1) to invoke the proto-Izu-Bonin arc arriving at Japan near its present-day location (i.e., fixed Japan triple junction model) [*Kimura et al*., 2005]. However, we will also show a plate model (i.e., Model 1b) that considers the alternative migrating Japan triple junction model and proto-Izu-Bonin arc arrival farther west near Kyushu [*Hall*, 2002; *Kimura et al*., 2014]. In Model 1b the Philippine Sea plate was moved with significant clockwise rotation relative to Japan after 15 Ma [*Hall*, 2002; *Kimura et al*., 2014] until 6 Ma, at which point the proto-Izu arc was aligned to the Boso peninsula, SW Japan. For Model 1b, between 6 and 2 Ma Philippine Sea plate motions were determined by interpolating from its 6 Ma position to its 2 Ma position, which is described below.

From ~2 Ma to the present day we invoked the Philippine Sea plate to move with its present-day WNW motions in all models. A Philippine Sea plate motion change around 2–1 Ma has been suggested by a change in Okinawa Trough back-arc extension pattern after 2 Ma [*Sibuet et al*., 1987], Mariana Trough back-arc spreading rate and clockwise rotations after 2 Ma [*Yamazaki et al*., 2003], Suruga and Sagami Trough morpho-bathymetric patterns [*Nakamura et al*., 1987], Boso Peninsula stress inversions from fault slips [*Yamaji*, 2000], and Kyushu fault slip and basin evolution [*Itoh et al*., 1998]. A 2 Ma Philippine Sea plate motion change would also be consistent with evidence we show in section 3.4 for a short (i.e., maximum 400–500 km E-W length) Eurasian slab, which could only account for maximum ~6 Ma duration of Philippine Sea subduction relative to present-day ~90 mm/yr WNW convergence rates south of Taiwan, in contrast with the estimated 15–20 Ma initiation of the northern Luzon arc.

2.4.4. Spatial and Temporal Positioning of Unfolded Slabs Within the Global Plate Model

With few exceptions, we assume that slabs sink vertically except for flexural effects; therefore, we generally place unfolded slabs initially at their barycenter overlying their deformed position within the GPlates environment. This unfolded position of a subducted slab will, of course, completely overlap existing lithosphere at the surface of the present-day Earth. However, as we move the global plate model backward in time, there must be a point at which the unfolded slab no longer overlaps and can be placed at the Earth surface. At this point, we expect that it will share at least one common edge, within mapping and unfolding uncertainties, with another plate to which it can be linked and then be moved backward in time within the plate kinematic model. If this is impossible, then there is generally some inconsistency in the slab-mapping interpretation or a problem in our plate-kinematic model, which must be discovered by inspection and corrected. This is a 4-D jigsaw puzzle in which the pieces have to be discovered by tomographic mapping. Unfolded slab constraints from this study were input into the global plate model in sequential hierarchical fashion, as follows.

1. *Attached slabs* for the major surrounding Indian Ocean, Australian, and Pacific plates were attached to their "mother" plate and moved according to a *Seton et al*. [2012] global plate model with updated Indian Ocean-Australian motions [*Gibbons et al*., 2013]. Seafloor spreading within key attached slabs (e.g., the Philippine Sea plate Shikoku slab and South China Sea slab) was modeled by arbitrarily extending their GPlates static plate polygons according to our unfolded slab lengths.
2. *Regionally extensive, flat detached slabs* not connected to any known plate (e.g., the East Asian Sea and proto-South China Sea slabs) were then added to the plate reconstruction. These slabs were restored with minimal correction (i.e., radial unfolding) and kept static within the mantle reference for the most straightforward reconstruction. Other smaller detached slabs were not reconstructed at this stage but later fit into the reconstruction by inspection as they became exposed to the surface. These smaller slabs provide evidence for the locations of transient subducting boundaries.
3. *Philippine Sea plate origin and plate motions* were modeled by first constructing a 52 Ma plate reconstruction. Our strategy was to search within a reconstructed slab map at 52 Ma for possible Philippine Sea plate-sized gaps or holes into which the Mesozoic plate nucleus might fit, given the range of 52 Ma Philippine Sea plate sizes discussed in section 1.3. This exercise revealed two permissible Philippine Sea

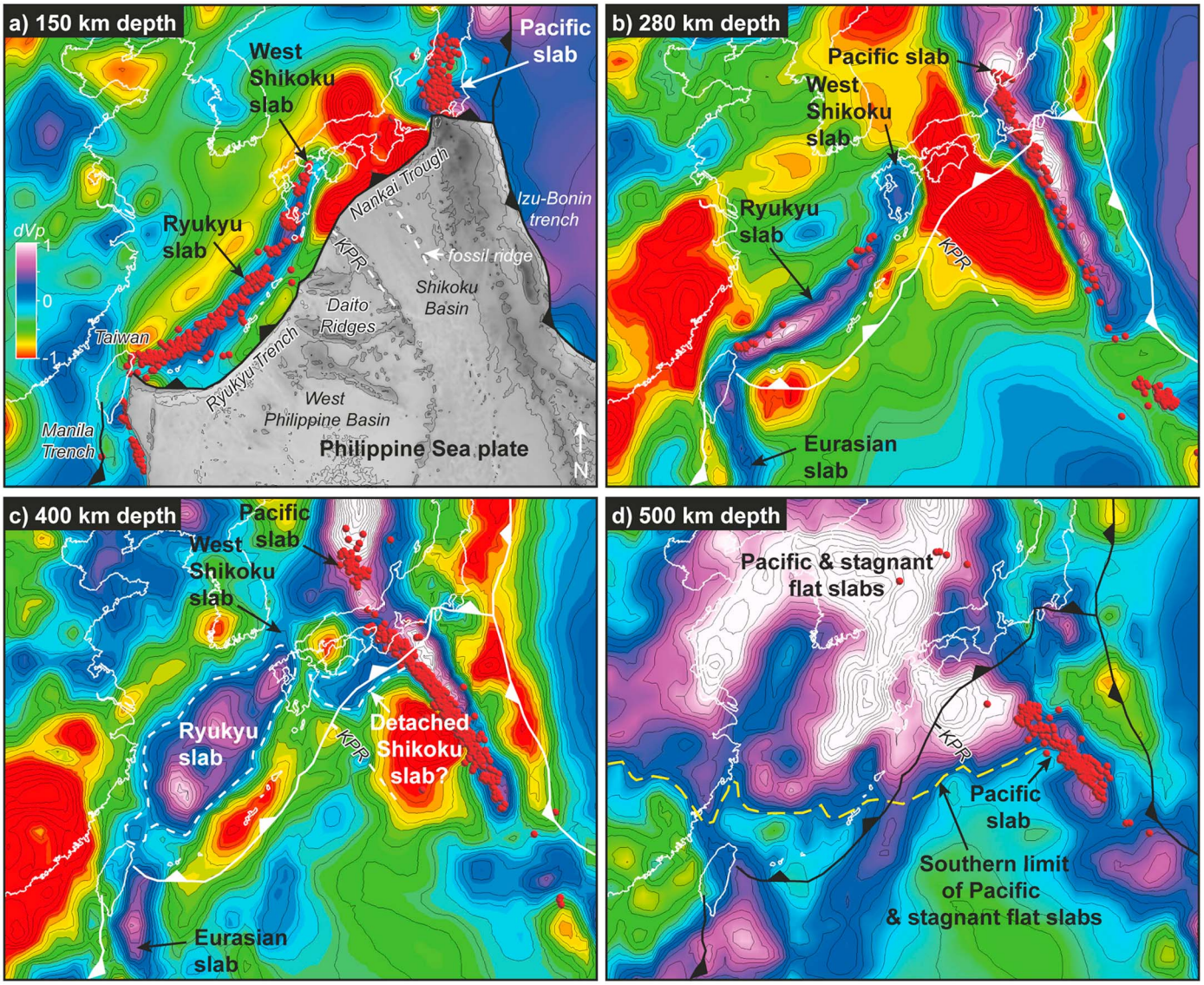

Figure 9. Slab anomalies under the northern Philippine Sea shown by MITP08 seismic tomography horizontal depth sections at (a) 150 km, (b) 280 km, (c) 400 km, and (d) 500 km. At 150 to 400 km depths, the Ryukyu Benioff zone and slab anomalies terminate to the west near Taiwan and to the east downdip of the Kyushu-Palau ridge (KPR). At 400 km depth the Ryukyu slab has subducted and flattened above deeper Pacific and stagnant slabs seen in the 500 km depth section. The Philippine Sea plate DEM has been overlain in Figure 9a. Surface trench locations are shown in Figures 9a to 9d. Red spheres show projected seismicity within 20 km.

plate origins, described later. We then modeled Philippine Sea plate motions from these two possible points of origin by progressively deducing its position over time, minimizing gaps and overlaps with adjacent plates, using minimal rotation poles, and maintaining reasonable plate velocities within the larger regional context of fast Pacific and Indo-Australian plate convergence toward Eurasia. We chose to reconstruct the Philippine Sea plate at its early Cenozoic origin using the newer *Ishizuka et al.* [2013] West Philippine basin spreading model (see review in section 1.3). We modeled this in GPlates by modifying the timing of the *Seton et al.* [2012] GPlates Philippine Sea age grid and poles. To accommodate other Philippine Sea spreading models, we will consider a range of plate sizes when reconstructing its pre-40 Ma early history and also allow for some flexibility (i.e., gaps or overlaps) in the fit between the Philippine Sea and adjacent plates during these periods.

4. *Smaller regional plates* outside the global plate circuit were fit within the remaining gaps in the *Seton et al.* [2012] global model and slab constraints.

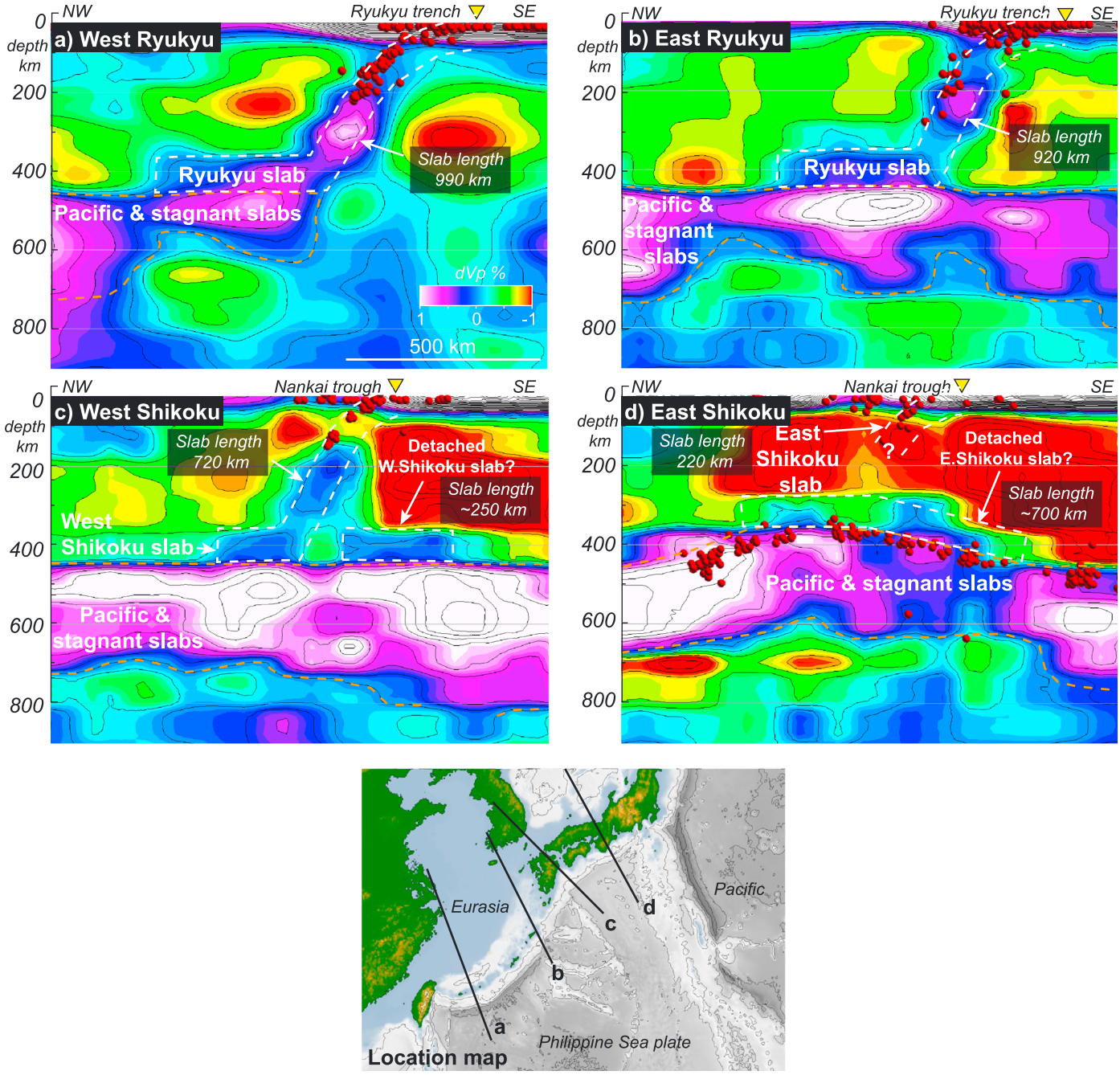

Figure 10. (a to d) MITP08 seismic tomographic cross sections across the Ryukyu trench and Nankai trough. Simple 2-D unfolded Ryukyu slab lengths in Figures 10a and 10b are 920 to 990 km. Shikoko attached slab unfolded lengths are shorter but approach ~1000 km lengths when detached slab fragments in Figures 10c and 10d are included. Red spheres show projected seismicities within 20 km. Yellow triangles denote surface trench positions.

2.4.5. Timing and First Appearance of Input Slab Constraints

The unfolding methods in this paper (described above in section 2.3) were used to estimate the presubduction total slab areas and geometries. No attempt was made to progressively restore the slabs within the mantle as they subducted [cf. *Lister et al.*, 2012]. Our unfolding is a direct geometric transformation from the present size, shape, and location of a slab to an estimate of its initial size, shape, and location at the initiation of subduction, based on assumed conservation constraints and in most cases vertical sinking. Simply put, each unfolded slab appeared in its entirety at a chosen time within our plate model (Table S1). Therefore, to model the unfolded slabs within the GPlates reconstruction, it was necessary to choose

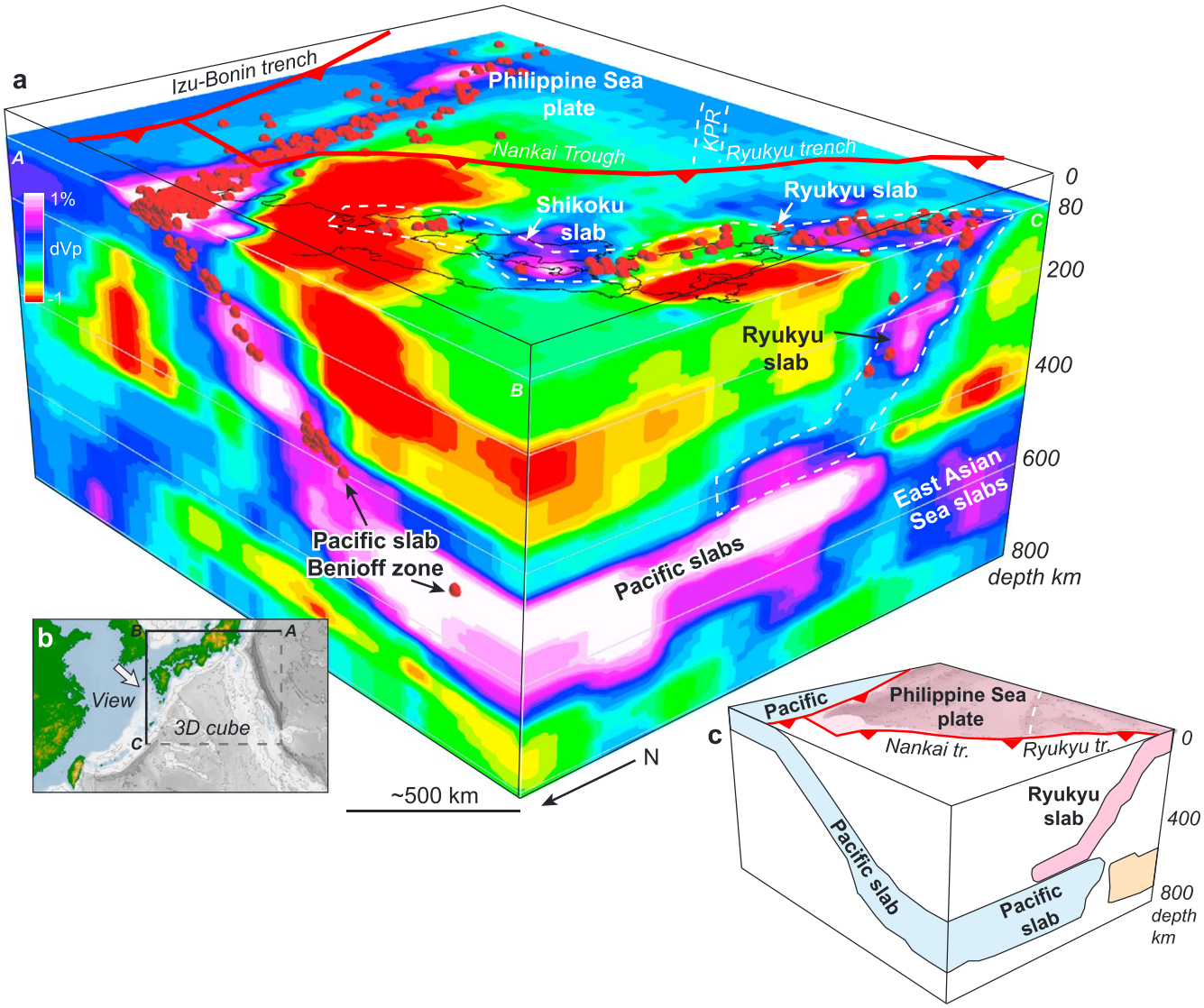

Figure 11. (a) Three-dimensional cube visualization of MITP08 seismic tomography and projected seismicity showing the northern Philippine Sea Ryukyu-Shikoku slabs and Pacific slabs near the Japan trench triple junction. (b) A location map. The Pacific slabs generally show a relatively higher velocity dV_p anomaly that is distinct from the lower dV_p Ryukyu slabs. We interpret that the northern Philippine Sea "Ryukyu slab" is on the order of ~1000 km length and has subducted above deeper, flat-lying Pacific and stagnant slabs. (c) Cartoon showing the interpreted slab geometries.

a time when the slab should first appear at the Earth surface as a tectonic plate (i.e., first appearance time in Table S1).

We chose the slabs to appear in our plate model based on two considerations. First, we had to estimate the age of the mapped subducted slab lithosphere (see supporting information Text S1 and Table S1), as some of the mapped slabs in this study were formed after our 52 Ma reconstruction time window due to seafloor spreading, and these slabs should obviously not appear before they were formed. For example, the Pacific Marianas slabs were likely formed in the Mesozoic based on published reconstructed Pacific age grids [*Müller et al.*, 2008], and thus, these unfolded slabs were eligible to be shown within our 52 Ma reconstruction. In contrast, the Philippine Sea plate Shikoku slabs were likely formed after 30 Ma based on seafloor magnetic anomalies and ocean drilling age dates, which have been incorporated into the *Seton et al.* [2012] global plate model. Hence, we chose the Shikoku basin slabs to appear after 25.2 Ma (Table S1) following the Shikoku basin age polygons from *Seton et al.* [2012]. In total, we inferred from published slab age models and the results in this study that 17 of the 28 unfolded slabs in this study

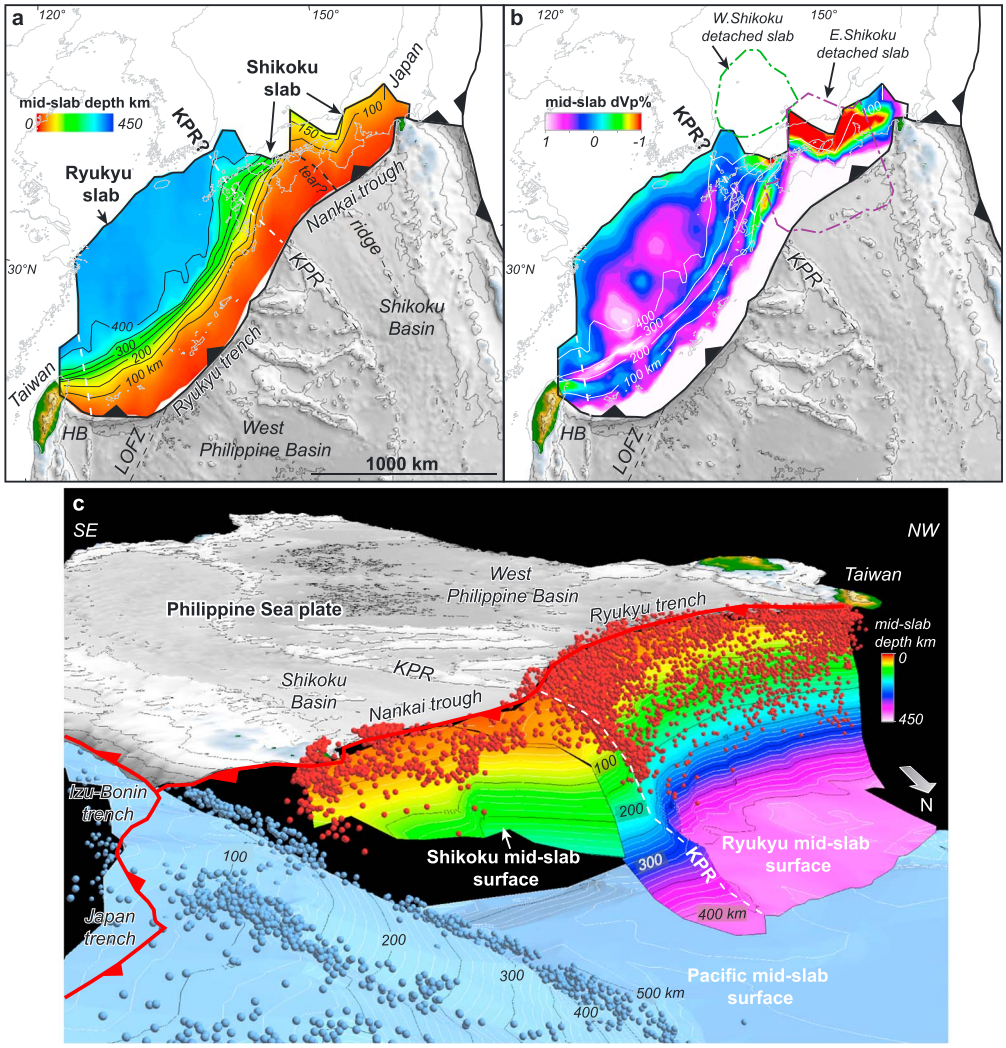

Figure 12. Ryukyu and Shikoku slab geometries shown by (a) midslab surface map and (b) MITP *P* wave velocity perturbation dV_P extracted along the Ryukyu and Shikoku midslab surfaces. Detached Shikoku Basin slab locations are shown by the dashed black lines in Figure 12b. (c) Three-dimensional slab model showing the attached Ryukyu and Shikoku slabs subducted above the Pacific slabs. Seismicity within 50 km of the Ryukyu and Pacific slab models is shown in red and blue, respectively. HB, Huatung Basin; LOFZ, Luzon-Okinawa fracture zone; KPR, Kyushu-Palau ridge.

existed at the Earth surface at 52 Ma (Table S1). We thus invoked these slabs to appear at the 52 Ma starting point of our reconstruction time window (Table S1). The remaining slabs appeared in our plate model based on the ages of their associated marginal ocean basins, which largely followed *Seton et al.* [2012] (Table S1).

Second, we had to assess whether some portion of our unfolded slabs had already been subducted prior to our 52 Ma initial time window, since any part of a slab that was subducted prior to 52 Ma should obviously not appear in the 52 Ma plate reconstruction. While this was clearly a challenging task due to lack of plate circuit constraints and mantle reference uncertainties (Figures 5a and S5), our approach was to search for overlaps between unfolded slabs and existing plates within a 52 Ma plate reconstruction (white stars in Figure 23a). Our rationale was that any potential pre-52 Ma subduction could be revealed by a major overlap between an unfolded slab and the existing plates at 52 Ma, especially for the attached Indian Ocean and Pacific slabs. For example, we chose to exclude a minor (~200 km) portion of the Sunda slabs from our 52 Ma reconstruction based on an assessed overlap between the leading edge of our unfolded Indian Ocean (i.e., Sunda) slabs and Sundaland (Figure 23a). Although the absolute position of Sundaland is not well constrained by the global plate circuit at 52 Ma, magmatic records allow the possibility of some pre-52 Ma

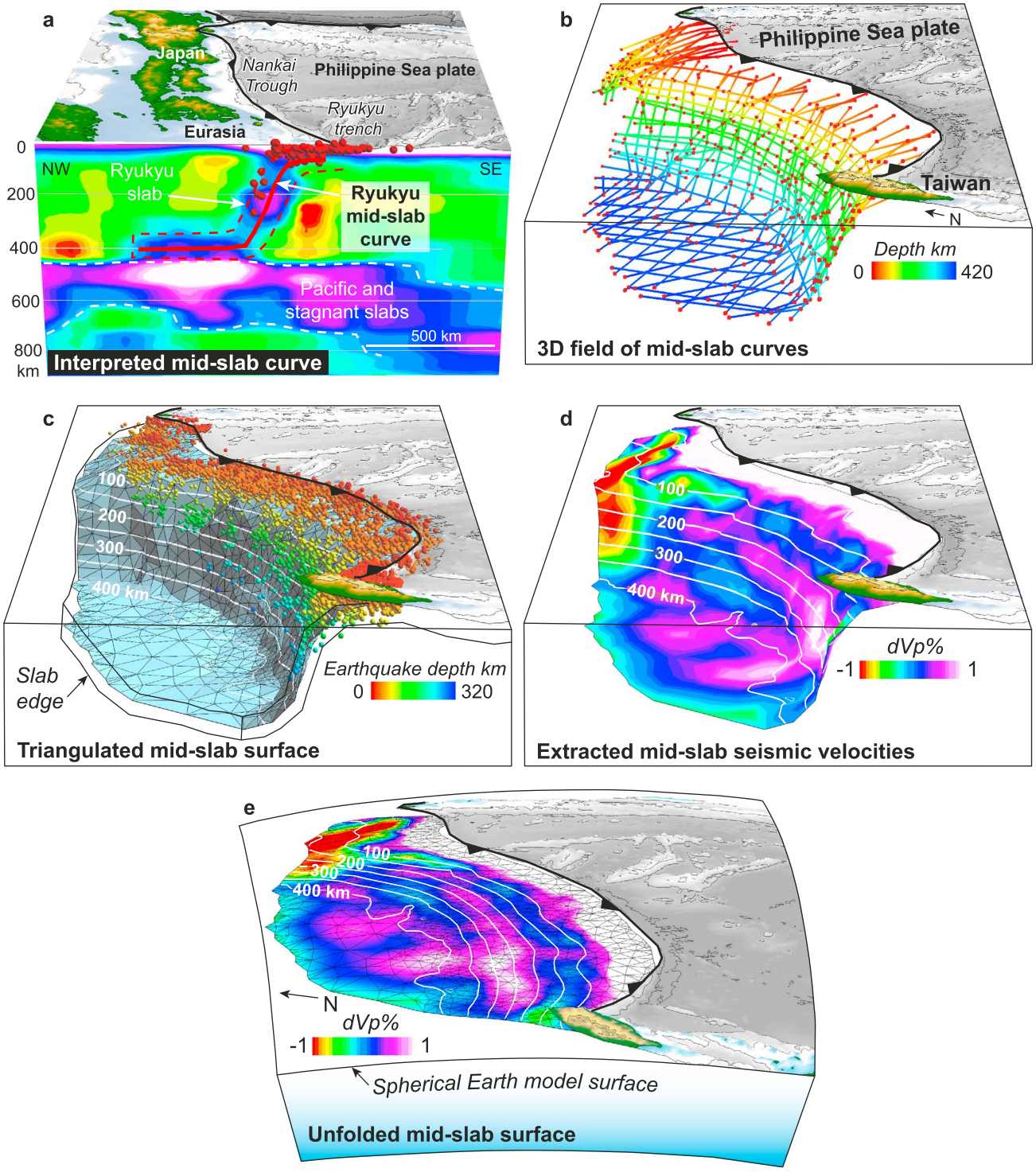

Figure 13. Flexural unfolding of the northern Philippine Sea plate Ryukyu slab. (a) Three-dimensional oblique view showing MITP08 seismic tomographic cross section across the Ryukyu trench and DEM. A Ryukyu slab "midslab curve" was interpreted along the center of the fast tomographic anomaly. (b) Three-dimensional view of midslab picks interpreted from variable cross-section orientations. (c) Triangulated midslab surface generated from the midslab picks in Figure 13b. Spheres show earthquakes projected from within a 50 km radius of the midslab surface. (d) *P* wave velocity perturbation dV_p extracted from the MITP08 tomography along the midslab surface. (e) Midslab surface unfolded to a spherical Earth model surface by flexural unfolding, minimizing changes in area and distortion. Midslab depth contours and seismic velocities are preserved in the unfolded slab.

subduction along southern or central Sundaland [e.g., *McCourt et al*., 1996]. In total, the test highlighted four areas with minor 200 to 500 km overlaps (e.g., white stars in Figure 23a) in noncritical areas that were excluded from our plate reconstruction.

3. Results

3.1. North Philippine Sea Plate: Ryukyu and Shikoku Slab Mapping

3.1.1. Tomographic Depth Sections

Figure 9 shows MITP08 tomographic sections at four depths across the northern margin of the Philippine Sea plate. We will herein use "Ryukyu slab" and "Shikoku slab" to refer to the subducted Philippine Sea plate at the Ryukyu trench and Nankai Trough, respectively (Figure 9a). At 150 km depth the Ryukyu slab and western Shikoku slabs are easily identified from their Benioff zone seismicity (Figure 9a). The slab tomographic anomaly is narrow, curvilinear, and nearly trench parallel. The slab anomaly and seismicity disappear east of the Shikoku Basin ridge (Figure 9a). At 280 km depth the Ryukyu slab anomaly is seismic, and the narrow slab anomaly parallels the trench strike similar to shallower depths (Figure 9b). At this depth the Ryukyu and Shikoku slab anomalies have a clear western limit near Taiwan and an eastern limit under Kyushu Island, Japan (Figures 9a to 9c). Similar anomalies at these depths have also been observed in regional *P* and *S* wave tomographic models [e.g., *Huang et al*., 2013; *Koulakov et al*., 2014; *Wang et al*., 2008].

The Ryukyu and west Shikoku slab anomalies broaden dramatically in the 400 km depth slice but have an east-west extent similar to shallower intervals (Figure 9c). We interpret this dramatic change in slab anomaly to show flattening of the Ryukyu and west Shikoku slabs above a swath of underlying Pacific and stagnant flat slabs (Figures 10 and 11). A key observation that underpins this interpretation is shown in a 3-D tomographic visualization in Figure 11. Here the Ryukyu slab anomalies show distinctly lower dV_p% values compared to the relatively fast velocity underlying Pacific and stagnant slab anomalies, which can be clearly identified from their Benoiff zone seismicity (Figure 11). Similar observations can be made in the tomographic cross sections particularly in Figures 10b and 10c. The Pacific slabs clearly show higher velocities than the Ryukyu slabs across a range of common depths (i.e., the upper 660 km) (Figure 11), and therefore, it is unlikely that these are tomographic depth-dependent parameterization artifacts. Instead, we attribute the observed slab velocity differences to the relative thermal contrasts of the older, colder Mesozoic-aged subducted Pacific lithosphere relative to the younger, warmer Cenozoic-aged Philippine Sea lithosphere.

Also visible in the 400 km depth section are fast anomalies between the Kyushu-Palau ridge and the Pacific Benioff zone, directly under the Nankai Trough (Figure 9c). We interpret these fast anomalies to be additional detached Shikoku slab remnants (Figures 9c and 10c). At 500 km depth the tomographic anomalies dramatically change to show a large swath of fast anomalies that have higher amplitudes compared to shallower intervals (Figure 9d). These anomalies are the well-known regional Pacific and stagnant flat-slab anomalies within the 410 to 660 km mantle transition zone documented by previous studies [e.g., *Fukao et al*., 1992; *Wei et al*., 2012]. The flat-slab anomalies can be correlated into the Pacific slab Benioff zone and generally show a higher-amplitude dV_p character relative to the overlying Philippine Sea slabs (Figure 11a).

3.1.2. Tomographic Cross Sections

In cross section the Ryukyu slab tomographic anomaly follows its steeply dipping Benioff zone seismicity but continues to greater depths, eventually flattening near 400 km depths (Figures 10–12, 13a, and 13b). Simple 2-D unfolded lengths measured from the cross section are on the order of 920 to 990 km (Figures 10a and 10b). The west Shikoku slab has a proximal steeply dipping and distal flat geometry similar to the Ryukyu slabs (Figure 10c). The west Shikoku slab has a simple 2-D unfolded length of ~720 km (Figure 10c), which is similar to estimates from regional tomographic models [*Huang et al*., 2013]. Additional detached slab fragments are potentially indicated by fast anomalies to the southeast under the Nankai trough, which could add about ~200 km slab length for a total of ~920 km (Figure 10c). At the east Nankai Trough we interpret a poorly imaged but seismic, short (~220 km length) attached east Shikoku slab (Figure 10d). Our 220 km unfolded length in Figure 10d is comparable to the seismicity-constrained SLAB 1.0 model [*Hayes et al*., 2012], from which we estimated a ~200 km unfolded length for the same location. Higher-resolution regional shear wave tomography of the Japan subduction zone also shows comparable slab lengths [*Asamori and Zhao*, 2015]. Similar to its counterpart west Shikoku slab, there are possible detached east Shikoku slab fragments that overlie the Pacific slab Benioff zone to the southeast that could add up to 700 km slab length for a total of 920 km length (Figure 10d).

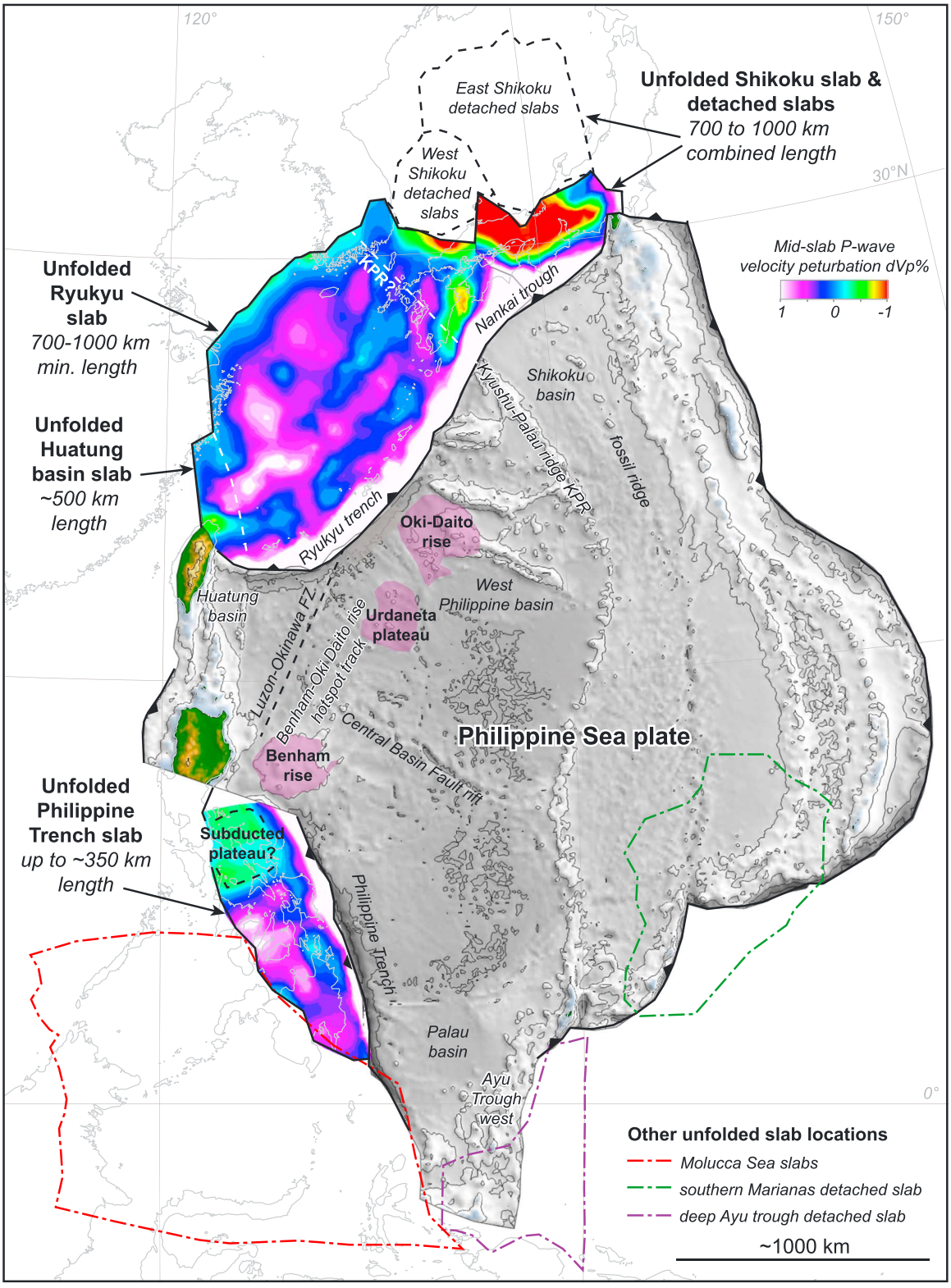

Figure 14. Philippine Sea plate DEM and unfolded slabs from this study. The unfolded slabs are colored by the *P* wave velocity perturbation dV_p extracted along the midslab surface. The unfolded Ryukyu and westernmost Shikoku slabs are on the order of ~1000 km length. The unfolded central and eastern Shikoku attached slabs are shorter (<400 km length) but approach ~1000 km lengths when combined with the unfolded East and West Shikoku detached slab fragments (dashed black lines). The slow-velocity area within the northern Philippine trench slab may indicate a subducted plateau that once existed along the proposed Benham-Oki-Daito rise hot spot track.

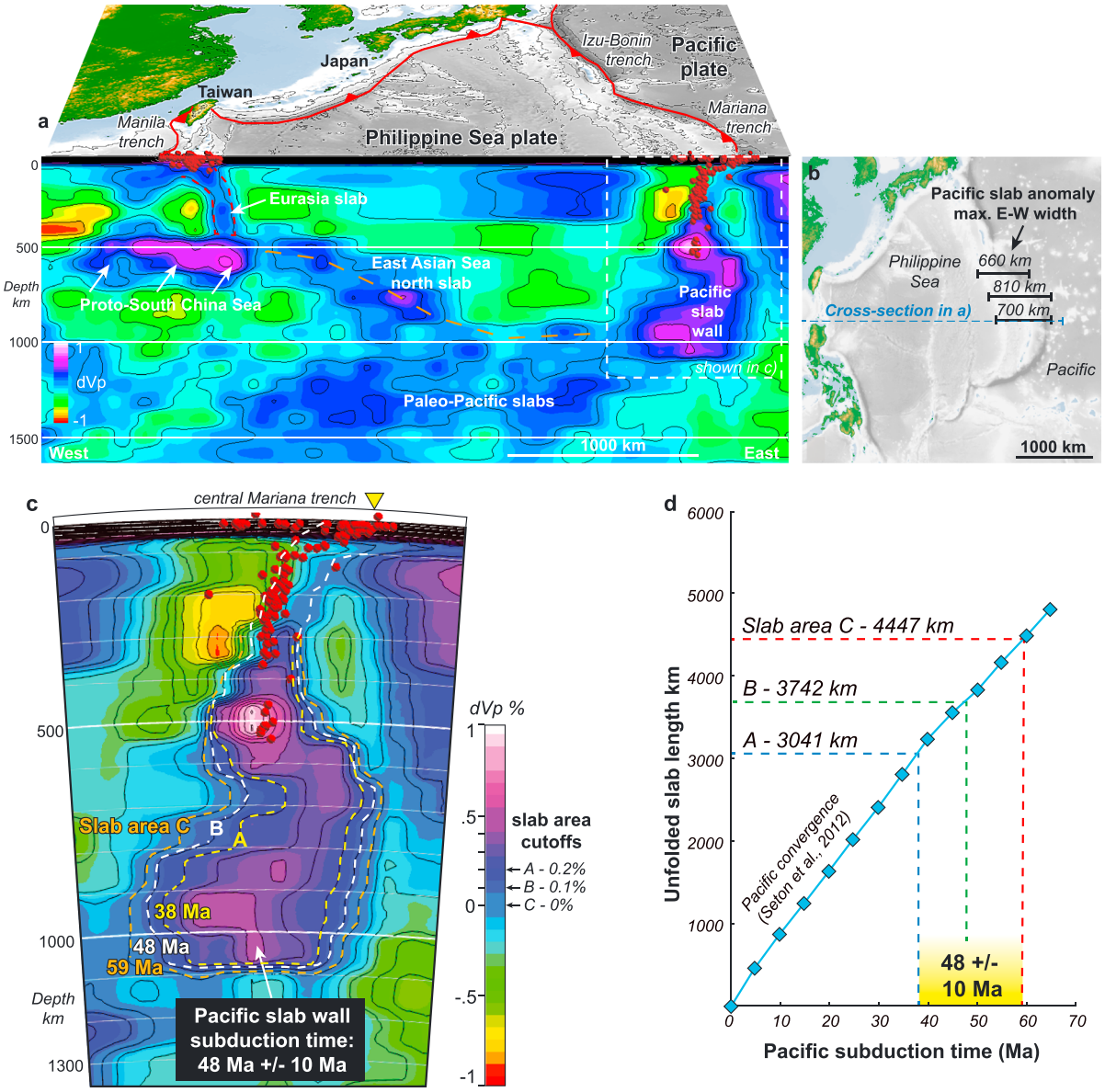

Figure 15. (a) MITP08 tomographic cross section oriented along the mean 0 to 50 Ma Pacific convergence direction showing the subvertical Pacific "slab wall" under the central Marianas. (b) Maximum E-W width of the Pacific slab wall anomaly under the northern and central Marianas calculated from a 0% dV_p cutoff along three transects. (c) Pacific slab wall from Figure 15a shown undistorted within spherical Earth model. Three possible Pacific slab areas A to C (dashed colored lines) were picked from the tomographic section that were guided by dV_p cutoffs of 0.2% to 0%, respectively. We measured unfolded slab lengths between 3041 km and 4447 km for areas A to C using cross-sectional area unfolding (for method, see Figure 8). Our unfolded slab lengths were corrected for PREM density-depth changes [*Dziewonski and Anderson*, 1981] and assumed an incoming 100 km thick Pacific slab. (d) Total Pacific slab subduction times for slab areas A to C was 48 ± 10 Ma, based on a comparison of unfolded Pacific slab lengths to the Pacific convergence rate at the central Marianas from *Seton et al.* [2012].

In summary, a simple 2-D unfolding of our interpreted northern Philippine Sea Ryukyu and Shikoku slabs, including their attached and detached segments, yields slab lengths on the order of 900 to 1000 km length.

3.1.3. Three-Dimensional Slab Maps

Based on our slab model, we produced a contour maps of the midslab depths and associated dV_p seismic velocities for the attached Ryukyu and Shikoku slabs (e.g., Figures 12 and 13). Our mapped Ryukyu slab has an approximately N-S western edge near Taiwan that supports previous interpretations by *Lallemand et al.* [2001]. A shallower dipping slab is revealed down dip of the Kyushu-Palau ridge by increased midslab depth contour spacing (Figure 12a). This may indicate the possible location of a subducted buoyant Kyushu-Palau arc (Figure 12a). Other slab maps produced from regional tomography show similar geometries [*Cao et al.*, 2014;

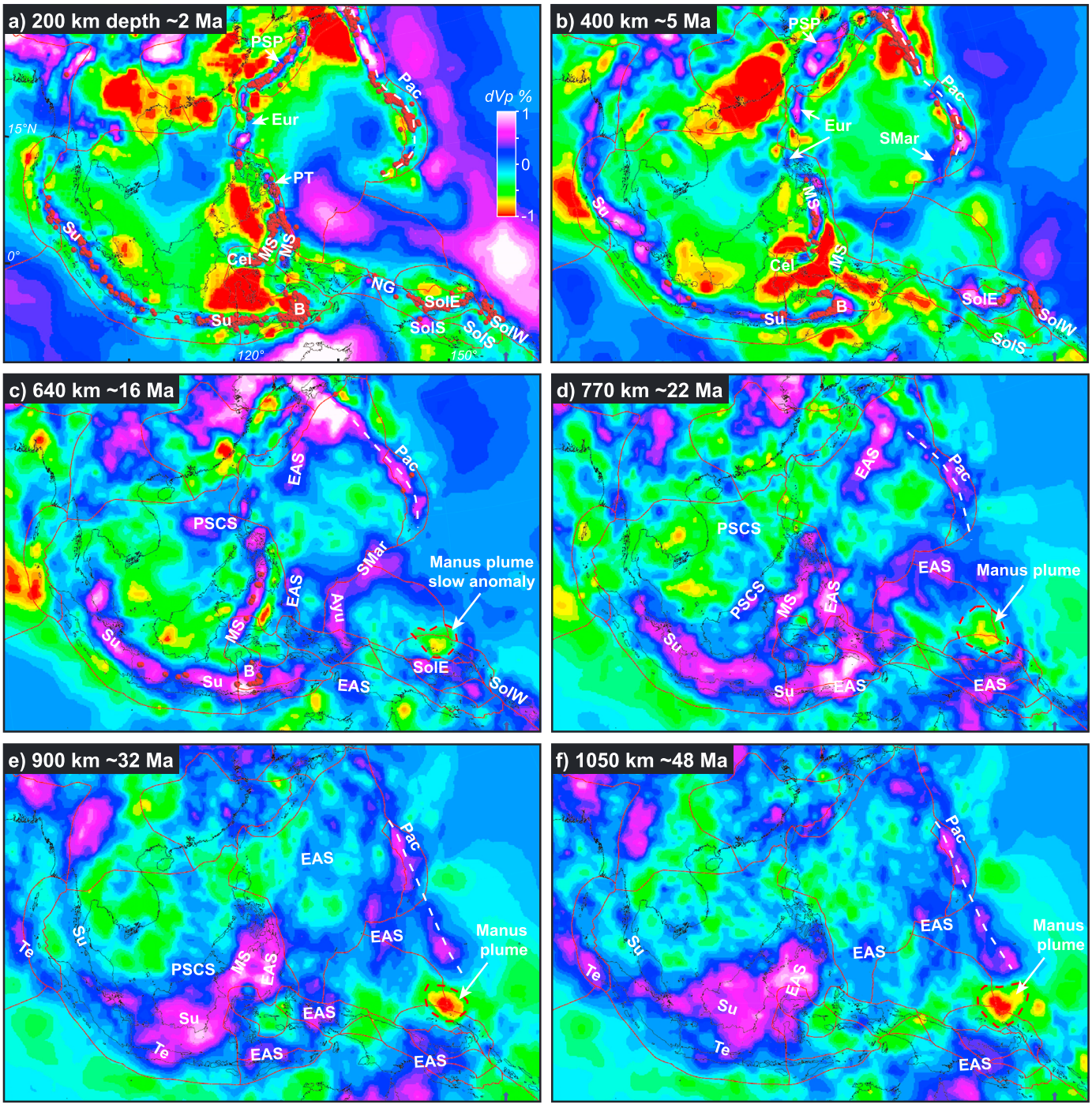

Figure 16. Mapped slabs from MITP08 tomographic depth sections and seismicity at (a) 200 km, (b) 400 km, (c) 640 km, (d) 770 km, (e) 900 km, and (f) 1050 km depths under East Asia. Subduction ages for each depth follow the Pacific slab age depth analysis in Table 3. Mapped slab anomalies are labeled as follows: Ayu, deep Ayu detached slab; B, Banda; Cel, Celebes Sea south; EAS, East Asian Sea; Te, Tethys; Eur, Eurasia; MP, Manus plume slow anomaly; MS, Molucca Sea; NG, New Guinea; Pac, Pacific slabs; PSCS, Proto-South China Sea; PSP, Philippine Sea Ryukyu and Shikoku; PT, Philippine Trench; SMar, southern Marianas detached slab; SolE, Solomon east; SolS, Solomon south; SolW, Solomon west; Su, Sunda slabs.

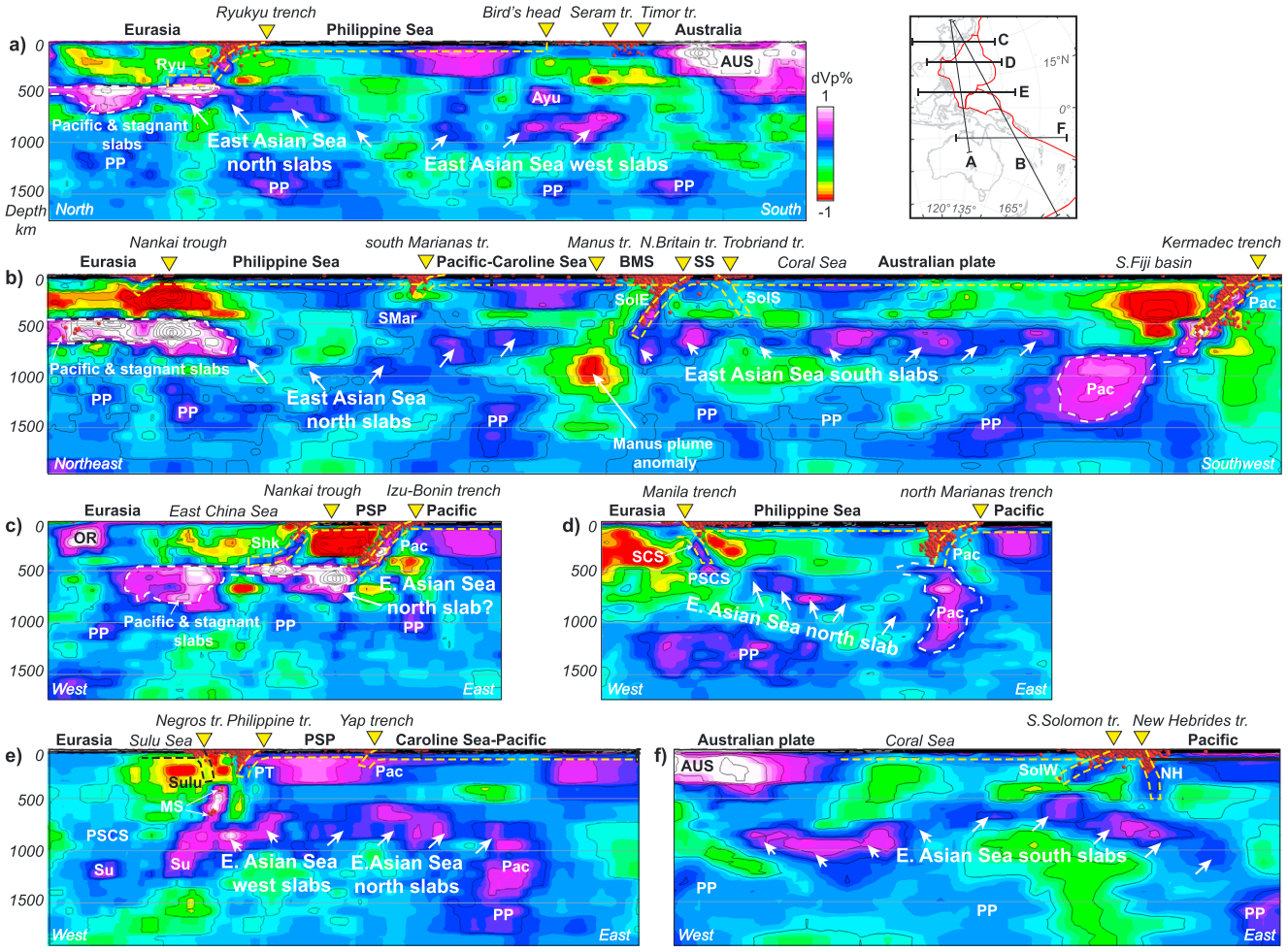

Figure 17. (a to f) Interpreted slabs and mantle structure under East Asia from MITP08 tomography vertical cross sections. The study area is dominated by subhorizontal, relatively lower amplitude detached slabs at 500 to 1100 km depths that we call the East Asian Sea slabs. Inset map shows section locations. Seismicity shown by red dots. AUS, Australian craton; Ayu, deep Ayu Trough slab; BMS, Bismarck Sea; MS, Molucca Sea slab; NH, New Hebrides slab; OR, Ordos block; Pac, Pacific slabs; PP, proto-Pacific slabs; PSCS, proto-South China Sea slabs; PSP, Philippine Sea plate; PT, Philippine Trench slab; Ryu, Philippine Sea Ryukyu slab; SCS, South China Sea and Eurasian slabs; Shk, Philippine Sea Shikoku slab; SMar, southern Marianas detached slab; SolE, Solomon east slab; SolW, Solomon west slab; SolS, Solomon south slab; SS, Solomon Sea plate; Sulu, Sulu Sea slab; Su, Sunda slabs.

Hasegawa et al., 2013]. The location of our mapped Kyushu-Palau ridge also coincides with an abrupt lateral change in slab seismicity (Figure 12c). Changes in slab length downdip of the Shikoku Basin fossil spreading ridge supports a previously proposed slab tear or slab window [*Cao et al.*, 2014; *Hasegawa et al.*, 2013].

3.2. Philippine Sea Plate Unfolded Slabs

Figure 13 shows how our mapped Ryukyu and Shikoku midslab surfaces were restored using 3-D flexural unfolding. Figure 14 shows a map of the Philippine Sea plate DEM and unfolded slabs from this study. The unfolded Ryukyu and Shikoku slabs were positioned relative to their outer western and eastern edges, respectively, to maintain their lateral positioning relative to the adjacent Eurasian and Pacific slabs (e.g., Figure 9b). Slab subduction within a spherical Earth commonly results in internal slab distortions (i.e., rips, tears, and buckling) [*Lister et al.*, 2012]. For our Ryukyu-Shikoku slabs the gaps and overlaps from unfolding were small (i.e., within the 100 km limits of maximum seismic resolution) and modeled within a poorly constrained tear or slab window area between the east and west Shikoku slabs (e.g., Figures 12a and 14). The detached west Shikoku slab was unfolded and positioned directly above its present-day location. The detached east Shikoku slab was unfolded and positioned ahead of the attached east Shikoku slab (Figures 9d, 9e, and 14).

Table 2. Unfolded Slab Lengths Calculated From A to C Pacific Slab Tomographic Areas at the Central Marianas (Shown in Figure 15a)[a]

Area	dV_p Cutoff	Slab Cross-Sectional Area (km^2)	PREM-Corrected Slab Area (km^2)	Unfolded Slab Length (km)	Pacific Subduction Time (Ma)
A	0.2%	247,509	304,077	3,041	38
B	0.1%	301,478	374,180	3,742	48
C	0%	357,425	444,704	4,447	59

[a]Slab lengths were calculated from corrected slab area by assuming a 100 km thick incoming Pacific slab. The restored slab lengths were compared to predicted Pacific convergence from the Pacific plate motion model of *Seton et al*. [2012] as shown in Figure 16c. We consider the intermediate slab "Area B" to be the most probable estimate.

The unfolded Ryukyu slabs are ~1000 km in NS length (Figure 14). The attached westernmost Shikoku slabs including the Kyushu-Palau ridge show a comparable unfolded length to the Ryukyu slabs (Figure 14). This seems reasonable given that the Shikoku basin was formed by NE-SW rifting of the Kyushu-Palau ridge [*Okino et al*., 1994]. The attached central and east Shikoku slabs are much shorter (<300 km N-S) when unfolded (Figure 14). However, when the detached Shikoku slabs are added, this segment has an unfolded length that is comparable to the ~1000 km length of the other Ryukyu and westernmost Shikoku slabs (Figure 14). We noted that the extracted Ryukyu and Shikoku slab dV_p seismic velocities showed generally faster velocities west of a major lithospheric age boundary at the Kyushu-Palau ridge (Figure 14). The faster Ryukyu slab dV_p seismic velocities appear to be consistent with an expected thermal signature of older and colder subducted Oligocene to Cretaceous lithosphere relative to the warmer, younger Oligocene to Miocene-aged Shikoku slab lithosphere.

The narrow slab downdip of the Huatung Basin (HB) near Taiwan is a conspicuously shorter ~425 to 500 km NS length relative to the Ryukyu slab (Figure 14). This seems to support the notion that the enigmatic Huatung Basin is not autochthonous but was added later to the Philippine Sea plate [*Deschamps et al*., 2000]. Alternatively, a fragment of the Huatung Basin may have been lost in the development of the Manila trench subduction zone.

Our unfolded Philippine trench slab at the SW margin of the Philippine Sea is on the order of 230 to 400 km length (Figure 14). Our mapping of the Philippine trench slab is further described below in section 3.4, but in general, the upper 200 km of our slab model was supported by Benioff seismicity and very similar to the published SLAB1.0 model [*Hayes et al*., 2012]. When unfolded, the extracted dV_p values within the northernmost Philippine trench midslab showed a distinct lower dV_p area (Figure 14) that could indicate a subducted oceanic plateau from Urdaneta Plateau (UP)-Oki-Daito Rise (OKR)-Benham Rise oceanic plateau chain as predicted by *Ishizuka et al*. [2013]. Our tests showed that unfolding of the SLAB1.0 Philippine trench slab model [*Hayes et al*., 2012] produced a similar intraslab dV_p pattern. The potentially subducted oceanic plateau revealed here is tectonically significant because it suggests the minimum age of the Philippine Trench slab lithosphere

Table 3. Cumulative Slab Areas and Pacific Age Depth Relationships for the Central Marianas Pacific Slab Wall in Figure 15a[a]

	Cumulative Unfolded Slab Length (km)			Pacific Subduction Time (Ma)		
Depth (km)	Area A	Area B	Area C	Area A	**Area B**	Area C
220	285	285	285	3	**3**	3
400	493	505	568	5.5	**5.6**	6.3
500	706	738	838	8.2	**8.4**	9.7
600	1020	1096	1263	11.8	**12.8**	15
670	1222	1346	1576	14.5	**16.1**	19.4
770	1513	1803	2129	18.3	**22**	26.3
800	1637	1942	2304	19.8	**23.8**	28.9
900	2148	2595	3056	26.6	**32.5**	38.5
1000	2685	3255	3817	33	**40.8**	49.7
1100	3041	3742	4447	38	**48**	59
Mean lower mantle slab sinking rate (cm/yr)				1.7	**1.3**	1.1

[a]The calculated Pacific subduction times imply lower mantle sinking rates between 1.1 and 1.7 cm/yr. The intermediate "Area B" estimates shown in bold were used to infer slab subduction age depths in Figures 16, 18, and 19.

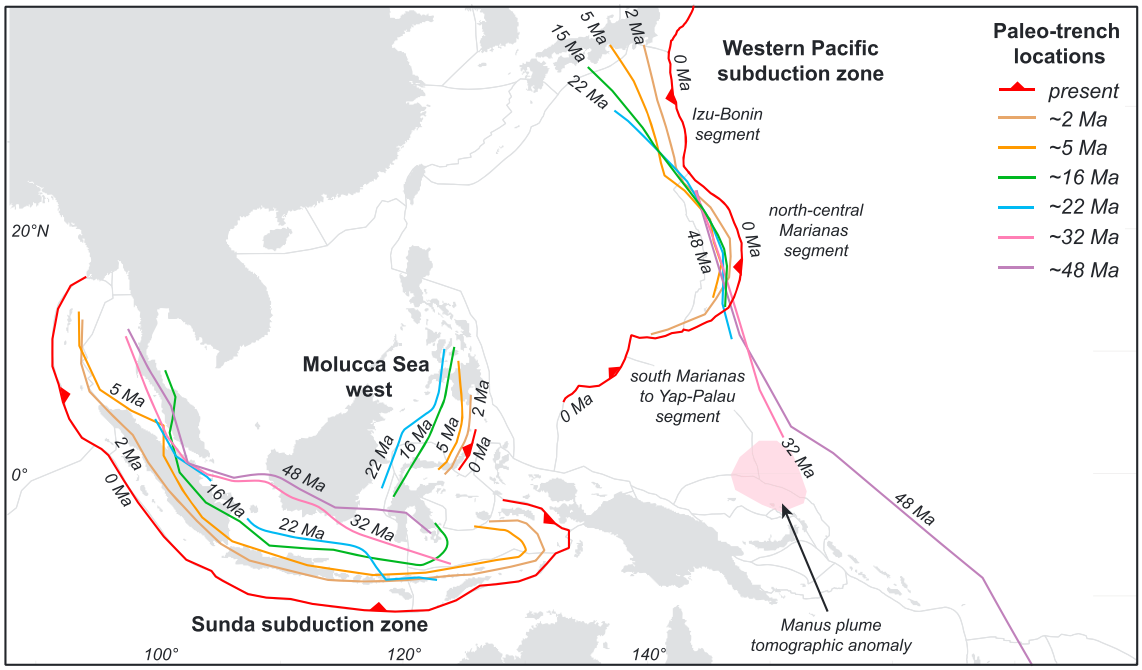

Figure 18. Western Pacific, Molucca Sea, and Sunda (i.e., Indian Ocean) mean paleotrench positions interpreted from the MITP08 tomographic anomalies shown in Figure 16. The results suggest a near-stationary north-central Marianas Pacific subduction zone since 47 Ma. In contrast, the Izu-Bonin Pacific subduction zone has retreated eastward maximum 500 km since 21 Ma, and the southern Marianas-Yap-Palau segment has advanced westward maximum 1500 km since 47 Ma. Vertical slab sinking was assumed. Paleotrench ages follow the mantle depths from Figure 16 and Table 3. Our slab-constrained plate reconstructions shown later also predicted similar Pacific paleo-trench patterns even though the paleo-trench analysis described here was not used to constrain our plate models (see Figure S8).

should be at least ~45 Ma following the plateau age progression model of *Ishizuka et al*. [2013]. We also note that the unfolded Philippine trench and Molucca Sea slabs display an edge-to-edge fit (Figure 14). This implies the Philippine Sea and Molucca Sea may have previously shared a common tectonic boundary. Further details on our mapped Philippine trench slab and other slabs under the southern Philippine Sea are shown in section 3.4.

In summary, we interpret the following about the Philippine Sea plate Ryukyu and Shikoku slabs based on our slab mapping and unfolding:

1. The unfolded Philippine Sea Ryukyu and Shikoku slabs are ~1000 km in NS length (Figure 14), which is short relative to the ~2000 km northward motion of the Philippine Sea plate since ~40 Ma based on paleo-latitudes (Figure 3). Therefore, we do not find tomographic evidence to support Philippine Sea plate anchored slab-style reconstructions (Figure 4b) that suggest the Philippine Sea plate filled the entire 2000 km gap south of the Ryukyu-SW Japan Eurasian margin at 40 Ma.
2. Instead, the short unfolded Ryukyu and Shikoku slabs require a late Cenozoic collision between the Philippine Sea plate and Eurasia along the Ryukyu-SW Japan continental margin, which we discuss in more detail in section 5.4.

3.3. Western Pacific Slab Constraints

3.3.1. Western Pacific Slabs Under the Central Marianas

MITP08 seismic tomography shows a subvertical slab wall anomaly under the northern and central Marianas Pacific Benioff zone down to at least 1100 km depths (Figures 15a, 16, and 17d). The imaged slab wall is consistent with previously published *P* and *S* wave tomographic cross sections [e.g., *Jaxybulatov et al*., 2013; *Miller et al*., 2006; *van der Hilst and Seno*, 1993]. Synthetic slab, checkerboard, and odd-even tomographic resolution tests indicate that the area has sufficient seismic raypath densities for slab imaging [*Jaxybulatov et al*., 2013]. The slab wall displays a clear NNW-SSE trend in MITP08 depth sections that continues southward near the equator at 900 and 1050 km depths (Figure 16). The maximum E-W width of the slab wall was ~600 to 800 km beneath the central and northern Marianas using a conservative 0% dV_p cutoff (Figure 15b). A slightly

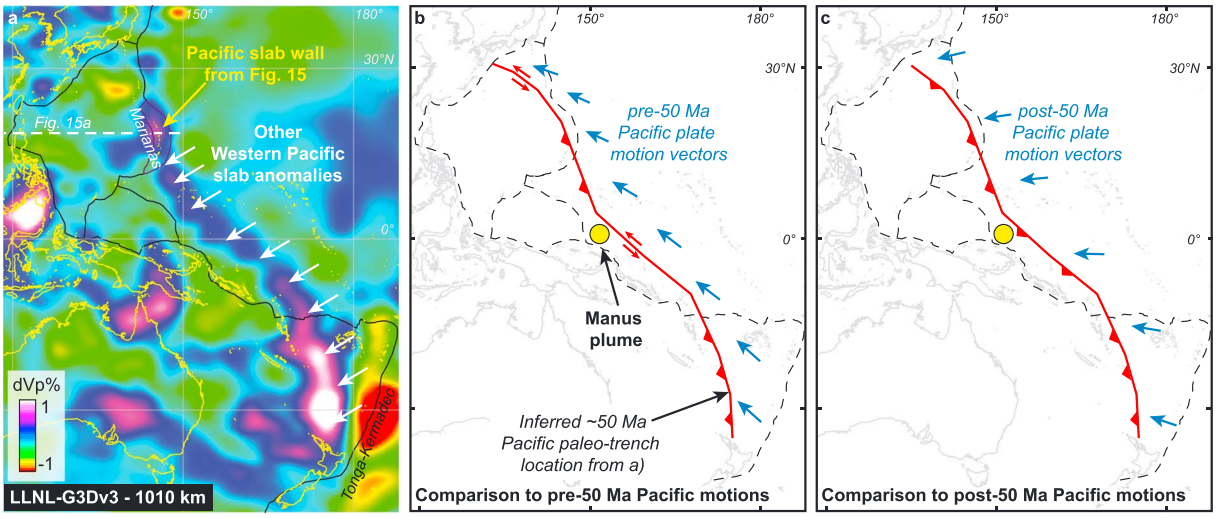

Figure 19. (a) Horizontal global tomography section from LLNL-G3Dv3 [*Simmons et al.*, 2012] at 1010 km depth showing continuation of the central Marianas Pacific slab wall anomalies in Figure 15 southward to west of present-day Tonga-Kermadec. Similar slab anomalies occur in other global tomography models (see Figure S3). We infer that the slab anomalies in Figure 19a reveal the regional western Pacific paleotrench location at ~50 Ma based on slab age depths (see Table 3). When the paleotrench orientation is compared to (b) pre-50 Ma and (c) post-50 Ma Pacific plate motion directions from *Seton et al.* [2012], we suggest that before ~50 Ma, this western Pacific boundary may have been characterized by highly oblique subduction or transforms. After 50 Ma, Pacific plate motions changed and fast subduction began. Our preferred reconstruction Model 1 places the Philippine Sea plate origin at an equatorial latitude near the inferred transform in Figure 19b shown by the yellow dot, which is the present position of the Manus plume interpreted in Figure 16.

positive dV_p cutoff (i.e., 0.1% dV_p cutoff used in our analysis in Figure 15c) would produce an even narrower E-W slab wall width estimate. We interpret the central Marianas slab anomalies to be subducted Pacific slabs based on (1) their continuation below the Pacific Benioff zone and (2) their regional continuity in the MITP08 tomographic depth sections. These conclusions are similar to those reached by previous tomographic studies [*Jaxybulatov et al.*, 2013; *Miller et al.*, 2006; *van der Hilst et al.*, 1993; *Zahirovic et al.*, 2014], but we provide additional evidence from slab unfolding below and a regional reconstruction with other unfolded slabs in section 4.

3.3.2. Tectonic Implications of the Northern and Central Marianas Slab Wall

The northern and central Marianas subvertical slab geometries are reminiscent of subducted slab walls produced by slab sinking and buckling below a stationary subduction zone in numerical models [e.g., *Čížková and Bina*, 2013] (Figures 8b to 8d). Other tomographically imaged subducted slab walls have also been inferred to have formed at stationary subduction zones [e.g., *Sigloch and Mihalynuk*, 2013]. If the northern and central Marianas slab walls had indeed formed below a near-stationary Pacific subduction zone, this would support the anchored slab Philippine Sea plate models but be incompatible with retreating trench models, which predict >2000 km of Pacific trench retreat since 50 Ma (Figure 4).

In the next section we will first apply our cross-sectional area slab unfolding method (see section 2.2) to unfold the central Marianas slab wall and estimate a range of possible subducted slab lengths. By comparing the unfolded slab lengths to known Pacific convergence rates, we show that the central Marianas slab wall began to form in the latest Paleocene to Eocene 48 ± 10 Ma. These ages would be consistent with the Izu-Bonin Marianas fore-arc basement and the recently drilled Amami Sankaku basin at IODP Site U1438 [e.g., *Arculus et al.*, 2015; *Ishizuka et al.*, 2011]. Additional evidence is presented below from other mapped regional slabs and a plate reconstruction that a near-stationary subduction zone has existed at the northern and central Marianas since ~48 Ma (section 3.4 and 4).

3.3.3. Slab Tomographic Area Unfolding of the Pacific Slabs Under the Central Marianas

Figure 15c shows the central Marianas slab wall within an undistorted spherical Earth model. The exact resolution of the MITP08 tomographic model under the central Marianas is difficult to fully assess and is at best ~100 km [*Li et al.*, 2008], but as mentioned earlier, synthetic slab tests indicate that the area has adequate raypath coverage for slab imaging [*Jaxybulatov et al.*, 2013]. We therefore chose to pick a series of possible cross-sectional slab areas based on dV_p contour intervals that could be reasonably "closed" around the fast slab anomaly (e.g., Figure 15c). As shown in Figure 15c the possible dV_p cutoffs ranged between 0.2% and

0% dV_p (slab areas A–C). We inferred that these isovalues were reasonable because they were located within a steep dV_p gradient that may indicate the slab edge. We also considered higher dV_p cutoffs that resulted in very small picked slab areas (i.e., the 0.3% dV_p contour), but these areas seemed unlikely given the implied unreasonably fast lower mantle sinking rates relative to published studies [e.g., *Hafkenscheid et al*., 2006; *Steinberger et al*., 2012; *van der Meer et al*., 2012].

Cross-sectional slab area unfolding based on the total areas of A to C produced unfolded slab lengths between 3040 and 4450 km (Table 2), with a most probable length of 3700 km ± 700 km using the intermediate area B. We also calculated the cumulative unfolded slab lengths with depth for areas A to C (Table 3), which enabled us to estimate a Pacific slab wall subduction age versus depth relationship, implied lower mantle slab sinking rates and regional slab ages. As described in section 2.2, all unfolded slab lengths were corrected for density-depth changes according to the PREM Earth model [*Dziewonski and Anderson*, 1981]. We assumed a 100 km thick Pacific lithosphere during initial subduction according to modeled Mesozoic subducted Pacific lithospheric ages [*Seton et al*., 2012] and known age-lithospheric thickness relationships [e.g., *Parker and Oldenburg*, 1973].

Comparison of the unfolded slab lengths A to C against published Pacific convergence rates suggests that the central Marianas slab wall accounts for Pacific subduction from 48 ± 10 Ma to the present day (Figure 15d and Table 2). The 48 ± 10 Ma slab age coincides with a major 50 to 53 Ma Pacific plate motion change and a regional plate reorganization [*Whittaker et al*., 2007], which implies that fast Pacific subduction at the central Marianas began after the major 50 Ma Eocene Pacific plate motion change. Similar slab area unfolding performed at other locations along the western Pacific (Kuril, Japan, Izu-Bonin, and Tonga-Kermadec subduction zones) also indicated similar Eocene to Paleocene slab ages and are displayed later in section 4 plate reconstruction.

We estimated lower mantle slab sinking rates of 1.1 to 1.7 cm/yr for the slab wall areas A to C based on the cumulative unfolded slab lengths with depth (Table 3 and Figure S2), assuming vertical slab sinking. These lower mantle sinking rates are comparable to 1.2 ± 0.3 cm/yr to 2 ± 0.8 cm/yr rates from previous global tectonics and numerical modeling studies [*Hafkenscheid et al*., 2006; *Steinberger et al*., 2012; *van der Meer et al*., 2010]. We note that the very small 0.3% dV_p slab area we discarded earlier produced a very fast 3.5 cm/yr lower mantle sinking rate that fell outside of these published rates. Our implied slab sinking rates are further discussed in section 5.8.

3.3.4. Western Pacific Paleotrench Positions

Figure 18 shows a map of our interpreted western Pacific and other regional paleotrench locations based on their midslab anomalies from the MITP08 horizontal tomographic sections down to 1050 km depths (Figures 16 and 17). Paleotrench ages were estimated from the central Marianas slab age depths derived from cumulative slab area unfolding (Table 3). Our paleotrench analyses assume the western Pacific slabs sank more or less vertically after subduction and are mean location estimates, given later slab deformation (e.g., buckling) and variable tomographic resolutions.

Our paleotrench analysis suggests that the north-central Marianas subduction zone has been near-stationary within a narrow 200 km zone from the Eocene ~48 Ma to the end-Pliocene ~2 Ma (Figure 18). After 2 Ma, the Marianas subduction zone retreated 200 km eastward to its present-day location (Figure 18). Even if the possibility of maximum ~600 km of initial slab rollback prior to lower mantle slab anchoring is considered [e.g., *van der Hilst and Seno*, 1993], our conclusion that the Marianas subduction zone has been near stationary since its Eocene inception may be a surprising conclusion, considering that the Shikoku-Parece Vela basins are inferred to have opened from slab rollback. We will later reconcile this apparent contradiction from our plate model by showing that the slab rollback that formed the Shikoku-Parece Vela basins was more complex than previously envisioned and was produced when the Philippine Sea was driven westward and rotated clockwise away from a stationary Marianas Pacific trench by the impinging Caroline Sea back-arc basin (see Model 1 in Movie S1).

In contrast to the Marianas subduction zone, the Izu-Bonin trench has retreated eastward a maximum of ~500 km since the Miocene (Figure 18). The Yap-Palau and southern Marianas trenches have advanced up to 1500 km westward after the earliest Oligocene ~32 Ma and were located much farther to the east in the Eocene (Figure 18). Similar evolutionary patterns for all three segments (i.e., the Izu-Bonin, Marianas, and southern Marianas-Yap-Palau) were interpreted by *Miller et al*. [2006] for the younger Miocene to present-day Pacific paleotrenches based on tomographic analysis of the upper mantle and transition zone only. Our slab-

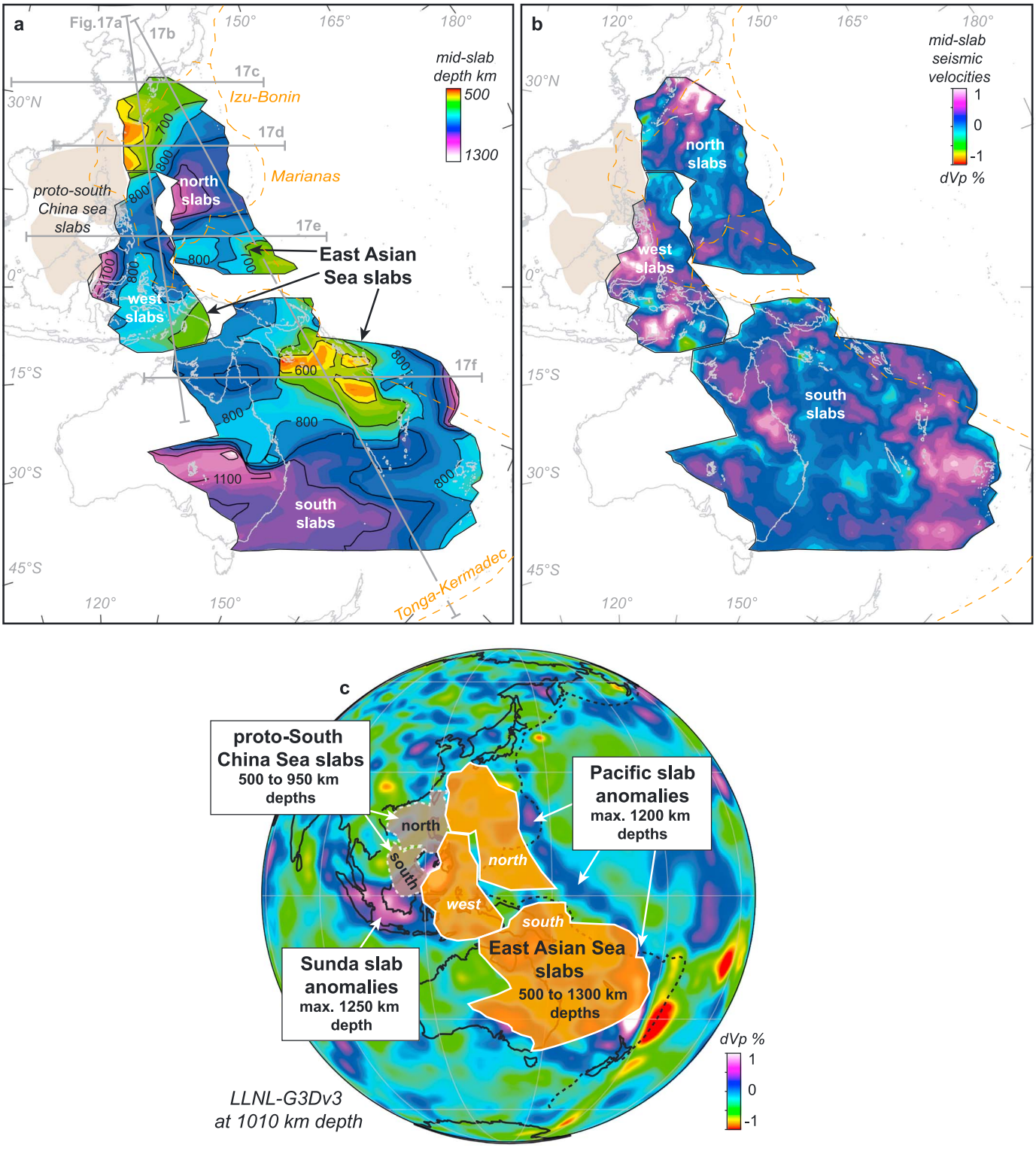

Figure 20. Maps of the East Asian Sea detached slabs in the mantle colored by their (a) midslab depth and (b) midslab seismic velocities. The proto-South China Sea flat slabs are shown in brown. Cross-section locations from Figure 17 are shown in Figure 20a. Present-day coastlines in grey and selected plate boundaries are in orange. (c) The projected position of the East Asian Sea flat slabs relative to slab tomographic anomalies at comparable depths. The East Asian Sea slabs generally fit east of the proto-South China Sea slabs and west of the deep Pacific slabs. The Sunda slab anomalies lie south of the proto-South China Sea slabs. The fit between the mapped slabs suggests that the East Asian Sea ocean basins once existed between the western Pacific and the proto-South China Sea (i.e., Eurasia). A comparison of regional slab anomalies from alternative global tomography models is shown in Figure S3.

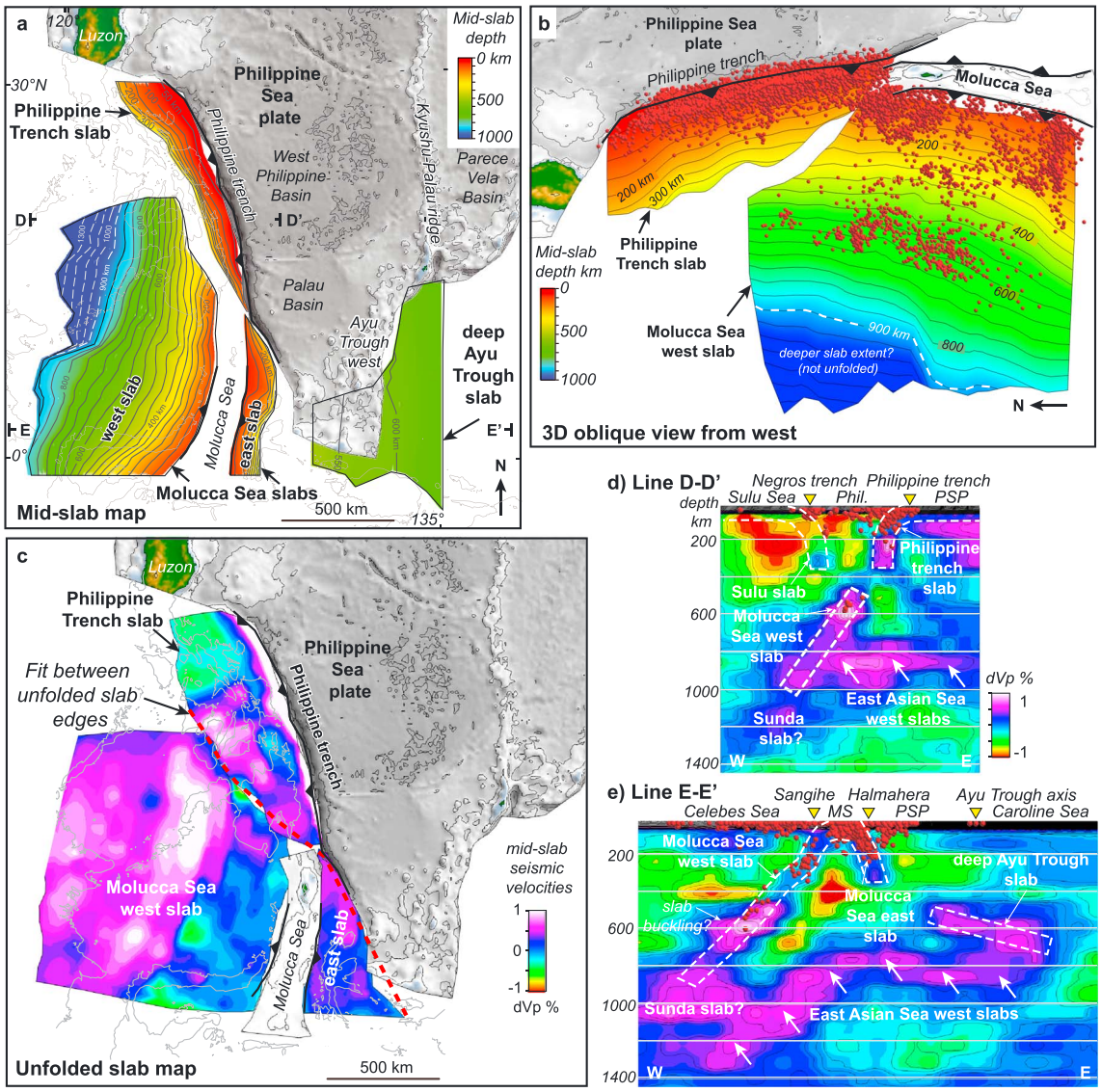

Figure 21. Slab constraints for the SW Philippine Sea and surrounding areas. (a) Philippine Trench slab, Molucca Sea slabs, and detached "deep Ayu Trough" midslab maps. (b) Three-dimensional oblique view from west showing projected seismicity within 50 km of the Philippine Trench and Molucca Sea west midslab surfaces. (c) Unfolded Philippine Trench and Molucca Sea slabs colored by their dV_p midslab seismic velocities. (d and e) MITP08 vertical tomographic cross sections and Benioff zone seismicity (red spheres) showing the interpreted fast-slab anomalies. Section locations are shown in Figure 21a. Note that the unfolded Molucca Sea slab in Figure 21c was the minimum length model. A longer unfolded Molucca Sea slab is possible based on possible deeper (>900 km) anomalies in Figure 21b and the slab buckling in Figure 21e. PSP, Philippine Sea plate; Phil, Philippines; MS, Molucca Sea.

constrained plate reconstructions shown later also predicted similar Pacific paleotrench patterns to Figure 18 (see Figure S8) even though we did not use the paleotrench analysis described here as a modeling constraint.

The base of the central Marianas slab wall anomalies that were dated at ~48 Ma in the previous section can be followed southward to a region west of Tonga-Kermadec and north of New Zealand within a number of *P* and *S* wave global tomographic models (Figures 19a and S3). We interpret the deep slab anomalies to be subducted western Pacific slabs. By assuming a central Marianas-like slab sinking rate (e.g., Table 3), the slab anomalies imply a once-continuous regional western Pacific subduction zone was located between the north-central Marianas and Tonga-Kermadec-New Zealand around ~48 Ma. The deep slab anomalies are oriented at high angles to post-50 Ma Pacific motions but have similar orientations to pre-50 Ma Pacific plate motions (Figures 19b and 19c). This is suggestive that the proto-Marianas to proto-Tonga Kermadec subduction zone was originally a pre-50 Ma Pacific transform or oblique subduction plate boundary.

Fastsubduction initiated across the subduction zone after the ~50 Ma major Pacific plate motion change and the deep slab anomalies were primarily subducted after 50 Ma, which would be consistent with the ~48 Ma central Marianas slab age date (e.g., Figure 15).

In summary, we interpret the following about the western Pacific subduction zone based on the slab constraints in this section:

1. The central Marianas Pacific subduction zone was established in the Eocene, with a probable age around 48 Ma ± 10 Ma. Assuming vertical slab sinking, the north-central Marianas Pacific subduction zone mean location was near stationary within ± 100 km until the latest Pliocene, when it retreated 200 km eastward to its present-day location (Figures 15 and 18).
2. Our interpreted near-stationary central Marianas subduction zone apparently supports anchored slab Philippine Sea reconstruction models (Figure 4b). Even if up to ~600 km of initial slab rollback prior to lower mantle slab anchoring is considered, our slab tomographic evidence does not support Philippine Sea retreating trench models that predict >2000 km of northeastward Izu-Bonin-Marianas Pacific trench retreat since the Eocene (Figure 18). In contrast, we find evidence for maximum 500 km eastward trench retreat only in the northernmost Izu-Bonin region during the latest Cenozoic (~22 to 2 Ma, Figure 18).
3. The Pacific slab anomalies south of the central Marianas (i.e., from the southern Marianas and along the Yap-Palau segment) indicate significant (up to 1500 km) westward trench advance after the earliest Oligocene ~32 Ma (Figure 18).
4. Fast Pacific subduction initiated around 50 Ma along the western Pacific subduction zones from the Izu-Bonin Marianas southward to Tonga-Kermadec-New Zealand. Prior to 50 Ma the western Pacific plate boundary was characterized by highly oblique subduction and/or transform motions (Figures 19b and 19c).

3.4. Other Mapped and Unfolded Slab Constraints

In this section we briefly describe other key mapped and unfolded slabs that will be used in our plate reconstruction in section 4. Our aim here is to assess first-order unfolded slab geometries for a plate reconstruction, and we limit discussion to implications for a Philippine Sea plate reconstruction.

3.4.1. East Asian Sea Slabs

Vertical tomographic cross sections reveal a swath of regionally extensive (8000 × 2500 km), subhorizontal, slab-like anomalies between SW Japan and New Zealand at 600 to 1200 km depths that we collectively call the *East Asian Sea* (Figures 17 and 20). The East Asian Sea flat-slab anomalies underlie the Philippine Sea, the Caroline Sea, New Guinea, and northern and eastern Australian plate and are not connected to any known present-day subduction zone (Figures 17 and 20). We interpret the East Asian Sea slabs to be a set of vanished oceans that once existed at East Asia, and our slab-constrained plate reconstruction in section 4 shows that the East Asian Sea at 52 Ma occupied a position between the proto-South China Sea, Eurasian margin, the western Pacific, northern Australia, and Indian Ocean. In particular, we note a good fit between the eastern limit of our East Asian Sea flat slabs and the deep Pacific slab anomalies (Figure 20c) that were estimated to be Eocene ~48 Ma in age (e.g., Figures 15 and 19).

Parts of the western and southern East Asian Sea slabs were also previously identified from other global tomography and interpreted to be vanished oceans [*Hall and Spakman*, 2002; *Rangin et al*., 1999; *Schellart and Spakman*, 2015; *Widiyantoro and van der Hilst*, 1997; *Zahirovic et al*., 2014]. *Hall and Spakman* [2015] identified part of the western East Asian Sea slabs from UU-P07 global tomography (i.e., their "P?" slabs). Although they acknowledged that their plate reconstruction did not adequately explain the existence of these slabs, they inferred that the slabs must somehow be linked to early Philippine Sea plate histories [*Hall and Spakman*, 2015]. We mapped the East Asian Sea slabs in three parts (i.e., the north, west, and south slabs) based on their midslab depths, lateral continuity, and seismic velocities (Figures 20a and 20b). An important contribution from our mapping is the newly identified northern East Asian Sea slabs, which lie at ~600 to 1000 km depths below the present-day Philippine Sea and are likely the proto-Philippine Sea (Figure 20). Tomographic resolution tests typically show these areas under the Philippine Sea plate to be less-well resolved, particularly at upper mantle depths, but the north East Asian slab anomalies also appear at similar depths in recent multiparameter adjoint tomography [*Chen et al*., 2015].

In the MITP08 global tomography the northern East Asian Sea slabs are in some places heterogenous and relatively faint (i.e., low dV_p perturbations) but generally show a gentle SE dip away from the present-day

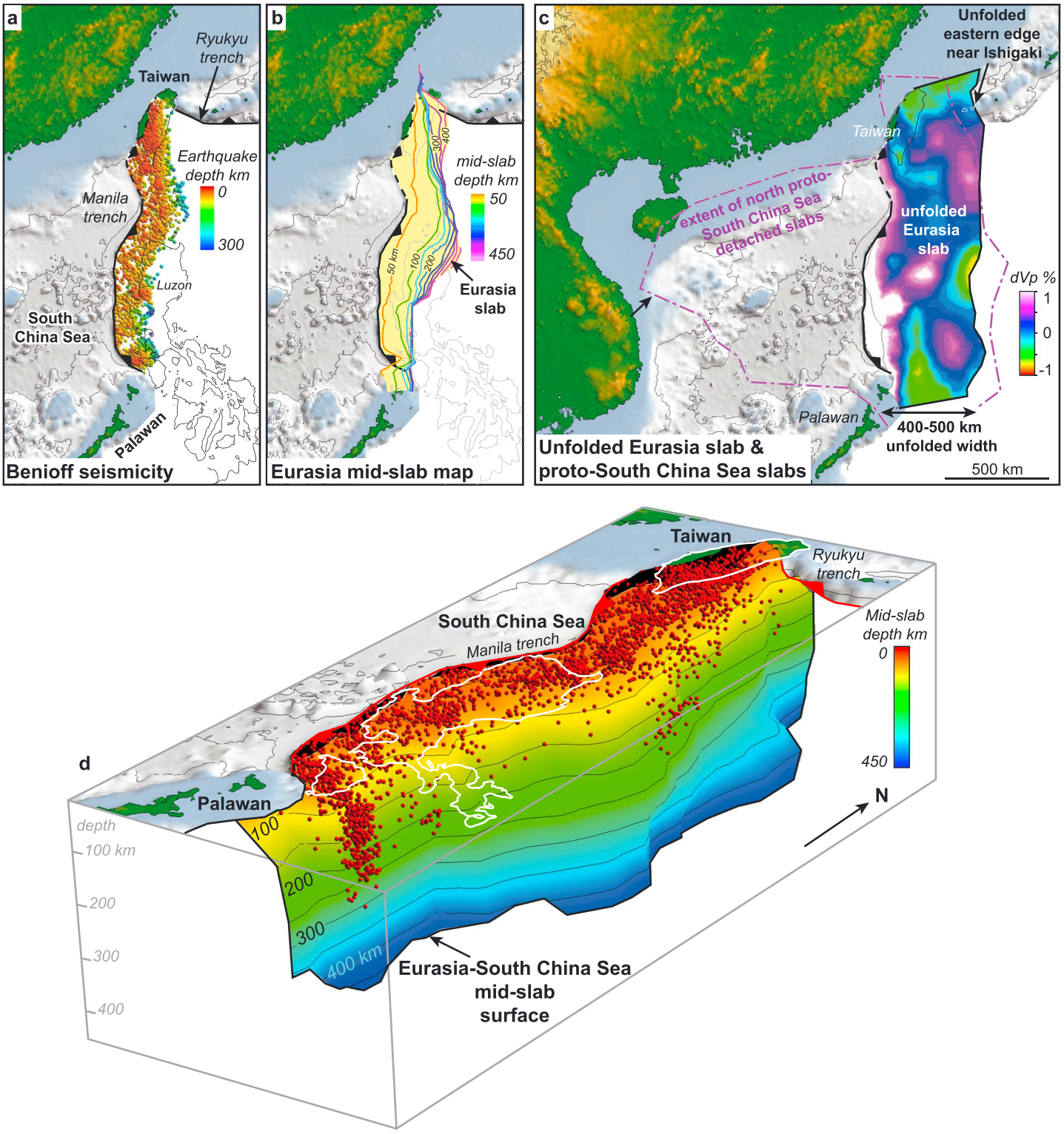

Figure 22. Eurasian slab constraints shown by (a) map of Benioff zone seismicity within 50 km of the midslab surface, (b) Eurasia midslab depth map. (c) Unfolded Eurasian slab colored by its intraslab seismic velocity dV_P. The unfolded Eurasian slab has a 400 to 500 km E-W width and has an eastern edge that terminates near Ishigaki at the Ryukyu Islands. Similarly, the unfolded northern proto-South China Sea detached slabs shown by the purple dashed line also have a similar eastern limit. This suggests a linked origin, namely, that the South China Sea opened as a back-arc basin through subduction of the proto-South China Sea. (d) Three-dimensional visualization of the subvertical Eurasian midslab surface between Taiwan and Palawan. Coastlines in white.

Eurasian margin near Taiwan and Japan (Figures 17a, 17b, and 20a). The SE dip of the northern East Asian Sea slabs generally conceptually fits with a general southeastward subduction beneath a northwest moving Philippine Sea plate. The northern limit of the northern East Asian Sea slabs is uncertain, and the slabs may partially underlie the regional Pacific and stagnant flat slabs under Japan (e.g., Figure 17a). The eastern limit of the northern East Asian Sea slabs terminates just west of the present-day north-central Marianas subduction zones (Figures 15a and 17d), which supports the earlier interpretation of a long-lived (~50 Ma), near-stationary Pacific subduction zone at the north-central Marianas in section 3.3.

3.4.2. Philippine Trench, Molucca Sea, and Ayu Trough Slabs

The size of the Philippine Trench slab (Figure 21) is important for reconstructing the tectonically complex southwest margin of the Philippine Sea plate and surrounding areas [e.g., *Lallemand et al*., 1998; *Pubellier et al*., 1999]. We mapped a ~350 km long Philippine Trench slab based on seismicity and tomography (Figures 14 and 21d). The upper 200 km of our mapped Philippine trench slab was generally consistent with the seismicity-constrained SLAB1.0 model [*Hayes et al*., 2012]. *Deschamps and Lallemand* [2002] also estimated a comparable 200 to 300 km length Philippine Trench slab. On the other hand, other studies suggest that the Philippine Trench slab cannot be traced clearly in tomography and instead attributed a shorter slab length of slightly over ~100 km [*Hall and Spakman*, 2015]. In any case, our Philippine trench slab length is relatively short (<400 km) and within the range of published plate reconstruction predictions shown in Figure 4.

The east and west Molucca Sea slabs are more substantial in size, based on their Benoiff zone depths, and more complex. Furthermore, they are important because of their potential relationships both to the adjacent Sunda slab of the Indian Ocean and to the Philippine Sea plate, to which it has been linked in some reconstructions [e.g., *Hall*, 1987; *Zahirovic et al*., 2014]. It has been long known that the Molucca Sea has subducted to both the west and east along the Sangihe and Halmahera thrusts based on Benioff zone seismicity (Figure 21e). In the eastern Molucca Sea, we interpreted a subducted slab to ~375 km depths based on a relatively clear and regionally mappable tomographic anomaly (Figure 21e). The maximum unfolded east Molucca slab length is ~400 km (Figure 21c). *Hall and Spakman* [2015] interpreted a comparable 400 to 450 km length for the eastern Molucca slab, which they called the Halmahera slab.

The western Molucca Sea slab has more uncertainty due to a number of fast tomographic anomalies down-dip of its ~660 km deep Benioff zone (Figures 21d and 21e). We interpreted a minimum-size west Molucca slab down to ~900 km or 1000 km depths based on 3-D mapping of its slab anomaly (Figures 16a to 16e, 21a, 21d, and 21e). It is possible that the western Molucca slab continues to greater depths (1200 km or deeper), but based on 3-D slab mapping, we preferred to interpret the deeper slab anomalies as Sunda slabs (e.g., Figure 21d). *Hall and Spakman* [2015] interpreted a shorter west Molucca slab (i.e., Sangihe slab) that did not extend past its deep Benioff zone [*Hall and Spakman*, 2015]. This interpretation required that the deeper fast anomalies were an unknown slab that was not in their current plate model. Other tomographic studies have also indicated ambiguity in interpreting the Molucca Sea slabs [*Richards et al*., 2007; *Widiyantoro and van der Hilst*, 1997]. Therefore, in this study we will unfold our minimum-size Molucca Sea slab for the plate reconstruction but permit gaps along its western limit to account for a possible longer slab.

When flexurally unfolded our minimum Molucca Sea plate size, including both the west and east slabs and a ~100 to 200 km upper flat section, varies from a maximum east-west length of 1550 km in the south to about 850 km in the north (Figure 21c). The west Molucca Sea slab accounted for a maximum 1050 km length (Figure 21c). Our total unfolded lengths are similar to the 1500 to 1600 km total length estimated by *Hall and Spakman* [2015] but much shorter than the 3400 km estimated by previous tomographic studies [*Rangin et al.,* 1999]. The larger Molucca Sea slab estimate of *Rangin et al.* [1999] included a number of slab anomalies that we mapped separately from the Molucca Sea slab based on our 3-D mapping and tomographic model (e.g., the deep Ayu Trough slab, East Asian Sea west slabs, and the Sunda slabs; Figures 21d and 21e).

We made a surprising observation that the Molucca Sea and Philippine trench slabs shared a common boundary that is only slightly offset in their present 3-D position (Figure 21b). Furthermore, the two slabs fit together edgewise within tomographic uncertainties when they were unfolded and positioned relative to their present-day trenches (Figure 21c). This could mean that the Molucca Sea and Philippine Sea plates were once together as a single plate and have since fragmented, a hypothesis that has been put forward by a number of published reconstructions [e.g., *Hall*, 1987; *Zahirovic et al*., 2014]. Alternatively, a NW-SE transform may have once existed between the two plates that has since subducted under the Philippines.

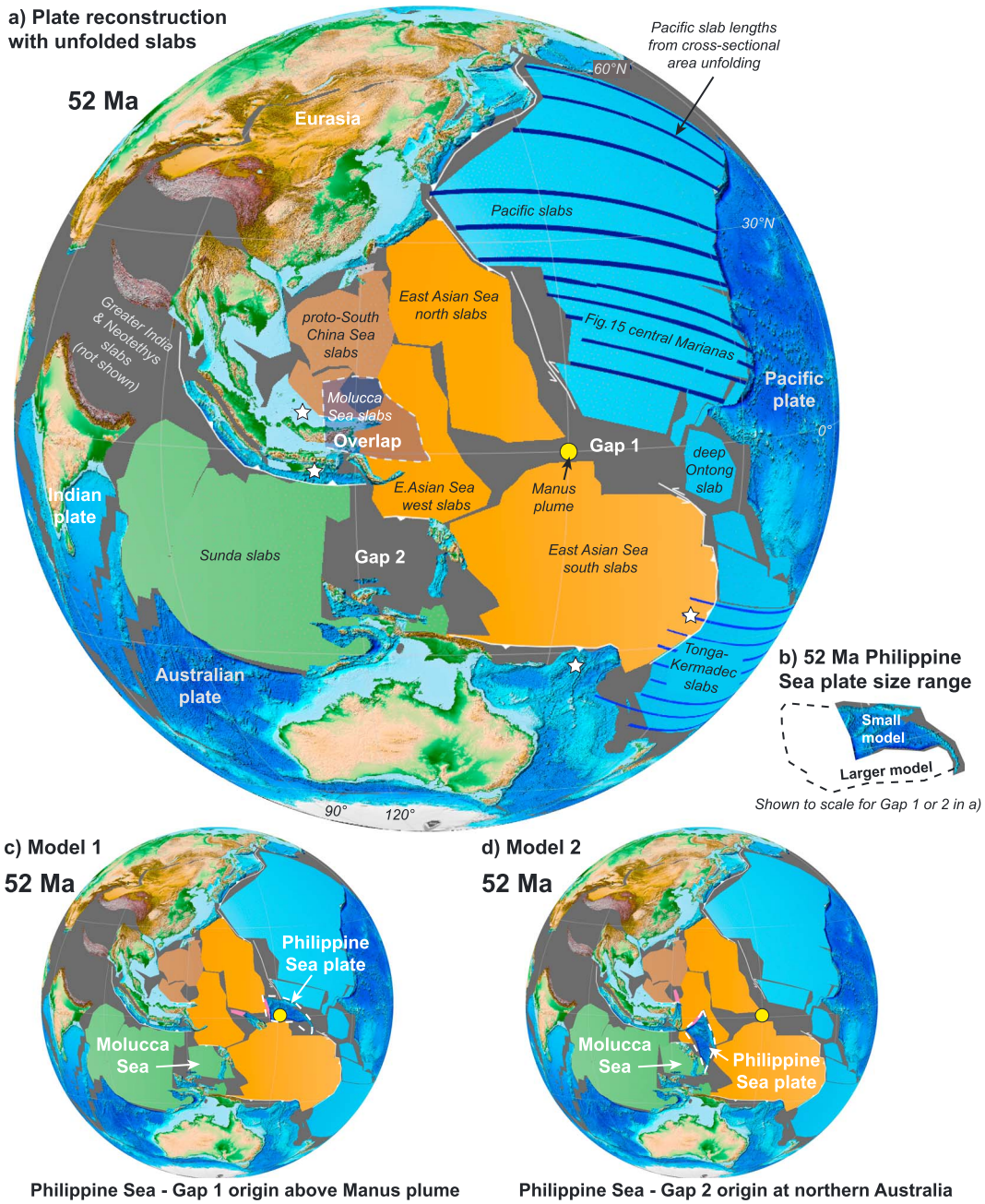

Figure 23. (a) 52 Ma plate reconstruction near the time of Philippine Sea plate initiation constrained by the subducted slabs and inferred trench locations from this study within the global plate reconstruction of *Seton et al.* [2012]. Supporting information Figure S4 illustrates reconstruction method in more detail. (b) The reconstruction revealed two reconstruction gaps of missing lithosphere at "Gap 1" and "Gap 2" that could accommodate the Philippine Sea plate nucleus at 52 Ma based on the range of plate sizes shown. (c) In our reconstruction Model 1, we originated the Philippine Sea plate at Gap 1 above the Manus plume with Luzon and the Huatung basin to the west. The minimum-size Molucca Sea plate was placed in Gap 2. (d) In Model 2 we originated both the Philippine Sea plate and the Molucca Sea at Gap 2 north of Australia. In Figure 23b the smaller 52 Ma Philippine Sea plate size consisted of the Oki-Daito province (OKP) and the Izu-Bonin-Marianas arcs similar to *Ishizuka et al.* [2013]. Some of the western Palau Basin was included as possible Marianas arc basement. The larger model (black dashed line) was based on *Hilde and Lee* [1984] and also includes the unfolded Ryukyu slab and Philippine Trench slabs from this study, which are of unknown age. The white stars in Figure 23a show minor (<500 km) reconstruction overlaps that could indicate active subduction during 52 Ma, or alternatively, errors in the Pacific cross-sectional area unfolding, the Sundaland plate model, or the mantle reference.

To the southeast of the Palau Basin, under the Ayu Trough, we mapped a detached slab that we call the "Deep Ayu Trough slab" at 550 to 600 km depths (Figures 21a and 21e). Our mapped Deep Ayu Tough slab has an eastern edge that roughly corresponds to a southward extension of the Kyushu-Palau ridge, within tomographic resolution (Figure 21a). The maximum east-west length of the Deep Ayu Trough slab is ~600 km. The location of this slab beneath the present Ayu Trough slow-spreading axis may seem puzzling, but it may be consistent with proposals for a former trench along the Ayu Trough, discussed in section 1.4. This shallow slab may provide evidence for relatively recent Philippine Sea-Caroline Sea plate convergence, and this is further discussed in section 5.6.

Below the Molucca Sea and Philippine trench slab anomalies, we observed deeper Sunda slab and the East Asian Sea detached slab anomalies (Figures 21c and 21d). These deeper slabs reveal the earlier history of this area before subduction at the Molucca Sea and Philippine trench.

3.4.3. The South China Sea-Eurasian Slab and Proto-South China Sea Slabs

The Eurasian slab subducted between Taiwan and Palawan displays seismicity to a maximum depth of ~300 km (Figure 22a). Based on tomography, we interpret the Eurasian slab to be subvertical and continue to a maximum ~450 km depth that is approximately constant between Taiwan and Palawan (e.g., Figures 15a and 22d). We mapped the detached proto-South China Sea slabs as two parts (Figure 20c). The northern proto-South China Sea slab is generally shallower (~500 to 900 km depths) and underlies a large part of the present South China Sea and extends below the Eurasian slab (Figures 15a, 20c, and 22c and Table 1). In contrast, the southern slab is deeper at ~850 to 950 km depths and underlies northern Borneo and the southern South China Sea (Figures 17e and 20c and Table 1). As shown earlier, our mapped proto-South China Sea slab locations roughly border other adjacent slabs (i.e., the East Asian Sea slabs and Sunda slabs) that are located at comparable depths in the mantle (Figure 20c).

A key observation from our 3-D slab mapping is that the Eurasian slab has subducted above the northern proto-South China Sea slab (Figure 15a). While it is possible that the slab anomalies have been smeared due to suboptimal seismic raypath coverage, we note that our slab interpretation allows for a tectonically viable link between the eastern margins of the South China Sea and proto-South China Sea; a simple visual unfolding of our Eurasian slab anomaly in Figure 15a would roughly align its restored eastern edge with the underlying proto-South China Sea eastern edge. In map view, both the unfolded Eurasian slab and the proto-South China Sea slab display roughly coincident N-S eastern edges (Figure 22c) that are subparallel to the South China Sea N-S opening direction [e.g., *Briais et al*., 1993; *Sibuet et al*., 2016]. Therefore, the pre-subduction eastern edge of the Eurasian slab could be easily reconstructed as a STEP fault ridge-trench transform, formed in association with the subduction of the northern proto-South China Sea. Our plate-tectonic model incorporates this interpretation, which is further discussed in section 5.7.

Our 3-D slab interpretation differs from previous tomographic interpretations based on individual tomographic sections that combined both our Eurasian slab and the deeper "northern proto-South China Sea" slab anomalies into one long (>1000 km length) overturned Eurasian slab [*Lallemand et al*., 2001; *Rangin et al*., 1999]. The inverted "T" junction (Figure 15a) in 3-D between the vertical and flat slabs is inconsistent with these one-slab interpretations. Furthermore, the newer MITP08 tomography augmented by the regional Chinese seismic network appears to clearly differentiate the Eurasian slabs from the higher-velocity proto-South China Sea slabs below (e.g., Figure 15a). Previous studies using the MITP08 tomography also similarly interpreted the deeper slabs to be the subducted proto-South China Sea and not part of the Eurasian slab [*Zahirovic et al*., 2014]. *Hall and Spakman* [2015] identified the flat slabs in the UU-P07 global tomography model, not including them as Eurasian slabs, but suggested that the slabs had stagnated in the transition zone during a much earlier phase of Mesozoic subduction. The history of the Proto-South China Sea is further discussed in section 5.7.

4. Plate Tectonic Reconstruction Using Subducted Slab Constraints

4.1. Philippine Sea Plate Origin: A 52 Ma Plate Reconstruction

In this section we build two alternative 52 Ma to present-day Philippine Sea and East Asian plate-tectonic models based on our 28 subducted slab constraints (Table 1), which are embedded in a recent global plate model [*Seton et al*., 2012]. We begin by assembling a single 52 Ma plate reconstruction (Figure 23a), which is the approximate beginning time of Philippine Sea growth and Pacific-Mariana subduction. This is a relatively

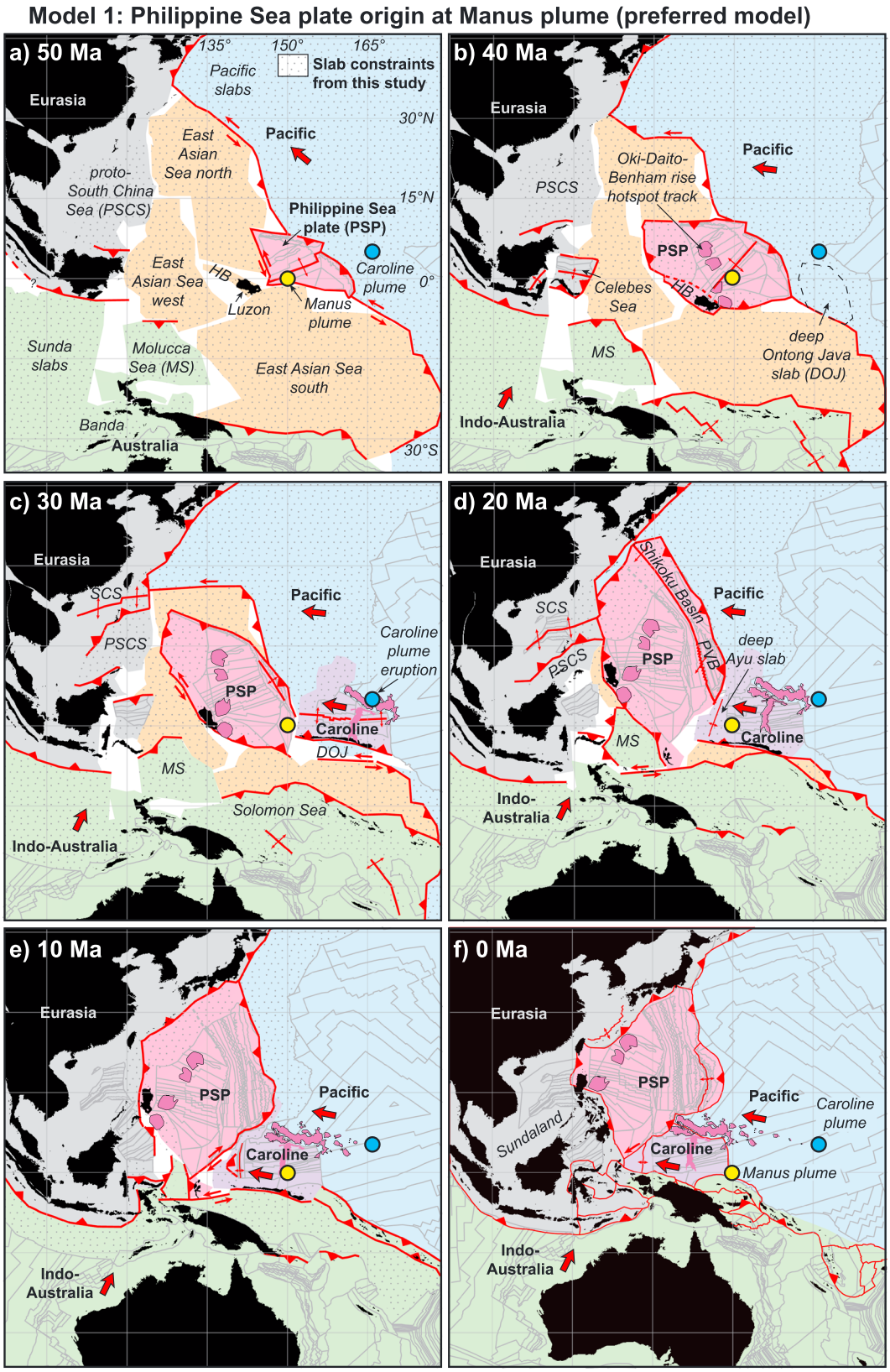

Figure 24. Preferred Philippine Sea plate reconstruction Model 1 showing its origin near the Manus mantle plume (yellow dot). Stippled areas show the unfolded slab constraints from this study. Purple polygons show oceanic plateaus from *Ishizuka et al*. [2013] and the UTIG University of Texas LIPs database [*Coffin*, 2011]. HB, Huatung Basin.

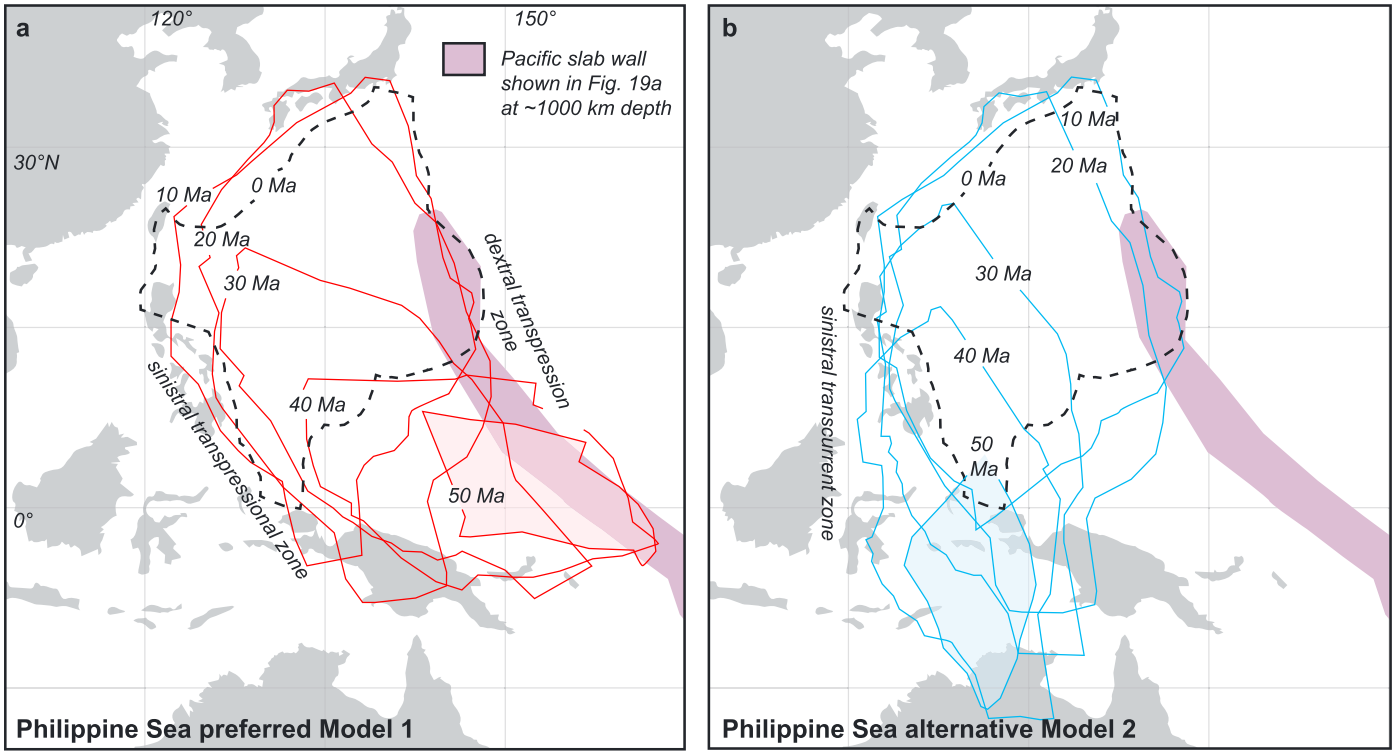

Figure 25. Comparison between (a) Model 1 and (b) Model 2 predicted Philippine Sea plate motions from this study. Philippine Sea plate outlines are shown at 10 Ma increments. Present-day coasts are shown in grey fill. The present-day Philippine Sea plate position is shown by the black dashed line. The trend of the Pacific slab wall anomalies from Figures 15 and 19 are shown in purple. Model 1 predicts that the eastern Philippine Sea plate boundary was a zone of dextral transpression against a Pacific plate boundary, which would be favorable to produce clockwise local block rotations. Model 1 also predicts that the western Philippine Sea plate boundary was a sinistral transpressional zone. In contrast, Model 2 predicts that the western Philippine Sea plate was largely a strike-slip tectonic boundary.

straightforward exercise of finding sufficient slabs that were age relevant for a 52 Ma reconstruction (i.e., the pre-52 Ma slabs in Table S1) to fill the very large hole defined by the locations of the major Pacific, Australian, and Eurasian plates at 52 Ma, shown in Figure 5a. Almost all of the hole is filled by the major subducted parts of the present Pacific and Indian Oceans (Sunda and Banda Sea slabs), plus the wholly subducted East Asian Sea and Proto-South China Sea, as shown in Figure 23a. All relevant unfolded slabs thought to exist at the surface at 52 Ma (Table S1), with the exception of the Philippine Sea, Molucca Sea, and a number of minor plate fragments, were added into the reconstruction following the reconstruction sequence of section 2.4 as shown in Figure S4. We note that the East Asian Sea and proto-South China Sea detached slabs were simply projected to the Earth surface (i.e., radially unfolded) and kept static in the mantle reference, which yields a straightforward reconstruction (Figure 23a).

4.1.1. Locating the Philippine Sea Plate Origin Using Reconstruction Gaps

Our strategy was to locate possible sites of Philippine Sea origin by searching for Philippine Sea plate-sized holes or gaps where no lithosphere has been identified within the 52 Ma slab reconstruction (Figure 23a). As reviewed earlier, published Philippine Sea plate spreading models predict a range of possible 52 Ma plate sizes. We estimated two model plate sizes: (1) a smaller Philippine Sea plate model at 52 Ma that included the Mesozoic-aged Oki-Daito province, the nascent Izu-Bonin-Marianas arcs, and minor arc basement behind the Marianas arc; and a (2) larger plate model was based on *Hilde and Lee* [1984] and included the unfolded Philippine Sea plate slabs from this study (Figures 23b and S4).

We located two substantial reconstruction holes or gaps (Gaps 1 and 2) that could potentially accommodate the "small model" Philippine Sea plate at 52 Ma (Figures 23b and S4). Gap 1 was near our mapped Manus plume anomaly centered at 150°E/0° whereas Gap 2 was located near 128°E and 10°S to 20°S latitudes, north of the reconstructed northern Australian margin (Figure 23a). Based on this analysis, we will present two Philippine Sea plate reconstruction models from these two possible sites of origin in section 4.2 (Figures 23c and 23d). In the case of Gap 2 we allowed some overlap with the southern "East Asian Sea west

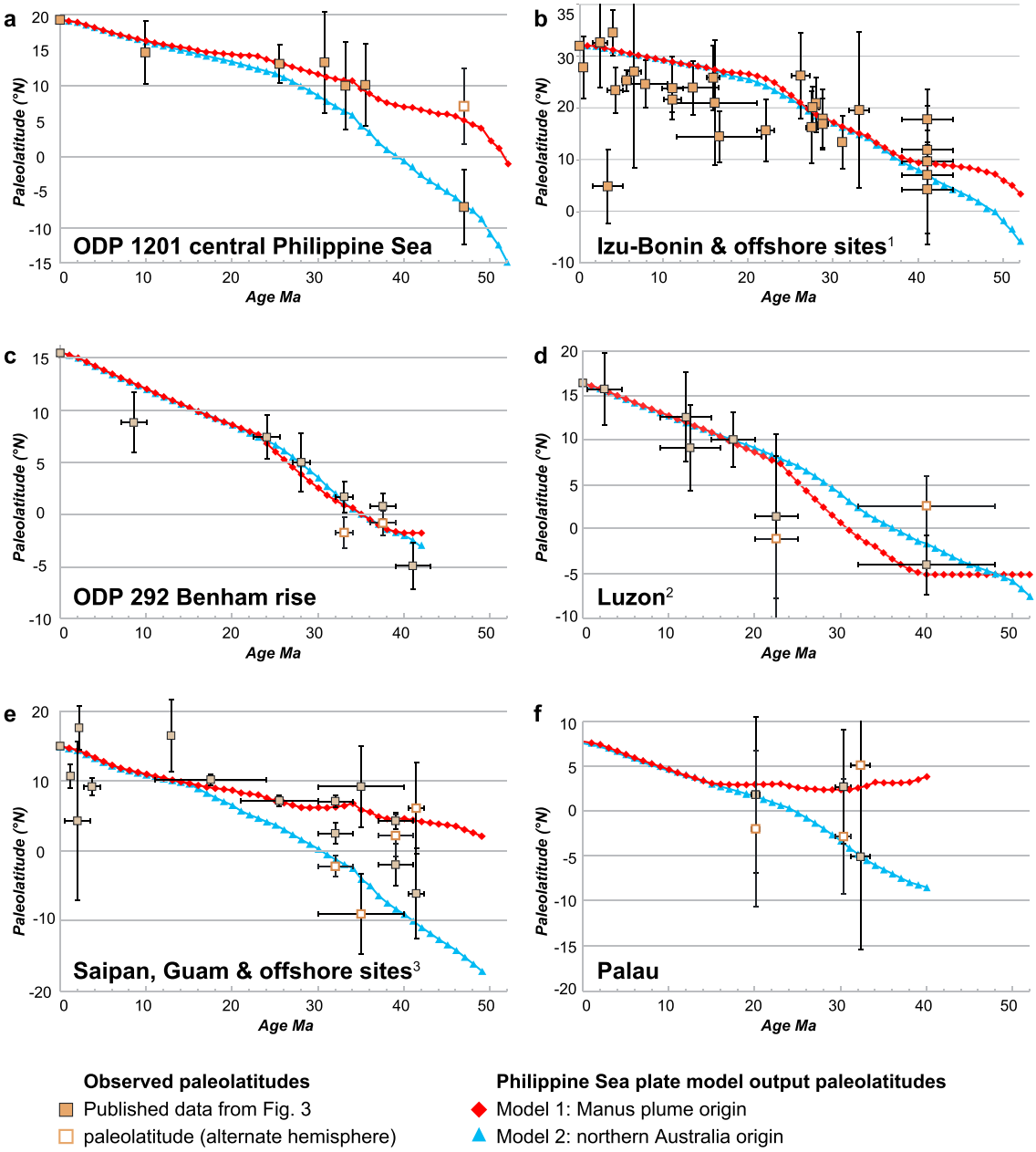

Figure 26. Comparison between modeled Philippine Sea paleolatitudes from this study (red and blue dots) against published Philippine Sea paleolatitudes for six widely scattered sites (see Figures 1 and 3 for locations and references). Alternate paleolatitudes (hollow brown dots) are shown for relevant data. The superscript 1 = Includes ODP DSDP site 782, 784, 786, 787, 792, and 793. Referenced to Izu 32°N, 140°E. The superscript 2 = Referenced to Baguio City 16.4°N, 120.6°E. The superscript 3 = Includes ODP DSDP site 453, 454, 456, 458, and 459. Referenced to Saipan 15.1°N, 145.7°E.

slabs" based on (1) tomographic uncertainties in the southern boundary of these slabs (Figure 17a) and (2) alternate mantle reference frames that suggest that the Australian plate absolute position was up to 5° farther south at 52 Ma relative to our chosen reference (Figure S5). Using the alternate mantle reference would create additional space to fit the Philippine Sea plate within Gap 2.

4.1.2. Major Reconstruction Overlaps: Reconstructing the Molucca Sea Plate

In addition to the reconstruction gaps, we note a major reconstruction overlap between the Molucca Sea slabs (restored at their present-day positions) and the "East Asian Sea west" slabs near NW Borneo (Figure 23a). Based on slab sinking, we infer that the deeper East Asian Sea west slabs subducted before the shallower Molucca Sea slabs (Figures 21d and 21e). Therefore, one way to solve the overlap would be

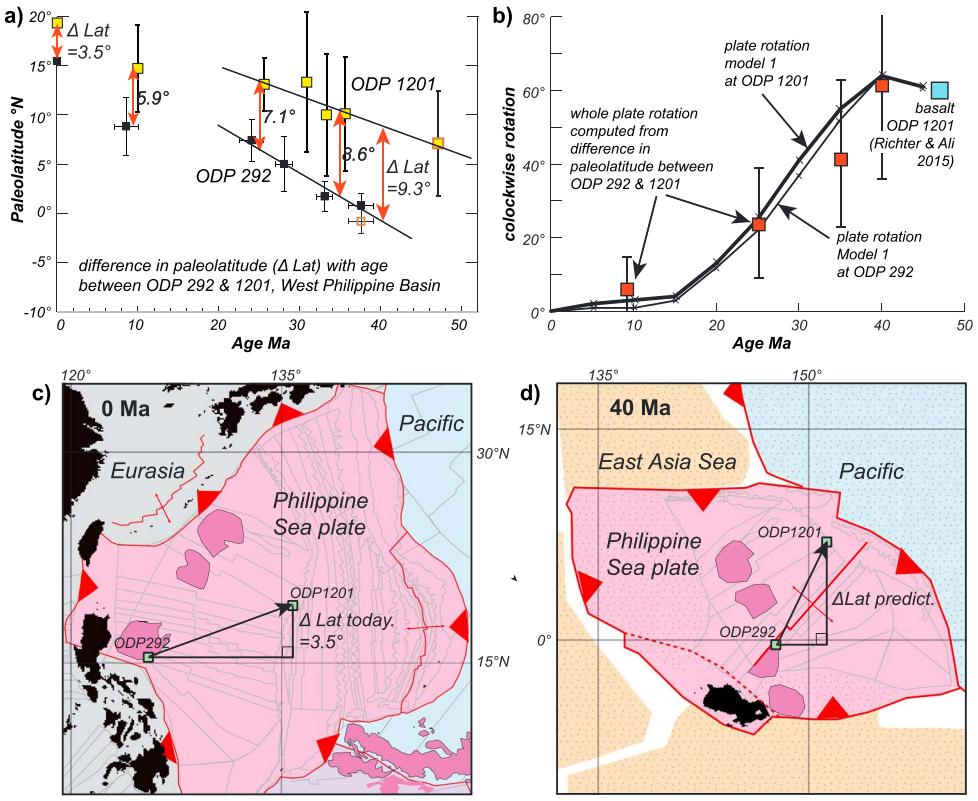

Figure 27. Whole-plate clockwise rotation of the West Philippine basin from differential changes in paleolatitude between ODP sites 292 and 1201 (Figure 1). (a) The current difference in latitude is 3.5° whereas their difference in paleolatitude is 9°–10° at 40 Ma, suggesting that the line connecting the two sites, which has an angular separation of 10.6°, was oriented more nearly N-S, in contrast with its current 71° azimuth. The contrasting rates of change of paleolatitude between the sites suggests whole-plate rotation during the period ~25–40 Ma. (b) Estimated whole-plate rotations compared to our preferred plate Model 1. Rotations were computed based on observed differences in paleolatitude (Figure 27b) corrected for our West Philippine basin seafloor-spreading model. In spite of large uncertainties, the estimated clockwise rotations are in broad agreement with our plate Model 1 and with paleomagnetic declination observations (e.g., Figure 28). (c) Present-day difference in latitude between ODP 292 and 1201. (d) 40 Ma difference in paleolatitude predicted by Model 1.

to place the Molucca Sea elsewhere at 52 Ma (i.e., within Gap 1 or Gap 2). Alternatively, the overlap between the Molucca Sea and the west East Asian Sea could be explained if the Molucca Sea were a young plate formed after 52 Ma, in which case it could be removed from the 52 Ma reconstruction. Unfortunately, the Molucca Sea has not been directly age dated because the plate has been overridden by the Sangihe fore arc from the west and none of the plate survives at the surface today [*Hall*, 2000]. However, it is reasonable to infer a minimum mid-Miocene age for the Molucca Sea based on the Neogene Halmahera arc, which likely formed during subduction of the eastern Molucca Sea [*Baker and Malaihollo*, 1996]. Early Cenozoic or Cretaceous ages for the Molucca Sea are also possible [e.g., *Hall*, 1987; *Hall et al.*, 1988].

In the absence of direct Molucca Sea age dates, we observe that the Molucca Sea slab has a very high amplitude velocity anomaly similar to the Sunda slab with which it is in contact (Figures 16 and 21) and a very deep Benioff zone extending to ~660 km, both suggesting that it is Mesozoic and old at the time of subduction. Therefore, we conclude that the Molucca Sea slabs could be reconstructed within "Gap 2" adjacent to the NS edge of the Sunda slab as part of the northern Australian plate at 52 Ma (Figures 23c and 23d). This implies an Indian Ocean origin for the Molucca Sea, which could fit with the apparent convergence between the Molucca Sea and Sunda (i.e., Indian Ocean) slab anomalies at depth (Figures 16, 18, 21d, and 21e). Other tomographic studies have chosen to similarly reconstruct the Molucca Sea with the Indian Ocean [*Richards et al.*, 2007].

4.1.3. Minor Reconstruction Overlaps

A number of smaller (200 to 500 km) reconstruction overlaps were also noted, shown by white stars in Figure 23a. At least some of these overlaps could be the result of mantle reference frame uncertainties

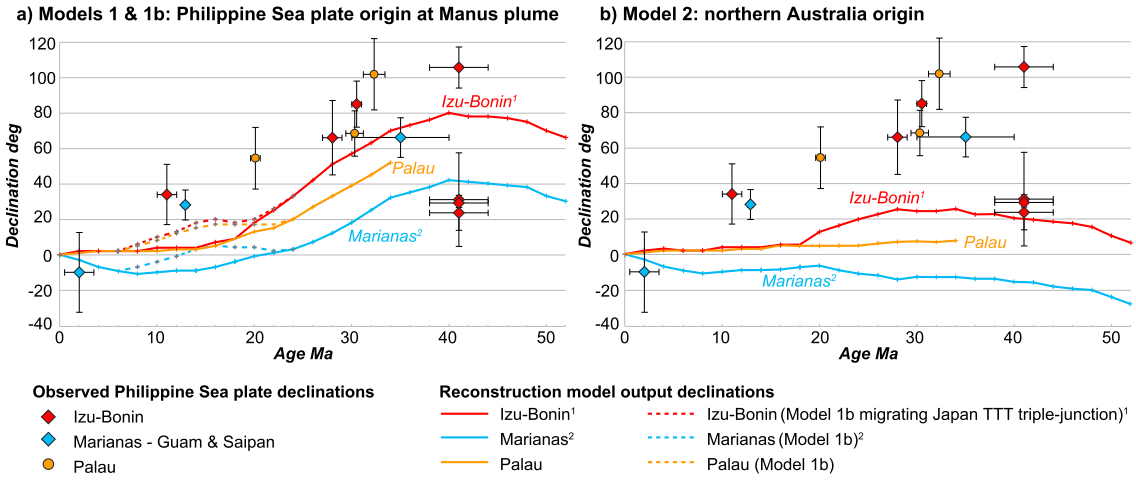

Figure 28. Comparison between published and the modeled Philippine Sea plate declinations for three locations along the eastern plate margin (see Figures 1 and 3 for site locations and references). (a) The whole-plate rotation Models 1 and 1b produced up to 80° clockwise Philippine Sea plate rotation. The migrating Japan triple junction Model 1b showed slightly higher (up to 20°) rotations in the Miocene. (b) The minimal rotation Model 2 showed small rotations (±25°) due to the opening of adjacent back-arc basins. All models from this study predict declinations that are generally less than the observed declinations. We consider our models to be viable from the limited perspective of paleomagnetic declination constraints because any gaps between the modeled and observed rotations could be ascribed to local block rotation along the Philippine Sea plate eastern margin. Modeled locations: superscript 1 = Izu (32°N/140°E); superscript 2 = Saipan (15.1°N/145.7°E).

(see Figures S5 and S6). Overlaps near southern Sundaland could be explained by minor pre-52 Ma subduction [e.g., *McCourt et al*., 1996], uncertainties in the relatively unconstrained Eurasian-Sundaland plate model, or an overestimate in our Sunda slab length; we consider the latter unlikely since the Sunda slabs were flexurally unfolded (Table 1) and therefore closer to a minimum length estimate. An overlap between the Tonga slabs and the East Asia Sea south slabs could suggest some minor pre-52 Ma Tonga subduction, which would be consistent with Tonga fore-arc ages [*Meffre et al*., 2012]. We interpret the overlap between the East Asian Sea south slabs and the NE Australian plate margin (Figure 23a) to be caused by slow subduction of the southernmost East Asian Sea under northern Australia after 84 Ma due to slow Australia-Antarctica northward spreading. This hypothesis has also been proposed by other slab tomographic studies [*Schellart and Spakman*, 2015].

4.2. Cenozoic Plate Tectonic Reconstructions of the Philippine Sea Constrained by Mapped and Unfolded Slabs

We identified two sizable regions of good tomographic coverage without identified lithosphere in our 52 Ma reconstruction (Figures 23 and S4), which are therefore potential sites of origin of the Mesozoic nucleus of the Philippine Sea plate. Gap 1 spans the equatorial junction between the East Asian Sea and the Pacific, extending east and west of the present position of the proposed long-lived (minimum 52 Ma) Manus plume [cf. *Macpherson and Hall*, 2001]. We will herein also adopt a stable, long-lived Manus plume in our plate models based on: (1) a prominent lower mantle slow-velocity anomaly in our MITP08 tomographic analysis at 0°/150° E (Figures 16c to 16f and 17b), (2) a plume-like low-velocity conduit in the lower mantle (i.e., the "Indonesia" anomaly) detected by a recent global shear wave velocity model SEMUCB-WMI [*French and Romanowicz*, 2015], and (3) plume-like helium isotope signatures within Manus back-arc basin rocks [e.g., *Macpherson et al*., 1998]. The part of the equatorial gap within the East Asian Sea west of the Manus plume is a region of poorer imaging and therefore potentially may not be a region of missing lithosphere. Gap 2 is east of the NS eastern edge of the Sunda slab and north of Australia at ~10–20°S latitudes (Figure 23a). We argued above in section 4.1 that the Molucca Sea likely reconstructs within Gap 2, just east of the Sunda slab, and is part of the 52 Ma NE Indian Ocean, north of Australia. However, Gap 2 is sufficiently large that it potentially could also contain the Mesozoic nucleus of the northern West Philippine basin and the Philippine Trench slab (cf. Figure 21c).

Presently available paleolatitude constraints for the Philippine Sea plate near 52 Ma are extremely limited. However, a 50 ± 5 Ma paleolatitude of 13.2°S ± 5.6° from ODP Site 294 at the southern edge of the Daito Ridge (Figure 1) [*Louden*, 1977] is consistent within errors with either Gap 1 or Gap 2. A few other sites 40 Ma

and older yielded −5° to 0° paleolatitudes, with equatorial ambiguity, including ODP 292 and 1201 (see Figures 26a and 26c). Therefore, either Gap 1 or 2 appears to be viable for a site of origin of the Philippine Sea plate from the point of view of available paleolatitude data (see also section 5.1).

We input our slab constraints and reconstructed Philippine Sea plate forward to its present-day location from its two possible origins, which we call "Model 1: Manus plume-derived" (Figure 24) and "Model 2: northern Australia-derived" (Figure S5). A comparison between the two models is shown in Figure 25. These plate-reconstruction figures show the major active tectonic features at progressive 10 Ma periods. Subduction zones were inferred from relative plate motions and tectonic relationships. Fully animated plate reconstruction movies and GPlates files are available in the supporting information. White gaps (grey gaps in Movies S1–S3) at each stage are unfilled spaces that could be due to slab unfolding or mapping errors, thermal erosion of slab tomographic anomalies, spreading ridges, or mantle reference errors. It is emphasized that each of these two reconstructions represents a separate class of solutions that can accommodate a number of second-order modifications in the light of existing or new constraints. The Manus plume-derived model (i.e., Model 1) is our preferred solution, based on comparison to Philippine Sea plate paleomagnetism and regional geology (sections 5.1 and 5.2); Model 2 is presented as an alternative. Comparisons between the two models in terms of Philippine Sea positions, predicted latitudes and declinations are shown in Figures 26–28, respectively. A summary of the comparisons between Models 1 and 2 is given in section 5.3.

4.2.1. Philippine Sea Plate Model 1: Manus Plume Origin

Model 1 represents a class of models that positions the small initial Mesozoic core of Philippine Sea plate at 52 Ma within the elongate equatorial Gap 1 that extends east and west of the present location of the Manus plume and places a minimum-sized Molucca Sea slab into Gap 2 north of Australia (Figure 23c). The present version of Model 1 has the main Philippine Sea core overlapping the present-day position of the Manus plume at 0°/150°E near a western Pacific transform plate boundary (Figure 24a). This choice is consistent with the Philippine Sea nucleating at a hot spot that formed the proposed Benham Rise-Oki-Daito hot spot track (Figures 1 and 14; see section 1.3). This starting Philippine Sea plate configuration allowed multiple plate orientations, and we chose to longitudinally align the Izu-Bonin-Marianas arcs along our inferred Pacific plate boundary (Figure 24a). This initial Philippine Sea plate configuration implied maximum ~80° whole-plate clockwise rotation, which would fit within published paleomagnetic declinations if a small amount (20° to 30°) of local block rotation were included (Figure 27). We positioned Luzon and the Huatung Basin to the west of the main nucleating Philippine Sea (Figure 23c), implying that these are fragments of the East Asian Sea that were amalgamated to the Philippine Sea during its subsequent westward and northward journey. Under this interpretation the Cretaceous Huatung Basin [*Deschamps et al*., 2000] is apparently the only remaining fragment of intact East Asian Sea oceanic crust, as opposed to arc crust.

At 52 Ma the Pacific plate was moving NW whereas the Eurasian and Australian plates were slow moving. These three major plates were separated by the East Asian Sea, a swath of now-vanished oceans that stretched from the Eurasian margin at ~30°N near proto-Taiwan and the Ryukyus to the northern Australian margin at 30°S (Figure 24a). The proto-South China Sea was located west of the East Asian Sea, between south China and Borneo (Figure 24a). The western Pacific plate boundary stretched NW-SE from south of Japan to offshore eastern Australia (Figures 19, 20c, and 24a). The orientation of the Pacific plate boundary relative to pre-50 Ma Pacific motions suggests transform or highly oblique subduction (Figures 19 and 24a). We reconstructed the Molucca Sea in Gap 2 to be part of the NE Indian Ocean north of the proto-Banda Sea. Slow northward drift of Australia from Antarctica drove slow Indian Ocean subduction along Java and east Sumatra (Figure 24a), and some subduction may have begun prior to 52 Ma (see section 4.1). East of New Guinea northward drift of Australia was accommodated by slow subduction of the southern East Asian Sea under NE Australia that may have began as early as 84 Ma within the global model.

After ~50 Ma there was a major regional plate reorganization. The Pacific plate changed direction to move rapidly WNW toward Eurasia, resulting in fast westward Pacific subduction under the East Asian Sea at the proto-Marianas (Figures 19 and 24b). North of the proto-Marianas, we infer the initiation of a STEP fault transform that accommodated westward motion of the Izu-Bonin Pacific flat slabs, which overrode and subducted the northernmost East Asian Sea slabs (Figure 24b). With continued Pacific motion the leading edge of the proto-Izu Bonin slabs eventually subducted under Eurasia to emplace the regional Pacific flat stagnant slabs (i.e., Japan slabs) seen in Figures 7d and 17c. During the same period the Tonga Pacific slabs began to subduct rapidly westward under eastern Australia and the southern East Asian Sea (Figure 24b). The Philippine

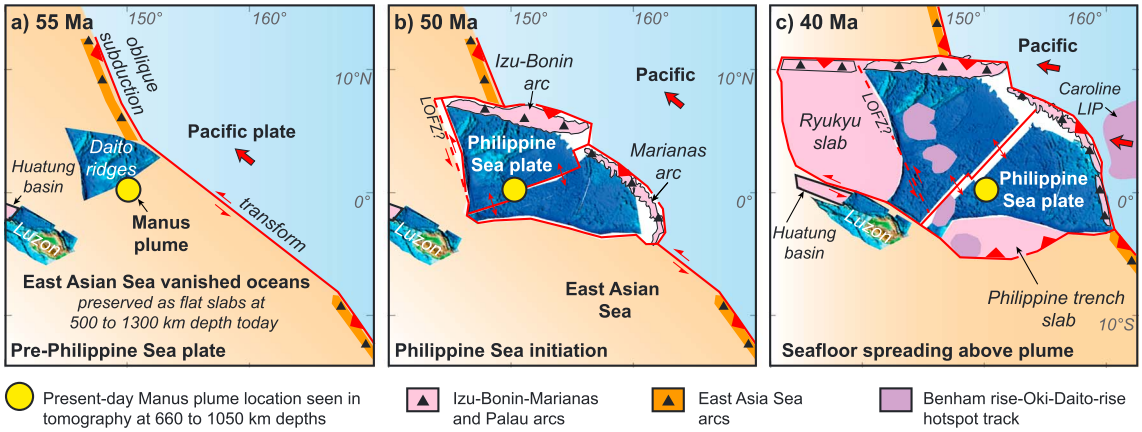

Figure 29. Philippine Sea plate initiation and growth based on our preferred Philippine Sea plate tectonic reconstruction Model 1. (a) The pre-Philippine Sea plate tectonic configuration was a NW-SE Pacific-East Asian Sea transform boundary near the equator. The Cretaceous-aged Daito ridges and Luzon-Huatung basin were located nearby. (b) The Philippine Sea plate initiated above the Manus plume at 150°E/0° and began to spread, centered above the hot spot. (c) The Philippine Sea plate remained stationed above the plume and grew outward by seafloor spreading, consuming parts of the East Asian Sea and Pacific plates by opposing subduction zones. The Ryukyu slab was formed during this period, potentially within a spreading center across the Luzon-Okinawa fracture zone (LOFZ). Excess plume magmatism formed an age-progressive chain of plateaus on either side of the spreading ridge (after *Ishizuka et al.* [2013]). The Huatung basin and Luzon were amalgamated to the Philippine Sea along a transpressive boundary shortly after 40 Ma. After 40 Ma the Philippine Sea plate was driven westward from the Manus plume by the newly formed, westward moving Caroline Sea plate in Figure 29c.

Sea nucleated and spread rapidly above the Manus plume, staying stationary with minor rotation behind the Pacific subduction zone (Figure 24b). During this stationary phase of the Philippine Sea plate, age-progressive oceanic plateaus formed across the Central Basin rift to produce the Benham-Oki-Daito Rise hot spot track, similar to the model envisioned by *Ishizuka et al.* [2013]. Philippine Sea plate spreading and growth were accommodated by East Asian Sea and Pacific subduction along circum-Philippine Sea plate subduction zones (Figure 24b). Luzon and the Huatung Basin were amalgamated to the growing Philippine Sea plate along a transpressional boundary between 52 and 34 Ma.

We reconstructed the Philippine Trench slab lithosphere to have formed prior to 45 Ma based on our interpretation of a subducted plateau within the Philippine Trench slab (Figure 14) and following a predicted ~45 Ma minimum plateau age from *Ishizuka et al.* [2013]. Reconstruction of the Ryukyu slab was more problematic because most of the slab is north of the Luzon-Okinawa fracture zone (Figure 14), which is a possible transform or major tectonic boundary. Magnetic age modeling of the small preserved part of the Philippine Sea plate north of the Luzon-Okinawa fracture zone indicates a nonsymmetric magnetic age sequence similar in age to the West Philippine Basin but progressively younger toward the Ryukyu Trench [*Doo et al.*, 2014]. The lack of conjugate magnetic anomalies implies that a subducted ridge may exist within the Ryukyu slab. Therefore, we reconstructed the Ryukyu slab to form within a separate subbasin offset from the West Philippine basin by the Luzon-Okinawa fracture zone (Figure 24b). The spreading of this subbasin was not modeled due to insufficient constraints but instead was approximated by artificially displaying the Ryukyu slab in its entirety at 40 Ma.

Around 40 Ma the Indian-Australian spreading ceased and the new combined Indo-Australian plate began to rapidly converge NNE toward Eurasia (Figure 24b). This resulted in faster northward subduction along the Sunda trench (Figure 24b). East of Java, the East Asian Sea subducted southward beneath the northern Molucca Sea (Figure 24b). We followed the global model to initiate ~43 Ma north-south Melanesian arc spreading at NE Australia and this further consumed southern East Asian Sea by fast southward subduction (Figure 24b). The Celebes Sea opened as a back-arc basin behind a rotating NW Borneo subduction zone, subducting the western East Asian Sea (Figure 24b).

Around ~36 Ma the Caroline Sea nucleated and began spreading N-S above the Caroline mantle plume near 5°N, 166°E (Figure 24c). Recent full-waveform global tomography indicates that the Caroline hot spot is deeply rooted to a plume-like slow anomaly that can be traced to the core-mantle boundary [*French and Romanowicz*, 2015]. Opening of the Caroline Sea was accommodated by southward trench migration over the Pacific plate (Figure 24c). The lost Pacific plate during Caroline Sea opening (i.e., proto-Caroline Sea Pacific slabs) is today in the lower mantle under the Ontong Java plateau (i.e., Ontong Java deep slabs;

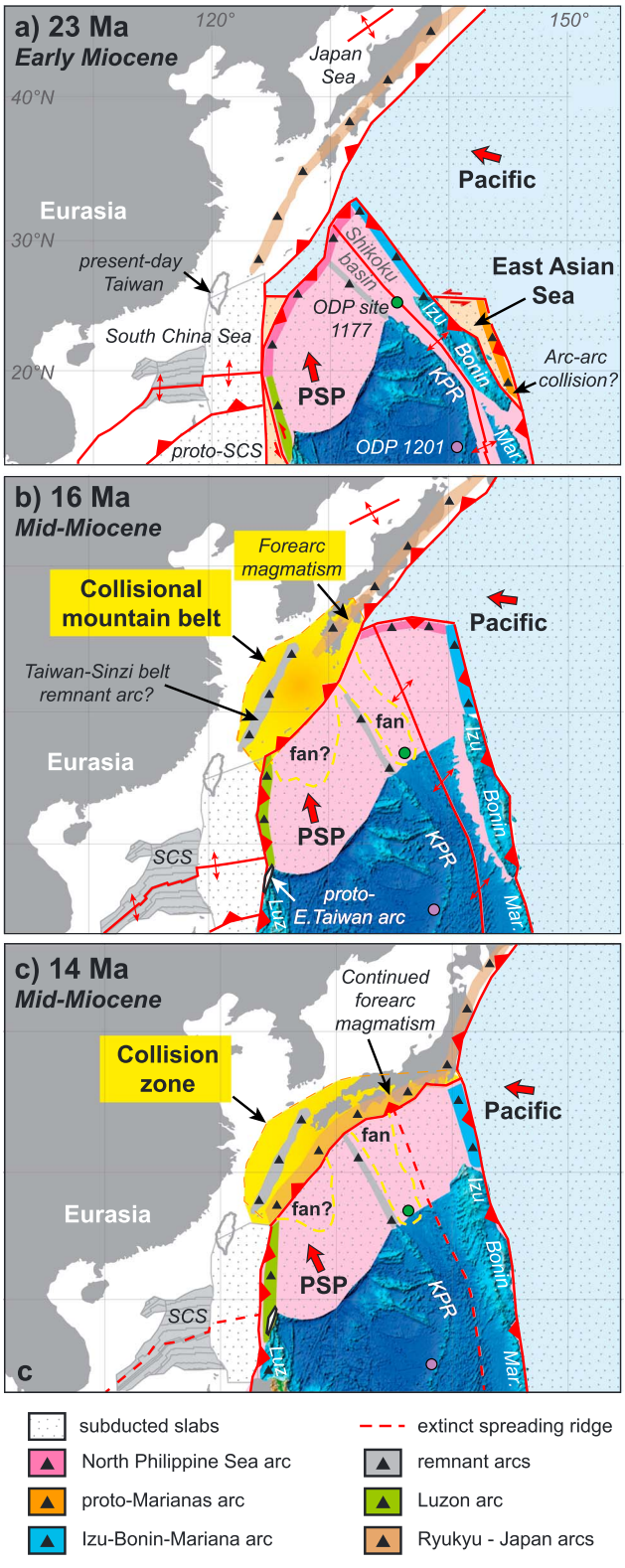

Figure 30. Early to mid-Miocene collision between the Philippine Sea plate and Eurasia predicted by the preferred Model 1 plate reconstruction. PSP, Philippine Sea plate; Mar, Marianas arc; Luz, Luzon arc; KPR, Kyushu-Palau arc.

Table 1 and Figures 24b and 24c). We tentatively interpret the southern Caroline Sea arc to be the Torricelli Terrane that collided with the leading arc of the Australian plate in the Miocene and is now incorporated into New Guinea (Figures 24d and 24e), as previously suggested by *Hill and Hall* [2003].

The N-S opening Caroline Sea impinged on the SE Philippine Sea around 34 to 30 Ma and apparently torqued the Philippine Sea plate (Figure 24c). This coincided with up to 60° clockwise rotation of the entire Philippine Sea plate between 40 and 20 Ma (Figure 27). With continued Caroline Sea westward motion, the Philippine Sea plate experienced an escape or extrusion to the north and west (Figures 24c–24e). In Model 1 the Philippine Sea rotational escape was accommodated by its overriding both the west and the north East Asian seas, with what became the northern Philippine Sea arc at the leading edge of the now subducted Ryukyu slab (Figures 24b–24d). The northern Philippine Sea arc eventually collided with the Eurasian margin along the Ryukyus and Japan around 20 Ma (Figures 24d and 28). Differential rotations between the Philippine Sea and Caroline Sea plates between 20 and 40 Ma were accommodated by spreading of a new ocean that was later subducted (i.e., deep Ayu Trough detached slabs in Figures 24d and 24e). During this phase our model indicates that the Palau basin at the southern Philippine Sea tracked across the Manus plume (Figure 24c). This suggests the enigmatic shallower bathymetry within the Palau Basin possibly could be a result of hot spot-related plateau eruptions or underplating. We interpret that West Philippine Basin spreading terminated around 34 to 30 Ma as it moved away from the Manus plume due to the Caroline Sea-SW Philippine Sea collision. Anomalous along-axis dextral shear recorded during the final West Philippine basin spreading phase [*Deschamps et al.*, 1999] could be an expression of this collision.

Shikoku-Parece Vela basin back-arc spreading began shortly after ~30 Ma

(Figures 24c and 24d). Our Model 1 suggests that the Shikoku-Parece Vela basins did not open fully by classic slab rollback, given the largely stationary Marianas subduction zone, but by westward motion of the Philippine Sea plate during the rotational tectonic escape driven by impinging Caroline Sea/Pacific plate (see Model 1 in Movie S1 between 30 and 15 Ma, discussed more fully in section 5.4). Furthermore, the two subbasins have different kinematics and plate tectonics. The Parece Vela basin widens southward associated with clockwise rotation of the West Philippine basin relative to the anchored Marianas. In contrast, the northward widening Shikoku basin began moving over the Pacific plate at the beginning of back-arc spreading ~27 Ma (Model 1 in Movie S1) and shows some evidence of Pacific slab rollback (Figures 18 and S8).

The Philippine Sea plate continued to be driven westward and rotated by the Caroline-Pacific leading plate edge until around 25 Ma, when the northern Indo-Australian margin converged and collided with the southern Philippine Sea plate and potentially contributed to the northward Philippine Sea motion (Figures 24c and 24d). The collision at ~25 Ma caused the Molucca Sea to be torn from the Indian Ocean along the Sorong strike-slip zone (Figure 24d). The Molucca Sea was then rapidly subducted westward under Sundaland at the Sangihe trench after ~ 25 Ma (Figure 24d).

As early as 25–20 Ma, a regional plate reorganization initiated as the northern Philippine Sea plate arc approached the Eurasian margin between Ishigaki in the western Ryukyus (Figure 22c) and southwest Japan (Figure 24d). Concurrently, the Bonin-Marianas arcs at the northeastern Philippine Sea margin approached the proto-Marianas arc at the eastern margin of the East Asian Sea (Figure 24d). The proto-Marianas arc was lost and subducted along with the East Asian sea slab during this arc-arc amalgamation or collision, which is further discussed in section 5.4. Our model suggests that the present-day preserved Izu arc segment was not involved in this amalgamation because it had moved across a transform at the northern margin of the East Asian Sea (Figures 24c and 24d). Continued convergence of the Indo-Australian, Philippine Sea, and Pacific-Caroline plates toward Eurasia caused the final remnants of the East Asian Sea to be subducted by 15–20 Ma (Figure 24d).

Between 15 and 20 Ma the northern Philippine Sea arc fully collided with the formerly subducting Eurasian margin, creating a collisional mountain belt that was formed between Ishigaki and southwest Japan (Figure 29b). Sediment from the collisional mountain belt was carried southward by extensive (~1000 km long) turbidite fans, one of which was drilled in the Shikoku Basin at ODP 1177, as well as within the Nankai accretionary prism (Figures 29b and 29c) [*Clift et al*., 2013; *Pickering et al*., 2013]. The Japan Sea opened and escaped eastward in response to the Philippine Sea-Eurasian collision between 16 and 14 Ma (Figures 29b and 29c). In this model we invoked the Izu-Bonin arc to arrive near Tokyo at 15 Ma, and therefore, Philippine Sea plate rotations are minimal after 15 Ma (Figure 27). However, our slab constraints also allow a migrating trench-trench-trench triple junction near Japan and Izu-Bonin arc arrival near Kyushu at 15 Ma. This alternative reconstruction is provided in the supporting information (see Model 1b in Movie 2) and will be later discussed. Around 16–17 Ma the Philippine Sea began to subduct northward under Japan and the Ryukyus east of Ishigaki, with associated fore-arc magmatism (Figures 24e and 29b). These effects of Miocene Philippine Sea plate collision are discussed more fully in section 5.4.

The Philippine Sea continued to be driven northward with a westward component by the Pacific-Caroline plates. By 15 to 20 Ma, South China Sea spreading was nearly completed and the Eurasian and newly formed South China Sea lithosphere between Ishigaki and Palawan-Mindoro began to subduct beneath the western Philippine Sea (Figures 22c, 24d, and 29b). A constraint on post ~15 Ma motions of the Philippine Sea plate is provided by the East Taiwan ophiolite, which is incorporated within the Pliocene-aged Lichi Melange of the Coastal Range, eastern Taiwan [*Suppe et al*., 1981]. This ophiolite formed at ~15 Ma and is generally interpreted as a preserved fragment of South China Sea spreading ridge or near-ridge seamount fragment [*Chung and Sun*, 1992; *Huang et al*., 1979; *Jahn*, 1986; *Suppe et al*., 1981]. This conclusion requires that the trajectory of the Taiwan Coastal Range arc and fore-arc accretionary complex pass over the South China Sea spreading axis after or synchronously with the formation of the ophiolite at 15 Ma. The dominantly northward motion of the Philippine Sea plate with small westward component in all of our models ensures that the Taiwan Coastal Range passes over the ridge at 10–15 Ma (e.g., Figures 30b and 30c).

After 15 Ma the southeast Philippine Sea plate-Caroline plate boundary became a NE-SW transpressive zone with limited, highly oblique subduction under the southern Marianas, Yap, and Palau trenches (Figure 24e). From 22 to 15 Ma the southern Caroline arc (i.e., the Torricelli Terrane) collided with predicted northern

Australian arcs whereas a final New Guinea arc-continent collision was much later (1 to 2 Ma). From 15 to 2 Ma the Philippine Sea plate moved NNW and the South China Sea and its margins were subducted at the Manila trench (Figures 24e, 24f, and 29c). At ~2 Ma the Philippine Sea began to move with its present-day, Pacific-like WNW direction, apparently due to greater coupling between the Philippine Sea and Pacific-Caroline plates (e.g., Figure 1b).

4.2.2. Model 2: Northern Australia-Derived Philippine Sea Plate Model

Model 2 (Figures 25b, Figure S7 and supporting information) is an alternative Philippine Sea plate reconstruction based on plate nucleation at northern Australia at 52 Ma within the reconstruction Gap 2 (see Figure 23d). A Philippine Sea plate origin north of Australia has been previously proposed by other studies [e.g., *Deschamps and Lallemand*, 2002; *Jolivet et al*., 1989] and is here tested within our new slab constraints. In this model we assume a small Molucca Sea with a maximum 900 km depth western slab (e.g., Figure 21 b), which allowed the Molucca plate to be fit southwest of the Philippine Sea (Figure S7a). Minor overlaps between plates in this reconstruction were allowed within the limits of uncertainties in early Philippine Sea spreading rates (Figure 23b), mantle reference (Figures S5 and S6) and Eurasian-Sundaland absolute positioning (see section 1.4).

At 52 Ma the Philippine Sea plate nucleated and grew northward by N-S spreading, subducting the western East Asian Sea (Figures S7a and S7b). We linked the West Philippine Basin and Celebes Sea spreading ridges based on their proximity and timing (Figure S7b), similar to suggestions from other published reconstructions [e.g., *Gaina and Müller*, 2007; *Hall*, 2002]. Counterclockwise rotation of Borneo resulted in southward subduction of the southern proto-South China Sea (Figures S7a and S7b). Luzon and the Huatung Basin were reconstructed as a plate fragment within the East Asian Sea in the vicinity of Borneo and the Celebes Sea (Figure S7a).

Northward motions of the Indo-Australian plate after ~40 Ma drove the Philippine Sea plate northward. Around 34 Ma the Celebes Sea was fragmented from the Philippine Sea and major West Philippine Basin spreading terminated (Figure S7c). The Philippines were trapped between a left-lateral transcurrent shear zone formed between the eastern Sundaland margin and the western Philippine Sea plate (Figure S7c). Luzon moved northward with the spreading Celebes Sea and was amalgamated to the Philippine Sea plate around 30 Ma. The East Asian Sea was subducted southward and overrun by the north moving Indo-Australian and Philippine Sea plates.

Between 30 and 20 Ma the north moving Philippine Sea began to approach the proto-Marianas arc on the East Asian Sea, particularly as a result of opening of the Shikoku and Parece Vela back-arc basins, resulting in amalgamation of the two convergent plate boundaries (Figures S7c and S7d). Similar to Model 1, around 15 to 20 Ma the final merger of the two subduction zones resulted in an arc-arc amalgamation between the Bonin-Marianas arc segments on the Philippine Sea plate and the proto-Marianas arcs according to Model 2 (Figure S7d). In either case, the proto-Marianas arc appears to have subducted as part of the East Asian Sea lithosphere (section 5.4).

After 25 Ma the Philippine Sea plate continued to move with Indo-Australia-like motions but a small component of westward motion was modeled in response to the incoming Caroline-Pacific plate indentor. The NNW Philippine Sea plate motions initiated highly oblique subduction of the Eurasian-South China Sea margin at the Manila trench by 20 Ma (Figure S7d). After 20 Ma both Models 1 and 2 similarly predict subduction of the final East Asian Sea remnants; collision between a northern Philippine Sea plate arc and the Eurasian continental margin near the Ryukyus and Japan around 22 to 15 Ma; a NE-SW transform margin between the southern Philippine Sea plate and Caroline Sea after 15 Ma and highly oblique subduction at the Manila trench (e.g., Figures 24 and S7). In contrast to Model 1, Model 2 allowed little to no rotation of the Philippine Sea plate and could not accommodate the migrating trench-trench-trench triple junction near Tokyo of Model 1b (supporting information Movie S2).

5. Discussion

In this study we have unfolded 28 subducted slabs within the upper 1300 km of the East Asian mantle (Table 1). We were able to successfully fit together the most important of these slabs within the space defined by the positions of the major existing Pacific, Australian, and Eurasian/Sundaland plates at 52 Ma, which was defined independently using a standard global plate model (Figures 5 and 23). The unfolded slabs were fit together using a straightforward procedure of sequential vertical projection to the Earth surface (Figure

S4). The 28 slabs have a total unfolded surface area of ~7.16×10^7 km^2 (Table 1), which is about one third larger than the present-day Eurasian landmass and ~25% of the Earth's oceanic lithosphere. This makes our study arguably the most extensive attempt to reconstruct plate tectonics using mapped and unfolded slabs as quantitative constraints.

Our slab-constrained plate models based on global tomography naturally have lower spatial and age resolution relative to traditional plate-tectonic reconstructions constrained only by Earth surface data, such as bathymetry and seafloor magnetic anomalies. However, in areas like East Asia dominated by subduction, traditional plate tectonic reconstructions suffer severely from large unconstrained regions of missing lithosphere (e.g., Figure 5). We have shown that large subducted slabs, once mapped and unfolded, can supply important first-order constraints in spite of the low spatial resolution of their edges (e.g., Figure 23). Even in tectonically intricate areas such as the Philippines, eastern Indonesia, and offshore north and east Australia where some slabs are small relative to their spatial resolution, the existence and location of these slabs helps to constrain the existence, location, and timing of transient subduction events (e.g., the Deep Ontong slab constrains the location of Caroline Sea opening attached to the Pacific plate, Figures 23 and 24). It is for these reasons that our plate models are successful at offering new insights for East Asian plate tectonics back to the time of global Eocene plate reorganization ~52 Ma, including relatively intricate intraoceanic subduction zone configurations and detailed motion histories for the enigmatic Philippine Sea plate. In this section we briefly discuss the plate model predictions and examine their implications for the Cenozoic to present-day geological history of East Asia.

In this study we found that two distinct classes of slab-constrained plate models are possible, each having different Philippine Sea plate starting positions, plate rotation histories, and geological implications. Our preferred Model 1 involves Philippine Sea nucleation above the Manus plume, near the western Pacific plate boundary, with large clockwise whole-plate rotation (Figures 24 and 25a). The alternative Model 2 has Philippine Sea nucleation north of the Australian plate with subsequent northward motions and minimal rotation (Figures S7 and 25b). Both plate models incorporate minimal input from regional geology and Philippine Sea plate paleomagnetism (see method in section 2.4). We now discuss our Philippine Sea plate models against these constraints and published plate models in the following sections 5.1 and 5.2. In section 5.3 we summarize the comparisons and justify of our preference for Model 1. In section 5.4, several major East Asian tectonic events that were robustly predicted by both plate models will be examined. These include a newly proposed Miocene Philippine Sea plate arc-continent collision at the Eurasian Ryukyu-Japan margin, and a possible Miocene arc-arc collision between the Izu-Bonin-Marianas arc and the proto-Marianas arc at the eastern edge of the East Asian Sea. Section 5.5 discusses the potential origins of the East Asian Sea vanished oceans. Our reconstruction of the Caroline Sea plate with Pacific-like motions plays a critical role in our models, and we discuss this component against alternative models in section 5.6. In section 5.7 we briefly discuss our plate model implications for South China Sea and proto-South China Sea tectonic histories due to their implications for Cenozoic regional plate reconstructions. Finally, our 28 retrodeformed slabs provide a rich history of the East Asian mantle back to the early Cenozoic, and we examine their geodynamic implications for slab sinking rates and reconstructing other convergent regions in section 5.8.

5.1. Comparison to Published Philippine Sea Plate Paleomagnetism

5.1.1. Paleolatitudes

Figure 26 shows a comparison of predicted time histories of latitude for Models 1 and 2 against published paleolatitudes at six widely separated Philippine Sea plate locations. We note that at three locations Models 1 and 2 make very different predictions (Figures 26a, 26e, and 26f), which result from contrasts in whole-plate rotation between the models. At the remaining three locations, Models 1 and 2 make similar predictions for paleolatitudes (Figures 26b–26d). In these studies near-equatorial paleolatitudes can be interpreted in either the Northern or Southern Hemisphere given age uncertainties; these important equatorial ambiguities were indicated by hollow brown squares in Figure 26. We will first consider the ODP Site 1201 paleolatitudes [*Richter and Ali*, 2015], which we regard as our most important point of comparison because of (1) its long time series (0 to 47 Ma) relative to the Philippine Sea plate age and (2) its central Philippine Sea location, far from plate boundary deformation zones. In addition, our Model 1 and 2 latitudes at ODP1201 diverged significantly prior to ~20 Ma (Figure 26a), and therefore, the published ODP1201 paleolatitudes may help distinguish between our models.

Models 1 and 2 latitudes were both viable within the ODP1201 paleolatitude constraints due to equatorial ambiguity in the ODP1201 47 Ma constraint (Figure 26a). We prefer Model 1 based on its closer fit to the full suite of ODP1201 observations when the 47 Ma constraint is interpreted north of the equator (Figure 26a). *Richter and Ali* [2015] acknowledged a northern location for the ODP1201 at 47 Ma was possible but argued for a Southern Hemisphere interpretation based on comparison to other DSDP and ODP site paleolatitudes and to the *Hall* [2002] and *Queano et al*. [2007] plate reconstructions. Our results suggest that a Northern Hemisphere location for ODP1201 at 47 Ma should not be dismissed (Figure 26a). We also argue that the published Philippine Sea paleolatitudes from the earliest plate history (Figure 3a) have sufficient uncertainty to accommodate both Models 1 and 2 origins (see also discussion of ODP Site 294 at 50 ± 5 Ma, section 4.2).

Our modeled absolute Philippine Sea positions were dependent on our chosen moving Indo-Atlantic hot spot mantle reference [*O'Neill et al*., 2005]. To test its effects, we output our Philippine Sea plate models within an alternate *Torsvik et al*. [2008] global moving hot spot mantle reference for comparison to ODP1201 (Figure S6). Model 1 predicted latitudes within the Torsvik mantle reference continued to fit within the published ODP1201 paleolatitudes whereas Model 2 predicted latitudes fell outside (up to 4° south) of paleomagnetic error bounds at 30–35 Ma (Figure S6). Therefore, Model 1 is robust within either mantle reference whereas Model 2 is more viable with our chosen mantle reference (Figure S6). We conclude that Model 1 is our preferred plate model because it shows a superior fit to ODP1201 paleolatitudes, especially at ~25–35 Ma (Figure 26a), and is also robust within an alternate mantle reference (Figure S6).

Our modeled latitudes for the Izu-Bonin sites at the northeast Philippine Sea plate generally fit within widely scattered published paleolatitudes (Figure 26b). Between 0 and 25 Ma our modeled latitudes were inside error limits but systematically offset about 5° north of the published paleolatitudes (Figure 26b). We argue that the published Izu-Bonin paleolatitudes are suspect because other Philippine Sea paleolatitude studies also show more northerly values over the same time period (Figure 3a), including recent studies from the northern Philippine Sea, southern Philippine Sea, Luzon, and ODP 1201 [*Ali and Hall*, 1995; *Queano et al*., 2007; *Richter and Ali*, 2015; *Yamazaki et al*., 2010]. The suspect 0 to 25 Ma Izu-Bonin paleolatitudes also compared poorly to other Philippine Sea plate models [*Hall et al*., 1995c].

At Luzon and the Benham rise ODP Site 292 both our modeled latitudes showed a good fit to the published paleolatitudes (Figures 26c and 26d). Our two plate models produced comparable latitudes for these locations (Figures 26c and 26d), and therefore, we cannot distinguish between our models on the basis of these sites. The 40 Ma Luzon paleolatitude could be interpreted within either the Northern or Southern Hemisphere due to its proximity to the equator (Figure 26d). Both our models agree with the suggestion that Luzon was more likely at the southern subequatorial location at 40 Ma [*Queano et al*., 2007] (Figure 26d).

The easternmost Saipan-Guam and southernmost Palau sites also show the large contrasts between our Models 1 and 2 predicted latitudes (Figures 26e and 26f), similar to ODP 1201. The differences between the Models 1 and 2 latitudes once again can be traced to the large clockwise Philippine Sea plate rotations in Model 1 compared to minimal rotations in Model 2 (Figure 25). Therefore, comparison of our modeled latitudes to these sites should in theory help distinguish between our models. Unfortunately, both Models 1 and 2 latitudes show relatively comparable fits to the published constraints due to paleomagnetic ambiguity near the equator, wide errors, and lack of long time series at single locations (Figure 26e). At Saipan-Guam we noted that rotational Model 1 showed a better fit to the published paleolatitudes between 15 and 25 Ma whereas the nonrotational Model 2 predicted latitudes that are slightly too far south by 4 to 5° (Figure 26e). Both Models 1 and 2 fall outside the 13 Ma Saipan-Guam paleolatitude error bounds by 1 to 2° (Figure 26e). Although not shown in Figure 26e the migrating Japan trench triple junction Model 1b had a better fit and showed a more northerly ~13°N latitude at 13 Ma (see supporting information Movies S1–S3). As Model 1b is a variant of Model 1, we suggest that the Saipan-Guam 13 Ma paleolatitude can fit the range of possibilities within Model 1 but is less easily more accommodated within the nonrotational Model 2. We ignore comparisons to the improbable, widely scattered published Saipan-Guam values between 0 and 4 Ma (Figure 26e). In summary, we conclude that both Models 1 and 2 generally fit the Saipan-Guam and Palau paleolatitudes, with rotational Model 1 showing a slightly better fit to Saipan-Guam.

5.1.2. Whole-Plate Rotation From Time Variation in Differential Paleolatitudes

It should be noted that the two paleolatitude time series in the West Philippine basin (ODP sites 292 and 1201, Figure 1) suggest significantly different total changes in paleolatitude since 40 Ma, based on simple least squares fitting of the two time series prior to 20 Ma (Figures 26a and 26c). However, we note that the

two time series were undertaken in different studies [*Louden*, 1977; *Richter and Ali*, 2015] making any such comparison is necessarily tentative. The current difference in latitude is 3.5°, in contrast with the current angular separation between the sites of 10.6°, whereas their difference in paleolatitude is about ~9–10° at 40 Ma and ~7° at 25 Ma (Figure 27a). This observation suggests that the line connecting ODP 292 and 1201, which has a current azimuth of 19°, had an orientation at 40 Ma close to NS (cf. Figures 27c and 27d). Furthermore, the differences in rates of change in paleolatitude during the period 25 to 40 Ma (Figures 26a and 26c) are consistent with clockwise whole-plate rotation during this period.

These observations do not lead to very robust estimates of the whole-plate rotation history given the uncertainties in paleolatitudes, ages, and history of seafloor spreading in the West Philippine basin between the two ODP sites. Nevertheless, if we correct the differential paleolatitudes using our seafloor spreading model we can obtain estimates of whole-plate rotation of the West Philippine basin that are consistent with predictions of our preferred plate-tectonic Model 1 (Figure 27b), whereas the nonrotational Model 2 is inconsistent with these observations. This agreement should be no surprise because the paleolatitudes already agree reasonably with Model 1 (Figures 26a and 26c). These results are also consistent with a tentative rotation estimate based on declinations of 47 Ma basalts from ODP 1201 present-day field overprints [*Richter and Ali*, 2015] (Figure 27b).

5.1.3. Rotation From Paleomagnetic Declinations

Philippine Sea paleomagnetic declinations indicate increasing clockwise rotation with age up to a maximum of ~110° at about 40 Ma (Figures 3b and 28). The extent to which this reflects whole-plate rotation as opposed to small-block tectonic rotations has been controversial, particularly because almost all declination data come from widely scattered land sites close to the plate margins, which is an environment in which small block rotations have been widely documented in southeast Asia and elsewhere (see review in section 1.2). Furthermore, declination data younger than ~20–25 Ma indicate rotations that are greater than the maximum possible rotations allowed by the size of the Philippine Sea plate relative to the space into which it must fit (Model 1b approximates this maximum allowed 0–25 Ma rotation, see supporting information Movie S2). Differences in rate of change in paleolatitude with time between ODP Sites 292 and 1201 in the West Philippine Basin, as well as Saipan and Guam data, are consistent with large clockwise rotation (~60°) but insufficient to accurately constrain the rotation history, as discussed above (Figure 27b). Therefore, it appears likely that both small-block and whole-plate rotations are present and need to be deconvolved.

In this section we compare observed paleomagnetic declinations with plate model predictions. Figure 27 shows a comparison of our modeled rotations relative to published paleomagnetic declinations at three sites near the eastern Philippine Sea plate margin (i.e., Izu-Bonin, Marianas, and Palau). As expected, the rotational Philippine Sea plate Models 1 and 1b showed large (maximum ~80°) predicted clockwise rotations, whereas the nonrotational Model 2 predicts minimal rotations (±25°) that can be ascribed to opening of adjacent back-arc basins (Figure 27). Both Models 1 and 2 predict declinations that are generally less than observed declinations (Figure 28); therefore, both plate models require a component of small-block rotation to explain the observed declinations. We consider that both models are viable from the limited perspective of paleomagnetic declination constraints because any gaps between the modeled and observed rotations could be ascribed to block rotation. Nevertheless, the two models have different implications for local small block rotation at the Philippine Sea plate margins, as we briefly discuss these below.

The Model 1 predicts a progressive increase in Philippine Sea plate clockwise rotations with time that lie ~20 to 40° below the maximum published values (Figure 28a). Therefore, one possible interpretation is that about 20° to 40° local small block rotation has occurred at the Izu-Bonin, Marianas, and Palau sites. These small block rotation magnitudes seem reasonable considering our model predicts long-lived dextral shear along the eastern Philippine Sea plate margin, which would be favorable conditions to produce clockwise local block rotation (Figures 24 and 25a). A second possible explanation is that our 52 Ma the starting Philippine Sea plate orientation for Model 1 was underrotated by 20 to 40°. This is possible as greater Philippine Sea plate clockwise rotations are allowable within Model 1 due to uncertainties in Philippine Sea size, shape, and orientation at 52 Ma relative to the reconstruction gaps (Figures 23a and 23b). Our current Model 1 rotation values reflected our choice to align the Izu-Bonin-Marianas arcs along an inferred Pacific plate boundary at 52 Ma (Figure 24a). Model 1b had a migrating Japan trench triple junction between 23 and 6 Ma instead of the fixed Japan trench triple junction in Model 1 (see supporting information Movies S1–S3). The Model 1b showed slightly elevated Miocene rotations that were effectively indistinguishable from Model 1 relative to published

declinations (Figure 28a). Therefore, we conclude that both Models 1 and 1b are equally viable within the published Philippine Sea plate declinations.

Large clockwise rotation Philippine Sea plate have been proposed by a number of paleomagnetic studies, as reviewed in section 1.2 [*Hall et al*., 1995c; *Keating and Helsley*, 1985; *Koyama et al*., 1992; *Yamazaki et al*., 2010]. The more testable solutions include a proposed clockwise 90° Philippine Sea plate rotation between 50 and 15 Ma around a pole at 23°N, 162°E with a mean angular velocity of 2.57°/Ma based on a fit to paleolatitudes [*Yamazaki et al*., 2010]. For comparison we calculated a single-pole Model 1 solution of 22.4°N, 149.4°E, 1.80°/Ma that shows similarities to *Yamazaki et al*. [2010]. However, we prefer that plate rotations should begin later at 40 Ma based on a plume origin as discussed below. *Hall et al*. [1995c] modeled rotation poles against published paleomagnetism and proposed a detailed and discontinuous rotation history in which the Philippine Sea plate rotated clockwise 50° between 50 and 40 Ma, 34° between 25 and 5 Ma, and 5° between 5 and 0 Ma. Model 1 shows similarities to the large clockwise rotations of *Hall et al*. [1995c], but our model suggests that the timing of initial rotation could be later at 40 Ma. Using our new slab constraints, Model 1 suggests that the majority of Philippine Sea plate rotations were driven by collision with a west moving Caroline Sea plate, which began spreading around 36 Ma due to an eruption of the Caroline plume several Ma earlier (Figure 24). We therefore suggest that clockwise Philippine Sea rotations began later around ~40 Ma (Figure 28a), much later than the initial rotations of *Hall et al*. [1995c] or *Yamazaki et al*. [2010]. Published Philippine Sea plate declinations peak at 40 Ma, and there are no indications of additional rotations before 40 Ma (Figures 3b and 28).

Our Model 1 suggests that clockwise rotation of the entire Philippine Sea plate continued in a relatively continuous fashion until the mid-Miocene to latest Miocene, or later (Figure 28a). We cannot more accurately constrain the end of Philippine Sea plate rotations because they are mainly the consequence of our plate model inputs. In any case, we agree with *Hall* [2002] that by 25 Ma, a substantial portion of Philippine Sea plate rotation had already occurred (Figure 24). By ~25 Ma, our slab constraints suggest that the Philippine Sea plate was essentially trapped between the major regional Pacific, Eurasian, and Indo-Australian plates and was driven northward by the Indo-Australian plate with less rotation (Figure 24). This can explain the apparent similarities in Philippine Sea and Indo-Australian plate northward motions after 25 Ma and possibly earlier (Figure 3a). There is also geological and paleomagnetic evidence from the Sorong fault zone that the southern Philippine Sea plate collided and formed a left-lateral shear zone with northern Australia around 25 Ma [e.g., *Ali and Hall*, 1995].

Model 2 has no whole-plate Philippine Sea rotation (Figures 25b and S7) and therefore implies that the majority (up to 80°) of published clockwise declinations were due to local small block rotations at the plate margins. As already discussed for Model 1, these rotations are within the realm of possibility [e.g., *Ali et al*., 1996; *Lee et al*., 1991; *Weiler and Coe*, 1997, 2000] especially since Model 2 predicts that the Izu-Bonin, Marianas, and Palau sites were located along a clockwise plate boundary shear zone (Figure 25b). Other minimal rotation Philippine Sea plate models also similarly infer large local block rotations at the Philippine Sea plate margins [e.g., *Byrne and DiTullio*, 1992; *Jolivet et al*., 1989; *Seno and Maruyama*, 1984; *Zahirovic et al*., 2014]. In summary, we conclude that Models 1, 1b, and 2 are not easily differentiated from the limited perspective of paleomagnetic declination data alone. We prefer Models 1 and 1b on the basis of their simpler explanation for published Philippine Sea plate declinations, specifically that the entire Philippine Sea plate has rotated clockwise up to 80° with additional small (20° to 40°) local block rotations. Furthermore, it appears likely that we can exclude nonrotational Model 2 and favor Model 1 based on contrasting rates of change in paleolatitude for the two paleomagnetic time series ODP 292 and 1201 from the West Philippine basin, even though observational uncertainties do not allow a very well constrained rotational history (see Figure 27b).

5.2. Comparisons to Philippine Sea Plate Geology

5.2.1. Philippine Sea Plate Origin

The origin of the Philippine Sea plate has been widely debated [*DeBari et al*., 1999; *Hickey-Vargas*, 1998; *Uyeda and Ben-Avraham*, 1972]. Our Models 1 and 2 also offer very different predicted Philippine Sea plate starting locations (e.g., Figure 25) that we discuss here. Our preferred plate Model 1 suggests the Philippine Sea plate originated above the Manus plume (Figure 24), assuming that the plume has been relatively fixed within our moving hot spot mantle reference [e.g., *O'Neill et al*., 2005]. Our Manus plume location was interpreted from a vertically extensive, slow tomographic anomaly near 150°E/0° (Figures 16 and 17b) under an active magmatic

area and interpreted hot spot in the eastern Bismarck Sea with plume-like helium isotope signatures [e.g., *Johnson et al*., 1978; *Macpherson et al*., 1998]. A plume-like conduit was also detected in the lower mantle below the Bismarck Sea (i.e., the Indonesia anomaly) by a recent global shear wave velocity model SEMUCB-WMI [*French and Romanowicz*, 2015]. The observed deep mantle conduit and plume-like geochemistries both suggest the viability of showing a long-lived and stable Manus plume in our plate models.

A Philippine Sea plate plume origin is consistent with a number of features within the West Philippine basin, including ocean island basalt (OIB) isotopic signatures [*Hickey-Vargas*, 1998], widespread uplift [*Chamley*, 1980], widespread high heat flow inferred from the Izu-Bonin-Marianas boninites [*Macpherson and Hall*, 2001], highly disorganized seafloor spreading [*Deschamps and Lallemand*, 2002], and a proposed hot spot track documented in the West Philippine basin [*Ishizuka et al*., 2013]. A Philippine Sea plate origin specifically from the Manus plume was first proposed based on a geochemical comparison of Philippine Sea plate lavas and a modeled Manus plume track along the Kyushu-Palau ridge [*Hall*, 2002; *Macpherson and Hall*, 2001]. Other studies have also reconstructed the early Philippine Sea plate above an unspecified mantle plume [e.g., *Deschamps and Lallemand*, 2002; *Ishizuka et al*., 2013]. Our Model 1 slab constraints and paleolatitude data of the Benham rise hot spot (ODP Site 262) support a Manus plume origin for the Philippine Sea plate in association with the Benham rise-Urdaneta plateau-Oki-Daito plume track [*Ishizuka et al*., 2013], discussed below.

Plume-driven, oceanic plateau formation near the West Philippine basin spreading center until ~35 Ma has been proposed based on bathymetry, geochemistry, and age dating of the Benham rise-Urdaneta plateau-Oki-Daito rise volcanic chain [*Ishizuka et al*., 2013]. Their model predicted a subducted plateau within the Philippine trench slab [*Ishizuka et al*., 2013] that is consistent with an anomalous slow seismic velocity zone within our mapped Philippine Trench slab (Figure 14). An important implication is that the West Philippine basin formed at a fixed spot (i.e., a mantle plume) centered near the West Philippine spreading axis [*Ishizuka et al*., 2013], a scenario that seems likely given the overlapping timing of West Philippine Basin spreading and the Benham rise-Urdaneta plateau-Oki-Daito rise plateau ages. Other Philippine Sea plate models that have considered a plume origin have also invoked a stationary Philippine Sea plate until 35 Ma [*Deschamps and Lallemand*, 2002]. In contrast, the *Hall* [2002] model nucleated the Philippine Sea plate at 55 Ma above the Manus plume but then moved the plate rapidly westward. By 40 Ma, the Benham rise-Urdaneta-Oki-Daito oceanic plateaus of the West Philippine basin were displaced more than 2000 km west of their starting location [*Hall*, 2002], too far to have received continued magmatism from a near-stationary Manus plume. In contrast, Model 1 has the Philippine Sea plate stationed near the present location of the Manus plume until 40 Ma (Figures 24 and 29). Our slab constraints show no reason to move the Philippine Sea plate until after ~40 Ma, when the plate began to be driven westward by the nucleating Caroline Sea plate (Figures 24 and 29c).

Our alternative plate Model 2 proposes that the Philippine Sea plate originated north of the Australian margin in the early Cenozoic (Figures 25b and S7). A Philippine Sea plate origin north of Australia was proposed by the earliest reconstructions and as well as more recently [e.g., *Deschamps and Lallemand*, 2002; *Jolivet et al*., 1989; *Uyeda and Ben-Avraham*, 1972; *Xu et al*., 2014]. A northern Australian Philippine Sea plate origin is intriguing as it places the Mesozoic core of the Philippine Sea plate (i.e., the Oki-Daito province) close to other Mesozoic-aged ocean crust of the Indian Ocean and Molucca Sea (Figure S7a). We found that the northern Australian-Philippine Sea origin also allowed the contemporaneous West Philippine basin and Celebes Sea spreading events to be connected (Figure S7b). This style of reconstruction has been favored by several other studies [*Deschamps and Lallemand*, 2002; *Gaina and Müller*, 2007; *Hall*, 2002]. A potential weakness of Model 2 is that it requires the Philippine Sea plate to have formed above a plume that no longer exists today, a challenge that is also acknowledged by other similar plate models [e.g., *Deschamps and Lallemand*, 2002]. A further weakness of Model 2 is that at 52 Ma, it places no presently recognized lithosphere in the large eastern equatorial hole extending east of the Manus plume (Gap 1 in Figure 23).

5.2.2. Philippines-Luzon Arc

Models 1 and 2 differ significantly on their predictions for the Eocene to Oligocene history of the western Philippine Sea plate boundary that includes the Philippine archipelago and Luzon (Figure 25). Although our plate models did not attempt to reconstruct the Philippines in detail, our modeled positions were viable with respect to published paleolatitudes (Figure 26d), and we can examine our predictions against Philippines-Luzon geology at a coarse scale. Models 1 and 2 differ most on their predictions for Oligocene magmatism at Luzon. In Model 1, Luzon experienced long-lived Eocene to Oligocene subduction along the western Luzon margin except for a mid-Eocene to late Eocene hiatus between 40 and 33 Ma due to transform

motions (see supporting information Model 1 in Movie S1). In contrast, Model 2 predicts that Luzon and the Philippines were primarily along a transcurrent plate boundary and would have had minimal subduction-related magmatism since the early Cenozoic (supporting information Model 2 in Movie S3). *Deschamps and Lallemand* [2002] reviewed Philippines magmatism and found widespread Eocene-Oligocene magmatism at Luzon that was interrupted by a potential hiatus between 43 and 36 Ma. Other studies similarly indicate magmatic activity at Luzon in the Eocene to Oligocene [e.g., *Florendo*, 1994; *Hollings et al*., 2011]. These magmatic patterns best fit Model 1 and are less compatible with Model 2. South of Luzon, the Philippine archipelago also shows widespread Eocene and Oligocene volcanism [*Deschamps and Lallemand*, 2002], but a finer-scale reconstruction would be required to properly assess these areas.

5.2.3. Palau Arc

The Palau arc indicates that the SE Philippine Sea plate margin has experienced some plate convergence during its history. Various studies have indicated Palau volcanism in the early Oligocene to early Miocene [*Meijer et al*., 1983] and/or possibly the Eocene [*Cosca et al*., 1998; *Meijer et al*., 1983], but it is generally agreed that dates are uncertain. Model 1 suggests that Palau had a history of convergence from the Eocene to mid-Oligocene that could be compatible with its magmatic record (Figure 24). Model 1 predicts that Palau was first situated above a Pacific subduction zone in the Eocene, then experienced a collision with the Caroline plate between the late Eocene to mid-Oligocene, and then separated from the Caroline plate from 28 to 15 Ma due to clockwise Philippine Sea plate rotations (supporting information Model 1 in Movie S1). In contrast, in Model 2 the Palau arc was located along a trailing edge of the Philippine Sea plate that did not experience significant convergence until the mid-Miocene (supporting information Model 2 in Movie S3). Therefore, Model 2 is less compatible with the Palau arc history, although it is possible that unknown spreading events within the East Asian Sea produced the plate convergence along the Palau margin. We note that published plate models that move the Caroline and Philippine Sea plates together [e.g., *Deschamps and Lallemand*, 2002; *Hall*, 2002; *Zahirovic et al*., 2014] would also have difficulty explaining any post-Eocene Palau volcanism, since the Palau margin would be trapped between the coupled plates after 40 Ma. However, there is sufficient ambiguity in our current understanding of the Palau arc to accommodate these models.

5.2.4. Halmahera Arcs

Halmahera is a collection of Cretaceous to present-day arcs formed on early Mesozoic ophiolitic basement [*Hall et al*., 1988]. Paleomagnetic evidence indicates that the Halmahera arcs have been at low latitudes (±10°) since the Cretaceous ~80 Ma [*Ali and Hall*, 1995]. The arcs were possibly in the Northern Hemisphere prior to 45 Ma [*Ali and Hall*, 1995]. After the early Miocene Halmahera moved ~10° northward to its present equatorial position from the Southern Hemisphere [*Ali and Hall*, 1995; *Hall et al*., 1995a]. The paleomagnetic and magmatic history of Halmahera arcs have been used as key constraints for Philippine Sea plate motion histories [*Ali and Hall*, 1995; *Hall*, 2002; *Hall et al*., 1995a]. However, it has not been fully established whether Halmahera was coupled to the Philippine Sea plate during its entire history (see review in section 1.2). Halmahera was only shown after 20 Ma in our study, but we can infer some of its earlier history from our plate models. We placed Halmahera at the southern Philippine Sea and to the east of our Molucca Sea east slab at 20 Ma (Figure 24d) based on its arc magmatic history relative to the Molucca Sea [*Baker and Malaihollo*, 1996; *Hall et al*., 1995b]. This position implied that Halmahera was at ~10°S and just north of our restored northern Australian plate boundary at 20 Ma (Figure 24d), which is roughly consistent with paleomagnetism, geological studies, and published plate reconstructions [*Ali and Hall*, 1995]. Our modeled 20 Ma position was also near the western limit of the southern Caroline arcs (Figure 24d).

Our plate Model 1 suggests two possible ways that Halmahera can be reconstructed to a subequatorial Northern Hemisphere position at the early Cenozoic. First, Halmahera could have moved with the southern Philippine Sea plate as envisioned by *Hall* [2002]. Alternatively, Halmahera moved with the southern Caroline arcs from an initial position along our restored Pacific-East Asian Sea plate boundary in the early Cenozoic (see Model 1 in Movie S1). In this scenario, Halmahera was transferred to the Philippine Sea plate from the Caroline arcs in the late Oligocene to early Miocene and therefore did not move with the Philippine Sea plate for its entire history.

5.2.5. Huatung Basin

The Huatung basin offshore eastern Taiwan is undrilled and has an enigmatic tectonic history [cf. *Deschamps et al*., 2000]. Our northern Philippine Sea slab mapping showed a markedly shorter ~500 km Huatung basin slab relative to the 700 to 1000 km length Ryukyu slab (Figure 14). This suggests that the Huatung basin could be allochthonous to the adjacent West Philippine Basin, and this is further reinforced by interpreted shear and

convergence at the eastern Huatung basin boundary along the Gagua ridge [*Deschamps et al*., 1998; *Eakin et al*., 2015]. Our preferred plate Model 1 indicates that the Huatung basin is a preserved East Asian Sea fragment (Figure 24), and later in section 5.5, we infer that the East Asian Sea was likely Cretaceous-aged based on regional tectonics. This would be consistent with an early Cretaceous age for the Huatung basin from radiometric dating (115–125 Ma), radiolarians (115 Ma), and geomagnetic modeling (119 to 131 Ma) [*Deschamps et al*., 2000]. However, other geophysical studies suggest that the Huatung basin is younger and formed in the Eocene [*Hilde and Lee*, 1984], Oligo-Miocene [*Kuo et al*., 2009], or in two episodes between the Eocene and Miocene [*Sibuet et al*., 2002]. A Cenozoic age for the Huatung basin age could be feasible within our Model 2 reconstruction that placed the Huatung basin near eastern Sundaland and nucleating Celebes Sea in the Eocene, but we consider Model 2 inferior to Model 1 based on Philippine Sea paleomagnetism (see section 5.1).

5.3. Summary of Comparisons Between Models 1 and 2

The results from this paper constrain Philippine Sea plate reconstructions into two distinct classes of solutions (Figure 25). The two solutions correspond to two possible near-equatorial starting points for the small Mesozoic initial nucleus of the Philippine Sea plate, which we identified as regions of missing lithosphere (i.e., Gaps 1 and 2) in a 52 Ma reconstruction of existing East Asian lithosphere and subducted slabs (Figures 23 and S4). Our preferred Model 1 and its variant Model 1b suggest that the Philippine Sea nucleus started in Gap 1 above the Manus plume at 150°E/0° near a Pacific transform (Figures 24, 25a, 29, and supporting information Movies S1–S2). The Philippine Sea was driven westward and rotated ~80° clockwise after 40 Ma by the westward moving Caroline Sea-Pacific. Alternative Model 2 suggests the Philippine Sea originated near northern Australia and was driven northward by the Australian plate with little rotation (Figures S7, 25b, and supporting information Movies S3).

At present, we consider both classes of plate model viable, broadly satisfying a number of available observational constraints, the most important of which are summarized below. Nevertheless, in four to five of the following comparisons between models and observations, the available evidence favors our preferred rotational Manus plume Model 1 over the nonrotational Australian Model 2:

1. Both models have potential sites of origin for the Mesozoic nucleus of the Philippine Sea plate, as defined by two sites (gaps) of significant missing lithosphere in the 52 Ma reconstruction (Figure 23) and very limited paleolatitude data. Model 1 is more successful in that it fills both holes with lithosphere, whereas Model 2 leaves the elongate eastern hole empty (gap 1 in Figure 23) with no presently known lithosphere to fill it.
2. Model 1 originates at a reconstruction hole near the present-day Manus plume, agreeing with the paleolatitude of the Benham Rise hot spot track. No current hot spot exists near the site of origin of Model 2.
3. Both models agree with the existence of subducted slabs between the Caroline plate and the southern Philippine Sea plate, in contrast with previous models.
4. Both models broadly satisfy paleolatitude data at widely separated sites (Figure 26). Nevertheless, Model 1 provides a better overall match to data at the ODP 1201 long time series in the West Philippine basin and to Saipan, Guam, and a set of offshore sites (Figures 26a, 26e, and S6). Model 2 provides a simple explanation for the northward motion of the Philippine Sea plate, similar to the Australian plate (Figure 2a). Northward motion of Model 1 is supplied by rotation driven by the Caroline/Pacific plate after 40 Ma, followed by northward extrusion after ~20–25 Ma, also driven by the Caroline/Pacific plate (Figure 24).
5. Rotational Model 1 satisfies large clockwise rotation suggested by differential changes in paleolatitude between ODP sites 292 and 1201 in the West Philippine basin (Figure 27). In contrast, the nonrotational Model 2 does not satisfy these observations.
6. Model 1 broadly agrees with the widespread observation of large clockwise rotation based on paleomagnetic declination data but requires some additional local block rotation in addition to whole-plate rotation (Figure 28). Model 2 requires that the declination data reflect local block rotation. Model 1 provides a mechanism for the clockwise whole-plate rotation and its timing in terms of interactions with the Caroline plate, linked to the Pacific motions.
7. History of plate convergence in Model 1 properly predicts current understanding of the history of Eocene-Oligocene arc magmatism in the Philippines, as well as Palau (Figure 25a), whereas Model 2 is less successful, predicting largely transform, nonconvergent motions at this time (Figure 25b).
8. Both models predict Miocene arc-arc collision of the Philippine Sea plate with the Ryukyu-southwest Japan margin (Figure 30).

9. Both models provide straightforward explanations for the existence of the East Asian Sea flat slabs and fixed Marianas Pacific subduction (e.g., Figures 19, 20, and S3).
10. Model 2 provides a straightforward explanation for the close link between the Molucca Sea and Philippine Trench slabs (Figures 14 and 21) and provides a link between the spreading of the West Philippine basin and Celebes Sea (Figure S7b). Model 2 assumes a transform attachment of the two plates, similar to the transform attachment of the Cretaceous Huatung basin to the West Philippine Basin (Figure 29).
11. The dominantly northward trajectories of both models since ~20 Ma, with secondary westward motion, are confirmed by the incorporation of ~15 Ma East Taiwan Ophiolite of South China Sea axial ridge origin into the accretionary complex of the Coastal Range of eastern Taiwan (e.g., Figures 30c and 30d).

In summary, we prefer Model 1 based on its superior fit to: (1) published paleolatitudes at ODP Site 1201 and differential changes in paleolatitude between ODP 292 and 1201 in the West Philippine basin, consistent with large clockwise rotation, (2) published declinations that suggest large whole-plate clockwise rotations, and (3) Luzon-Philippines and Palau Oligocene to Eocene magmatic histories, in comparison to model plate trajectories. In addition, Model 1 fills both reconstruction gaps at 52 Ma with significant known lithosphere, whereas Model 2 does not (Figure 23). Finally, the Benham Rise-Oki-Daito rise hot spot track has a well-defined origin near the current location of the Manus plume in Model 1, in agreement with paleolatitude constraints.

5.4. Predicted Philippine Sea Plate Collisional Events

5.4.1. Miocene Arc-Arc Collision Between the Northern Philippine Sea Plate and the SW Japan and Ryukyu Continental Margin

The existence of a major Miocene arc-arc collision between the Philippine Sea plate and Eurasian SW Japan-Ryukyu continental margin is a robust feature of both of our plate models (Figures 24, 30, and S7) for two reasons. First, our observation that the Ryukyu slab is short (~1000 km) relative to the ~20° northward Philippine Sea motion since ~40 Ma requires some form of collision to bring the northern Philippine Sea plate into contact with the Japanese Eurasian margin (Figures 3, 14, and 25). This ~20° northward motion from equatorial latitudes is robust from both paleolatitude observations (Figure 3) and the existence of two possible slab-constrained sites of equatorial origin for the Philippine Sea plate (Gaps 1 and 2; Figures 23 and S4). The expected subduction of a minimum ~1000 km of intervening ocean floor under the northward moving Philippine Sea plate is consistent with our observation of flat East Asian Sea and Pacific slabs under the northern Philippine Sea plate as far north as the Eurasian margin (Figure 20). These observations require a trench at the northern margin of the Philippine Sea plate.

Second, our regional slabs indicate a further geometric requirement that the collision took place over nearly the full ~2000 km width of the margin between the original eastern limit of the South China Sea (~400–450 km east of Taiwan) and SW Japan, given the large width to which the northern Philippine Sea plate had grown by ~20–25 Ma (e.g., see Figures 14, 17, and 25). The EW distance between the lateral constraints of the Mariana Pacific slab wall on the east and the Eurasian South China Sea slab on the west is nearly equal to the EW width of the Philippine Sea plate (Figures 18 and 22). Therefore, very little difference is possible between the orientation of the Philippine Sea plate in our models after ~25 Ma; Philippine Sea motion must be largely northward relative to Eurasia with no more than ~20° clockwise whole-plate rotation to avoid overlapping these lateral constraints. Our two plate reconstructions present closely similar scenarios for this collision (Figures 24, 25, and S7; supporting information Movies S1–S3).

Our reconstructions require the existence of a long-lived arc and subduction zone from at least 40 Ma until collision at ~20 Ma along what is now the northern margin of the subducted Ryukyu slab (Figures 24, 30, and S7). This northern margin of the slab has been close to its present orientation subparallel to the Eurasian Margin since 20–25 Ma in all our reconstructions, but prior to ~30 Ma in rotational Models 1 and 1b this leading edge of the Philippine Sea plate is oriented ~ NS and was moving rapidly westward, overriding the western East Asian Sea. Later, this trench is predicted to have run over the northern East Asian Sea, then crossed over an active EW transform between the East Asian Sea and the Pacific starting about 27–30 Ma (Figures 24c and 30a), and finally collided against the Eurasian margin near the Ryukyus and Japan islands in the early Miocene around 17 to 20 Ma (Figure 30 and supporting information Movies S1–S3).

This slab constrained Miocene arc-arc collision between the Philippine Sea plate and the Ryukyu-southwest Japan Eurasian continental margin has not been well documented or recognized in the literature, although

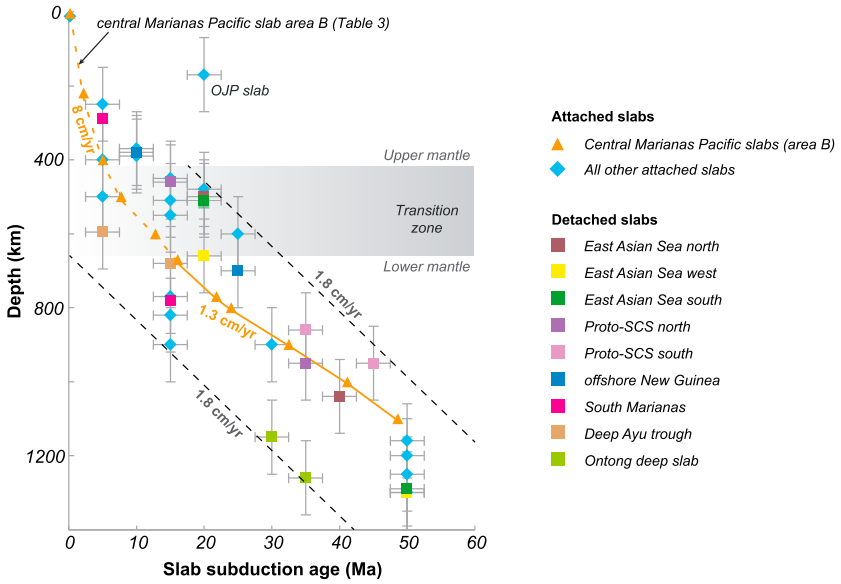

Figure 31. Age depth curve showing interpreted slabs from this study plotted from Table 1. The central Marianas Pacific slabs displayed a 1.3 cm/yr lower mantle sinking rate based on the intermediate slab "Area B." All reconstructed slabs from this study apart from the subducted Ontong Java plateau (OJP slab) fit within a 1.8 ± 0.8 cm/yr average lower mantle sinking rate. Slab sinking within the upper mantle was faster and within a 4 to 8 cm/yr range.

Hibbard and Karig [1990] clearly recognized a collision of the northern Philippine Sea plate in southwest Japan at ~15 Ma. Here we summarize fragmentary geologic evidence for an orogenic event in the area of this collision, as follows. (1) Asian-derived turbidite fans began to be deposited onto the Shikoku basin of the Philippine Sea plate starting ~15–16 Ma, indicating the arrival of the Philippine Sea plate at the Eurasian margin (Figure 30b) [*Clift et al*., 2013; *Pickering et al*., 2013]. These fans reached to ODP Site 1177 in the Shikoku basin which indicates a minimum transport onto the Philippine Sea plate of >1000 km from a Eurasian continental margin source (Figures 30b and 30c). Our Model 1b with a migrating Japan trench triple junction would reduce minimum sediment transport distances to within 500 to 600 km (see Model 1b in supporting information Movie S2). Detrital zircons indicate ultimate Yangtze River and North China craton sources [*Clift et al*., 2013], with redeposition likely given the setting of collisional continental-margin tectonics, with subaerial erosion of the margin widely documented at this time. (2) Widespread early to middle Miocene strong compressional deformation, uplift, and erosion, sealed by an upper Miocene angular unconformity, is documented in the Shimanto fore arc of southwest Japan, especially documented in Kyushu, and in Okinawa [*Letouzey and Kimura*, 1985; *Raimbourg et al*., 2014]. (3) Widespread Miocene compressive folding, uplift, and erosion at this time, capped by upper Miocene angular unconformities, is also documented in seismic images and drilling in the East China Sea, especially near the NW boundary of the Taiwan-Sinzi belt with deep Cenozoic rift basins (Figure 30) [*Cukur et al*., 2011, 2012; *Gungor et al*., 2012; *Su et al*., 2014]. Slow velocities and high anisotropic signatures from Rayleigh-wave phase velocity analysis also suggests that the southern East China Sea lithosphere has been highly deformed [*Legendre et al*., 2014]. (4) Widespread magmatism in the near-trench fore arc of southwest Japan at 14–16 Ma has been attributed to arrival of hot Shikoku Basin or arc of the Philippine Sea plate, or rapid migration of the trench-trench-trench triple junction [e.g., *Hibbard and Karig*, 1990; *Kimura et al*., 2014]. (5) A notable deceleration in Philippine Sea plate northward motions around 15 to 20 Ma based on paleomagnetism [*Richter and Ali*, 2015; *Yamazaki et al*., 2010].

5.4.2. Izu-Bonin-Mariana Arcs: An Early Miocene Arc-Arc Collision?

The Izu-Bonin-Marianas arc along the Pacific subduction system is a classic example of an intraoceanic convergent margin [e.g., *Stern et al*., 2004]. Our western Pacific slab observations place important new constraints on the location of this subduction system in a mantle reference frame since ~52 Ma (section 3.3). In particular, the central Marianas location of Pacific subduction has been relatively stationary (±200 km of its present location) since 52 Ma (Figures 15 and 18), with some possible (up to 600 km) initial rollback if the slab initially rolled back and steepened before it penetrated the lower mantle. As a consequence, our plate

reconstructions predict that a previously unrecognized arc-arc collision, amalgamation, or arc subduction event occurred between the Bonin-Marianas arc, which sits on the eastern edge of the Philippine Sea plate today, and a second, now-vanished "proto-Marianas" western Pacific arc that sat on the eastern edge of the East Asian Sea, both of which had the same polarity (Figures 24 and 30a).

It appears to be an unavoidable conclusion that the plate immediately west of the stationary central Marianas Pacific subduction zone (~15–25°N latitude) in the early Eocene could not have been the Philippine Sea plate. This is simply because in the early Eocene, the small (~600 × 700 km) Philippine Sea plate nucleus was near equatorial based on published paleomagnetism (see Figures 3, 15, and 23), which would place it about 1000–2500 km south or SW away from the fixed central Marianas subduction zone. Indeed, the Philippine Sea plate could have been even farther away to the south based on the most recent Philippine Sea paleomagnetic study, which argues for a Southern Hemisphere ~7.1°S ± 5° Philippine Sea paleolatitude in the middle Eocene [*Richter and Ali*, 2015]. Our two classes of Philippine Sea plate motion models make different predictions for how the Philippine Sea plate and the fixed central Marianas Pacific subduction zone came to be juxtaposed (cf. Figure 25), which we discuss below.

The small early Eocene (~52 Ma) nucleus of the Philippine Sea plate occupies two different possible equatorial sites in our two classes of plate model (Gaps 1 and 2 in Figure 23), giving rise to two classes of plate motion history that converge toward the present (Figure 25). In Model 1 the Philippine Sea nucleus begins in Gap 1 in the vicinity of the present position of the Manus plume and close to the ~52 Ma equatorial Pacific subduction location (Figures 19, 23, and S3 and Movie S1). The Model 1 Philippine Sea plate travels northwestward along the edge of the Pacific subduction system (Figure 25a), progressively overriding and replacing the East Asian Sea lithosphere at the surface and overriding the proto-Marianas arc from the south-southeast in the early Miocene ~23–17 Ma (Figures 24 and 25 and Movie S1). In Model 2 the Philippine Sea nucleus begins in Gap 2 adjacent to the Molucca Sea, ~3000 km to the southwest of the central Marianas (Figures 23d and S7 and Movie S2). The Model 2 nucleus of the Philippine Sea plate travels progressively northward over East Asian Sea lithosphere, but as a consequence of plate growth, the eastern convergent boundary moves toward the northeast (Figure 25b). In this model the East Asian Sea lithosphere is also overridden, with associated back-arc spreading of the Shikoku and Parece Vela Basins and collision with the proto-Marianas arc in the early Miocene ~20–17 Ma until coming into contact with the subducting Pacific (Figure S7 and Movie S2). We note that both our plate reconstructions suggest that the northern Izu arcs north of ~28°N today were not involved in the collision because they passed over an EW transform boundary onto the Pacific plate without having encountered the East Asian Sea arc (Figures 30a and S7c). The arc-arc collision was a robust feature of Models 1 and 2 (Figures 24 and S7) and is further examined below against geological observations.

Apparently, there is no direct geological evidence for a Bonin-Marianas arc-arc collision, amalgamation, or arc subduction event. The Izu-Bonin fore arc, Bonin ridge, and southern Marianas fore-arc rocks show similar ~52 Ma ages and geochemically consistent fore-arc basalt (i.e., FAB) signatures [*DeBari et al*., 1999; *Ishizuka et al*., 2011; *Reagan et al*., 2010]; these do not suggest the preservation an additional exotic accreted arc. This leaves the possibility that the proto-Mariana arc was fully subducted at the Izu-Bonin-Mariana trench during collision and disappeared with little to no trace. One potential analog for the complete disappearance of an arc is at the present-day Molucca region, where side-on arc-arc collision between the Sangihe and Halmahera arcs has caused the Halmahera arc to be almost completely overridden by the Sangihe fore arc [*Hall*, 2000]. With continued collision it is predicted that the entire Halmahera arc will disappear with almost no trace [*Hall*, 2000]. In contrast, at the Izu collision zone in Japan, end-on (i.e., orthogonal) active arc-arc collision between the Honshu and Izu arcs has left traces of the Izu arc within a complex and cryptic collision zone. The Izu supracrustal arc sequences are not easily located except possibly within two small ~5 km wide ophiolite sequences (the Mineoka and Setogawa ophiolites) [e.g., *Tamura et al*., 2010]. The Izu middle arc crust was partially melted and emplaced as plutonic bodies and the lower crust mantle was apparently delaminated [e.g., *Tamura et al*., 2010]. Reconstructions of the timing and initial configuration of the Honshu arc-arc collision continue to be highly controversial and widely debated [*Ali and Moss*, 1999; *Takahashi and Saito*, 1997; *Kimura et al*., 2014] despite the relative accessibility of this region compared to the intraoceanic Izu-Bonin-Marianas arcs.

Indirect evidence for arc-arc collision could include the dramatic change in Shikoku and Parece Vela basin spreading rate and direction at 20 ± 1.3 Ma [*Sdrolias et al*., 2004], which fits with our predicted timing of the arc-arc collision. It is also well known that the Bonin-Marianas fore arcs, including the Bonin ridge, show distinctive morphobathymetric ridges of uplifted Eocene basement that abruptly rise from the trench in

contrast to the gently sloping Izu fore arcs north of 30° [e.g., *Klaus and Taylor*, 1991; *Stern et al*., 2004]; these differences could possibly be effects of arc-arc collision. In any case, some form of Miocene juxtaposition of the fixed Marianas Pacific subduction zone with Philippine Sea lithosphere and associated loss of East Asian Sea lithosphere appears to be a robust consequence of our combination of slab, paleolatitude, and plate-size constraints. However, any detailed understanding of this juxtaposition and its implications for the presently preserved Izu-Bonin-Marianas arc and fore arc are at present necessarily tentative, requiring future studies.

5.5. Origin of the East Asian Sea Vanished Oceans

A key part of this study is our mapping of a major (8000 km × 2500 km) swath of detached lower mantle flat slabs, which we named the East Asian Sea vanished oceans (Figure 20a). The East Asian Sea slabs fit closely between the Pacific, Eurasian, and Australian plates in an early Cenozoic plate reconstruction (e.g., Figures 20c and 24), quantitatively filling a known gap in Cenozoic plate tectonic reconstructions [e.g., *Hall*, 2002; *Seno and Maruyama*, 1984; *Zahirovic et al*., 2014]. A number of lost microplates such as the "north New Guinea plate" [*Seno and Maruyama*, 1984] or "proto-Molucca Sea"-style oceans [*Rangin et al*., 1999; *Zahirovic et al*., 2014] have been previously proposed to fill this plate tectonic gap. Our slab constraints now show that these lost oceans were bordered to the west by the proto-South China Sea and shared a NW-SE boundary with the western Pacific plate boundary (Figures 4c, 20c, 24a, and 24b). Our slab-constrained reconstructions show that the East Asian Sea was completely subducted by 15 Ma due to Pacific, Philippine Sea, and Australian plate convergence (Figure 24). The final disappearance of the East Asian Sea at 15 Ma is consistent with the present-day ~500 to 660 km depths of the uppermost East Asian Sea slab fragments (Table 1) based on slab subduction timing depths from other East Asian studies [*Miller et al*., 2006] and our other mapped slabs (Figure 31) (see section 5.8).

Based on heterogeneities within the East Asian Sea slab anomalies, we divided the East Asian Sea into the northern, western, and southern East Asian Sea slab subparts (Figure 20). We suggest that our reconstructed East Asian Sea was probably not a single plate but formed of a number of smaller oceans. The northern East Asian Sea slabs are a new finding and were the "proto-Philippine Sea" in our plate models (e.g., Figure 24). Portions of the south and west East Asian Sea slabs have been previously identified from tomography to be vanished oceans [e.g., *Hall and Spakman*, 2002; *Rangin et al*., 1999]. Below we briefly discuss the possible origin of the East Asian Sea ocean basins in terms of their plate motion history. We also examine the northern East Asian Sea slabs relative to the Mesozoic to present-day tectonic history of southeast China and surrounding area.

We observed that the East Asian Sea displayed a reasonable fit with other slabs in a plate reconstruction when given an approximately stationary position within the mantle reference (e.g., Figure 24). The quasi-stationary East Asian Sea motions most resemble either the Eurasian plate or the pre-40 Ma Australian plate but are very different from the Pacific (see Model 1 in Movie S1). Therefore, it seems plausible that the pre-subducted East Asian Sea were marginal seas that were either loosely or rigidly linked to the Eurasian-Sundaland and/or Australian plates. Our plate reconstructions imply that the northern East Asian Sea were likely bordered by the proto-South China Sea to the west and the Ryukyu margin to the north (Figure 20c), both of which were probably also part of the Eurasian plate. Therefore, it seems reasonable that the northern East Asian Sea moved with Eurasian-like motions during its lifetime.

The simplest explanation for the origin of the northern East Asian Sea slabs is that they formed sometime after the mid-Cretaceous to late Cretaceous. During this period it is generally agreed that southeast China experienced a major transition from an active subducting margin to extension based on observed cessation of magmatism [*Li et al*., 2014; *Liu et al*., 2014; *Ren et al*., 2002]. Extensional tectonics was recorded by a series of oceanward younging Cretaceous to Eocene rift basins that formed along the south and east China Eurasian margin [*Ren et al*., 2002; *Sibuet et al*., 2004]. The proto-South China Sea also probably formed during this period [*Zahirovic et al*., 2014; *Shi and Li*, 2012]. Likewise, we suggest that the northern East Asian Sea formed as a back-arc basin or marginal seas adjacent to the proto-South China Sea during this period. Formation of the East Asian Sea oceans could have been accommodated by a rapid southeastward rollback, retreat, or jump of the paleo-Pacific subduction zone [*Zhou and Li*, 2000]. This scenario seems possible given our observed paleo-Pacific slabs that parallel the East Asian Sea slabs at greater depths and extend offshore from the Chinese margin (e.g., Figures 17a and 17d). At the very least, the extensive subducted slabs observed down to 1500 km depths under the current Philippine Sea plate (i.e., the northern East Asian Sea and

paleo-Pacific slabs) indicates that the region had a transient tectonic history and significant subduction history since the Cretaceous.

5.6. Caroline Sea Plate Motions: Pacific-Like or Coupled to the Philippine Sea Plate?

Our plate models showed that a Caroline Sea plate with Pacific-like motions fit well within a slab-constrained, fully animated and globally consistent plate reconstruction (e.g., Figures 24 and S7). An age-progressive Caroline LIPs-hot spot track straddles the Caroline and Pacific plates, suggesting a tectonic connection between the plates (Figure 6). We also showed that the observed Caroline LIPs track fits a Caroline hot spot track that was modeled with Pacific motions in a moving Indo-Atlantic hot spot frame (Figure 6). A Caroline Sea reconstruction with Pacific motions has also been previously suggested by other studies based on seismic profiles, paleomagnetism, petrography, radiometric dating, and plate reconstruction modeling [*Hegarty et al*., 1983; *Keating et al*., 1984; *McCabe and Uyeda*, 1983; *Yan and Kroenke*, 1993]. However, recent studies have followed *Hall* [2002] and moved the Caroline Sea with the Philippine Sea plate for most of its life [e.g., *Gaina and Müller*, 2007; *Zahirovic et al*., 2014].

The slab evidence presented in this study adds further support for a Caroline Sea reconstruction with Pacific-like motions, as follows: (1) Our mapped deep Ontong Java slabs fit the predicted proto-Caroline Sea slab location (i.e., the Pacific plate consumed during Caroline Sea opening). (2) Pacific paleotrench locations directly inferred from tomographic anomalies showed a significant (maximum 1500 km) westward advance of the southern Marianas to Yap-Palau trench segment after 32 Ma (Figure 18). The mapped paleo-Pacific trench advance in Figure 18 was consistent with the westward advance of the Caroline Sea with the Pacific in our models (Figure S8). (3) There is evidence for extensive subduction west of the Ayu Trough spreading axis, near the equator, and west of 135°E (i.e., the East Asian Sea west slabs, Molucca Sea slabs, and deep Ayu Trough slabs) (Figure 21e). When unfolded and restored, our reconstruction shows that these slabs can account for the $>$2000 km of coupled Pacific-Caroline convergence toward Eurasia since 36 Ma; subduction between the Caroline Sea and Pacific was not required. In addition, our Model 1 indicates that a young, fast-moving Caroline plate moving with the Pacific would have collided with the SE Philippine Sea in the late Eocene to early Oligocene (Figure 24c). This collisional model is consistent with the Philippine Sea plate having been pushed westward and torqued, producing clockwise plate rotations (Figure 24), a new and straightforward explanation for Philippine Sea plate rotations and extrusional motion.

Although some of our slab evidence can arguably fit other reconstructions, an important challenge for the coupled Caroline-Philippine Sea reconstruction models [e.g., *Hall*, 2002] comes from our "deep Ayu Trough" flat slabs, which were mapped at shallow 500 to 600 km depths under the Caroline Sea-Philippine Sea boundary (Figures 14, 16c, 17a, 21a, and 21e). These slabs exhibit a strong tomographic anomaly that can also be seen in other published tomography [*Hall and Spakman*, 2015; *Rangin et al*., 1999]. Comparison to the depths of our other reconstructed slabs suggests the "deep Ayu Trough slabs" subducted after the latest Oligocene or early Miocene (Figure 31), within the lifetime of the Caroline plate. Therefore, the presence of the deep Ayu Trough slab under the Caroline and Philippine Sea plates suggests that these plates converged some time after Caroline Sea nucleation, which is not easily explained by the fully coupled Caroline-Philippine Sea plate reconstruction of *Hall* [2002].

5.7. South China Sea and Proto-South China Sea History

The history of the proto-South China Sea is not a primary focus of our present study and has little impact on other aspects of Philippine Sea plate tectonics but is discussed here because of its importance for regional plate reconstructions. A great diversity of proto-South China Sea plate reconstructions have been proposed, including extrusion and subduction-type end-member models and various hybrids [cf. *Cullen*, 2010]. With the exception of extrusion-type models [e.g., *Replumaz and Tapponnier*, 2003], most published plate reconstructions generally agree that southward South China Sea opening was accommodated at least in part by south dipping subduction beneath Borneo [e.g., *Cullen*, 2010; *Hall*, 2002; *Taylor and Hayes*, 1983; *Zahirovic et al*., 2014]. In particular, several regionally extensive plate models show as much as 1500 km convergence between the north Borneo margin and SW Palawan between the early Cenozoic to Miocene [e.g., *Hall*, 2002; *Zahirovic et al*., 2014]. Tomographic studies including this study generally support the existence of proto-South China Sea slabs in the SE Asian mantle [e.g., *Rangin et al*., 1999; *Zahirovic et al*., 2014; *Hall and*

Spakman, 2015], which is apparently less compatible with pure extrusion-type models [e.g., *Replumaz and Tapponnier*, 2003]. However, proto-South China Sea slab interpretations have been highly variable with little agreement between studies [e.g., *Rangin et al*., 1999; *Zahirovic et al*., 2014; *Hall and Spakman*, 2015]. The implications of our slab reconstruction for proto-South China Sea is further discussed and compared to these previous studies below.

Our unfolded south "proto-South China Sea" slabs supports elements of the southward subduction models and indicates a limited 500 to 700 km of southward subduction under Borneo, mainly during the Eocene (Figures 24b and 24c). However, we also interpret that a large portion of proto-South China Sea slabs exist as subhorizontal slabs at 460 to 950 km depths under the present-day South China Sea (i.e., the "north proto-South China Sea" slabs) (Figures 15a, 16c, 16d, and 22c), where MITP08 tomographic resolutions are comparable to the rest of our study area [*Li et al*., 2008]. The northern proto-South China Sea slab anomalies were also identified from the other global tomography in this study (i.e., TX2011 *S* wave and LLNL-G3Dv4 *P* wave global tomography) and have been interpreted as slabs from the Utrecht tomography (UU-P07) [*Hall and Spakman*, 2015] and MITP08 [*Zahirovic et al*., 2014].

When reconstructed in our slab-prioritized plate model, we found that the north proto-South China Sea slabs naturally fit with a back-arc-style South China Sea opening after ~30 Ma (Figures 24c and 24d). In other words, our plate model implies that a large portion (up to 900 km) of the proto-South China Sea was subducted northwestward under the opening South China Sea in the Oligo-Miocene (~30 Ma to 15 Ma) (see supporting information Model 1 in Movie S1), concurrent with minor southward subduction under Borneo. Our predicted subduction style for the north proto-South China Sea slabs is reminiscent of post-30 Ma western Mediterranean subduction rollback [cf. *Faccenna et al*., 2014]. Furthermore, we can closely link the South China Sea back-arc-style opening to a progressive southwest propagation of the Ryukyu trench along the Eurasian continental margin between ~52 and 30 Ma that was driven by an east-west STEP fault transform between the Pacific and the northern East Asian Sea (Figures 24a–24c; Model 1 in Movie S1).

Our modeling of a back-arc-style subduction of the northern proto-South China Sea is controversial. The notion has been dismissed by past studies due to the lack of evidence for an associated volcanic arc [e.g., *Taylor and Hayes*, 1983], which nevertheless could have been subducted or underthrust along north Borneo. Other studies have alternatively suggested that the north proto-South China Sea slabs were subducted much earlier and stagnant in the mantle transition zone since the Cretaceous 80 to 90 Ma [*Hall and Spakman*, 2015]. Although we cannot fully rule out this interpretation, it would require an unconventional slab sinking history compared to the 28 slabs in this study (Figure 31). Alternatively, *Zahirovic et al*. [2014] suggested that the north proto-South China Sea slabs were subducted southward under north Borneo until the Miocene. Although this scenario is more consistent with our slab sinking rates in Figure 31, it was acknowledged that this reconstruction requires up to ~1000 km northward lateral advection of the slabs within the upper mantle and transition zone during the Neogene [*Zahirovic et al*., 2014]. Such lateral slab advection produces large gaps and overlaps that are absent in our 52 Ma reconstruction (Figure 23), which was based on the straightforward assumption of vertical sinking. Our north and south proto-South China Sea slabs fit together satisfactorily with adjacent lithosphere, including South China continent and East Asian Sea slabs of similar depths and subduction times for alternative mantle reference frames, which is consistent with vertical sinking (Table 1 and Figures 31 and S5).

In summary, we conclude that there is no current tectonic model that satisfactorily reconciles both the surface geology and mantle structure related to proto-South China Sea subduction. On this basis, we argue that the lack of a preserved or identified arc at the surface is not a sufficient reason to reject our back-arc-style model without consideration, even though the notion has been dismissed for many years. The proto-South China Sea subduction model presented as part of our East Asia study has advantages over existing models in that it identifies for the first time sufficient slab lengths to account for predicted ~1500 km lost lithosphere between Borneo and SW Palawan as predicted by *Hall* [2002] and *Zahirovic et al*. [2014]. Furthermore, our plate model also explains the apparently enigmatic slab anomalies in a natural and straightforward fashion, within a testable kinematic solution, and provides a sensible context for a back-arc-style subduction system.

5.8. Implications for Geodynamic Models

East Asia is a known global slab graveyard, a site where extensive subducted lithospheric remnants reside in the mantle [*Li and van der Hilst*, 2010]. Our slab reconstructions can now quantify this notion by showing that

an immense area (~25% of the area of the world's oceanic lithosphere, or about one seventh of the total Earth surface area) has subducted at East Asia since the major Eocene global plate reorganization at ~50 Ma, and these slabs now exist in the upper 1300 km of the mantle in our area of study (Table 1). Each of our 28 reconstructed slabs is a tracer for mantle flow; below we discuss the implications of our slab observations for slab sinking rates through the upper and lower mantle. We will also briefly comment on the implications of our new slab methods for plate tectonic reconstructions of convergent regions.

5.8.1. Upper and Lower Mantle Slab Sinking Rates

A plot of our mapped slab depths relative to their inferred subduction age is shown in Figure 31. Our observed upper mantle slab sinking rates generally ranged from 4 to 8 cm/yr with one exception for the subducted Ontong Java plateau (Figure 31). Previous global slab studies and geodynamic models have found comparable 5 to 10 cm/yr upper mantle sinking rates for mature oceanic lithosphere [*Goes et al*., 2011; *Sdrolias and Müller*, 2006; *Shephard et al*., 2012]. Within the lower mantle, our observed slab age depths fit within a 1.8 ± 0.8 cm lower mantle sinking rate (Figure 31). We attribute scatters in absolute slab age depths to differential sinking velocities through the 410 to 660 km mantle transition zone. Our cross-sectional area unfolded central Marianas Pacific slabs had comparable mean lower mantle sinking rates between 1.1 and 1.7 cm/yr (Table 3), and our preferred intermediate "Area B" estimate of ~1.3 cm/yr shown in orange shows a good fit with other slabs (Figure 31). Previous studies found comparable lower mantle sinking rates of ~2 cm/yr from the Tethyan slabs [*Hafkenscheid et al*., 2006], 2 ± 0.8 cm/yr from comparisons between geodynamic models and tomography [*Steinberger et al*., 2012], 1.2 ± 0.3 cm/yr from the global slab study of *van der Meer et al*. [2010], and maximum 1.5 to 2.0 cm/yr from geodynamic models [*Shephard et al*., 2012].

5.8.2. New Plate Tectonic Models for Convergent Regions

The integration of seafloor magnetic anomalies and hot spot tracks into a "global plate circuit" has been an important contribution that continues to underpin new advances in Mesozoic to present-day plate tectonics. However, vast areas of the Earth still lack sufficiently constrained plate reconstructions due to plate convergence. In convergent regions the plate circuit is broken by subduction zones. Furthermore, the lithospheric record lost at subduction zones is a major challenge for plate motion models; significantly more than two thirds of the Earth surface has been lost to subduction since ~200 Ma. These issues affect not only East Asian plate reconstructions but the Tethys, the entire Alpine-Himalayan realm, the western margin of North America, the Caribbean, and the Southern Hemisphere margins of the Pacific and Oceania. Numerous studies have used tomographic images of slabs to constrain or test plate tectonic models in these areas. However, the methods and approach used in this paper have arguably produced the first quantitative slab-constrained plate reconstruction model (e.g., Figure 24). This new generation of plate model shows unfolded slabs within a fully testable plate kinematics and brings new promise for reconstructions of large, previously unconstrained areas of the Earth (compare Figures 5 and 24).

6. Conclusions

We have presented a Philippine Sea and surrounding East Asia plate-tectonic reconstruction that has been arguably much improved by 28 subducted slab constraints. Each of the slabs were mapped in 3-D from global tomography, unfolded, and incorporated into a global plate reconstruction and given plate-tectonic kinematics using a new slab mapping and reconstruction workflow. The resultant plate reconstruction model is apparently the most extensive attempt to quantitatively recover subducted slab constraints for a plate-tectonic model.

Our mapped and unfolded slabs provide new first-order constraints that account, both in area and location, for a major 6000×10000 km region of post ~50 Ma lithospheric loss that is predicted by global plate models for East Asia (compare Figures 5a and 24a). Their surface area under East Asia and surroundings totaled 7.16×10^7 km^2 (Table 1), an area about 33% larger than the size of present-day Eurasia and about 14% of the total Earth surface area. This amounts to ~25% of the Earth's oceanic lithosphere that has been subducted in this region (Figure 23) since 52 Ma and now resides in the uppermost ~1300 km of the mantle.

Key new constraints for East Asian plate tectonics include: (1) the Marianas Pacific subduction zone remained within ±200 km of its present location since 48 ± 10 Ma based on a slab wall extending to >1000 km. Even if ~600 km of slab rollback prior to lower mantle slab anchoring is considered, the Marianas Pacific slab wall is incompatible with retreating trench plate models that predict >2000 km of

NE Izu-Bonin-Marianas trench retreat since the Eocene. Instead, we predict that the Shikoku-Parece Vela back-arc basin did not open by classic slab rollback, but by a more complex rollback resulting from westward motion and clockwise rotation of the Philippine Sea plate relative to a largely stationary Marianas subduction zone. Our plate model indicates that these Philippine Sea plate motions were largely driven by tectonic escape from the impinging Caroline Sea/Pacific plates; (2) a major (8000 km × 2500 km) set of lower mantle flat slabs represents a vanished East Asian Sea. These disappeared ocean basins fill the majority of an important and well-known plate reconstruction gap between the Pacific and Indian Oceans at 52 Ma and were the proto-Philippine Sea. The East Asian Sea finally disappeared by 15 Ma due to Pacific, Philippine Sea, and Australian plate convergence. (3) The northern Philippine Sea Ryukyu slab is short (~1000 km) relative to >2000 km northward Philippine Sea motion constrained by paleomagnetism. This requires an intervening now-subducted ocean south of the Ryukyu-SW Japan Eurasian margin, which our plate reconstructions show to be the northern East Asian Sea and the Pacific. Final closure of these oceans produced a mid-Miocene arc-arc collision between a northern Philippine Sea plate arc and the SW Japan-Ryukyu continental margin. Evidence for this collision includes widespread early to middle Miocene compressional deformation, uplift, and erosion in the East China Sea that is sealed by an upper Miocene angular unconformity.

The Caroline Sea has moved with the Pacific since its inception based on evidence from our mapped slabs and an overlapping coeval Caroline LIPs and hot spot track. When reconstructed with the other slab constraints, a Caroline Sea plate moving with Pacific-like, westward motions provides a clear and straightforward explanation for Philippine Sea westward motion and large ~90° clockwise rotations. We show that the Caroline Sea plate played an important role by driving the Philippine Sea plate westward to subduct the South China Sea-Eurasian margin and initiate Manila trench subduction. Today, GPS-derived global plate motion models indicate more complete coupling of the Caroline-Pacific plate to the SW Philippine Sea plate (Figure 1b), and all three plates now move with Pacific-like fast WNW motion.

This paper has demonstrated for the first time that plate-tectonic reconstructions of complex regions dominated by plate convergence can be substantially improved by methodologies involving systematic incorporation of mapped and unfolded subducted slabs as constraints into globally consistent plate-tectonic models. In the present example, focused on the Philippine Sea plate and adjacent East Asia, this strategy has allowed us to integrate diverse geologic and paleomagnetic constraints to provide a currently preferred class of plate tectonic models (Model 1) since the last 52 Ma. This should provide a starting point for more refined integration and modification based on new data and more detailed local studies of the surroundings of the Philippine Sea plate. Our inclusion of digital GPlates reconstruction files and unfolded slab polygons as a supporting information allows our models to be further tested by geodynamic numerical models and reconciled against regional geological data. Furthermore, our methodologies can be applied to other regions of the Earth dominated by convergent tectonics over the last ~200 Ma for which subducted slabs are sufficiently well imaged in the mantle. These slab-constrained models of plate tectonics will provide more data-rich, realistic motivations for diverse geodynamical models.

Acknowledgments

Jonny Wu's postdoctoral fellowship was funded by National Taiwan University grant 104R4000. John Suppe was funded by distinguished chair research funds from National Taiwan University grant 104R104051 and the National Science Council grant 104-2116-M002-028. Ravi Kanda and Renqi Lu were funded by National Taiwan University postdoctoral fellowship grant 10R40044. The authors would like to especially acknowledge many helpful discussions with our Taiwan academic colleagues including Yue-Gau Chen, Louis Teng, Ban-Yuan Kuo, Yuan-Hsi Lee, Yih-Min Wu, Hao Kuo-Chen, Cedric Legendre and Taiwan visiting professors Dennis Brown and Tim Byrne. Research assistants Chia-Yi Chou, Han-Fang Liu, Yi-Wei Chen, Chris Ding-Jyun Lin, Jia-Yu Fish Chen, Ponong Lee, and Wan-Yun Ho contributed valuable technical and administrative support. We benefited greatly from discussions on regional geology and geophysics with Jean-Claude Sibuet, Gaku Kimura, Kyoko Okino, Kenichiro Tani, Julia Ribeiro, Robert Hall, Serge Lallemand, Manuel Pubellier, Andrew Cullen, and Sabin Zahirovic. We are grateful for the many discussions on global tectonics and GPlates advice with the Sydney University Earthbyte Group including Dietmar Müller, John Cannon, Maria Seton, Simon Williams, Christian Heine, Nicolas Flament, Sabin Zahirovic, Ana Gibbons, Kara Matthews, and Grace Shephard. The ideas in this paper benefitted greatly from interactions with Douwe van Hinsbergen and Wim Spakman during a visit to Utrecht University. Douglas Wiens, Paul Tackley, and Vera Schulte-Pelkum provided helpful advice during their Taiwan visits. Peter Bunge and Sara Carena provided valuable geodynamics insights and Gocad software advice. John Liang at Geoforce Technologies provided Gocad software technical support. GPlates software was used for plate tectonic reconstructions. GMT was used for geographic projections. AreaErrorProp software from Rick Allmendinger was used for the cross-sectional slab area analysis. We thank Sabin Zahirovic and Marco Maffione for their thorough and constructive reviews. See supporting information for plate tectonic reconstruction movies and GPlates reconstruction files for all plate models and unfolded slabs in this study.

References

Ali, J., and S. Moss (1999), Miocene intra-arc bending at an arc-arc collision zone, central Japan: Comment, *Isl. Arc*, *8*(1), 114–123, doi:10.1046/j.1440-1738.1999.00218.x.

Ali, J. R., and R. Hall (1995), Evolution of the boundary between the Philippine Sea plate and Australia: Palaeomagnetic evidence from eastern Indonesia, *Tectonophysics*, *251*(1-4), 251–275, doi:10.1016/0040-1951(95)00029-1.

Ali, J. R., J. Milsom, E. M. Finch, and B. Mubroto (1996), SE Sundaland accretion: Palaeomagnetic evidence of large Plio-Pleistocene thin-skin rotations in Buton, *Geol. Soc. London Spec. Publ.*, *106*(1), 431–443, doi:10.1144/GSL.SP.1996.106.01.26.

Altis, S. (1999), Origin and tectonic evolution of the Caroline Ridge and the Sorol Trough, western tropical Pacific, from admittance and a tectonic modeling analysis, *Tectonophysics*, *313*(3), 271–292, doi:10.1016/S0040-1951(99)00204-8.

Arculus, R. J., et al. (2015), A record of spontaneous subduction initiation in the Izu-Bonin-Mariana arc, *Nat. Geosci.*, *8*(9), 728–733, doi:10.1038/ngeo2515.

Argus, D. F., R. G. Gordon, and C. DeMets (2011), Geologically current motion of 56 plates relative to the no-net-rotation reference frame, *Geochem. Geophys. Geosyst.*, *12*, Q11001, doi:10.1029/2011GC003751.

Asamori, K., and D. Zhao (2015), Teleseismic shear wave tomography of the Japan subduction zone, *Geophys. J. Int.*, *203*(3), 1752–1772, doi:10.1093/gji/ggv334.

Baker, S., and J. Malaihollo (1996), Dating of Neogene igneous rocks in the Halmahera region: Arc initiation and development, *Geol. Soc. London Spec. Publ.*, *106*(1), 499–509, doi:10.1144/GSL.SP.1996.106.01.31.

Bennis, C., J.-M. Vezien, and G. Iglesias (1991), Piecewise surface flattening for non-distorted texture mapping, *Comput. Graphics*, *25*(4), 237–246, doi:10.1145/127719.122744.

Bird, P. (2003), An updated digital model of plate boundaries, *Geochem. Geophys. Geosyst.*, *4*(3), 1027, doi:10.1029/2001GC000252.

Boyden, J. A., R. D. Müller, M. Gurnis, T. H. Torsvik, J. A. Clark, M. Turner, H. Ivey-Law, R. J. Watson, and J. S. Cannon (2011), Next-generation plate-tectonic reconstructions using GPlates, in *Geoinformatics: Cyberinfrastructure for the Solid Earth Sciences*, edited by G. R. Keller and C. Baru, Cambridge Univ. Press, pp. 95–113, Cambridge Univ. Press, Cambridge, U. K.

Bleil, U. (1982), Paleomagnetism of Deep Sea Drilling Project Leg 60 sediments and igneous rocks from the Mariana region, in *Leg 60 of the Cruises of the Drilling Vessel Glomar Challenger; Apra, Guam to Apra, Guam; March-May 1978*, edited by M. P. Lee, pp. 855–873, Texas A&M Univ., Ocean Drilling Program, College Station, Tex.

Briais, A., P. Patriat, and P. Tapponnier (1993), Updated interpretation of magnetic anomalies and seafloor spreading stages in the south China Sea: Implications for the Tertiary tectonics of Southeast Asia, *J. Geophys. Res.*, *98*, 6299–6328, doi:10.1029/92JB02280.

Byrne, T., and L. DiTullio (1992), Evidence for changing plate motions in southwest Japan and reconstructions of the Philippine Sea plate, *Isl. Arc*, *1*(1), 148–165, doi:10.1111/j.1440-1738.1992.tb00066.x.

Cande, S. C., C. A. Raymond, J. Stock, and W. F. Haxby (1995), Geophysics of the Pitman fracture zone and Pacific-Antarctic plate motions during the Cenozoic, *Science*, *270*(5238), 947–953, doi:10.1126/science.270.5238.947.

Cao, L., Z. Wang, S. Wu, and X. Gao (2014), A new model of slab tear of the subducting Philippine Sea Plate associated with Kyushu-Palau Ridge subduction, *Tectonophysics*, *636*, 158–169, doi:10.1016/j.tecto.2014.08.012.

Chamley, H. (1980), Clay sedimentation and paleoenvironment in the area of Daito Ridge (Northwest Philippine Sea) since the early Eocene, in *Initial Reports of the Deep Sea Drilling Project*, edited by G. deVries Klein et al., pp. 683–693, U. S. Gov. Print. Off., Washington, D. C.

Chatelain, J.-L., B. Guillier, and J.-P. Gratier (1993), Unfolding the subducting plate in the central New Hebrides Island Arc: Geometrical argument for detachment of part of the downgoing slab, *Geophys. Res. Lett.*, *20*, 655–658, doi:10.1029/93GL00681.

Chen, M., F. Niu, Q. Liu, J. Tromp, and X. Zheng (2015), Multi-parameter adjoint tomography of the crust and upper mantle beneath East Asia —Part I: Model construction and comparisons, *J. Geophys. Res. Solid Earth*, *120*, 1762–1786, doi:10.1002/2014JB011638.

Chung, S.-L., and S.-s. Sun (1992), A new genetic model for the East Taiwan Ophiolite and its implications for Dupal domains in the Northern Hemisphere, *Earth Planet. Sci. Lett.*, *109*(1), 133–145, doi:10.1016/0012-821X(92)90079-B.

Čížková, H., and C. R. Bina (2013), Effects of mantle and subduction-interface rheologies on slab stagnation and trench rollback, *Earth Planet. Sci. Lett.*, *379*, 95–103, doi:10.1016/j.epsl.2013.08.011.

Čížková, H., and C. R. Bina (2015), Geodynamics of trench advance: Insights from a Philippine-Sea-style geometry, *Earth Planet. Sci. Lett.*, *430*, 408–415, doi:10.1016/j.epsl.2015.07.004.

Clift, P. D., A. Carter, U. Nicholson, and H. Masago (2013), Zircon and apatite thermochronology of the Nankai Trough accretionary prism and trench, Japan: Sediment transport in an active and collisional margin setting, *Tectonics*, *32*, 377–395, doi:10.1002/tect.20033.

Coffin, M. F. (2011), Digital LIPs database (version 2011), PLATES Proj., UTIG Univ. of Tex. Inst. for Geophys. [Available at http://www.ig.utexas.edu/research/projects/plates/data/LIPS/.]

Cogné, J.-P., J. Besse, Y. Chen, and F. Hankard (2013), A new late Cretaceous to Present APWP for Asia and its implications for paleomagnetic shallow inclinations in Central Asia and Cenozoic Eurasian plate deformation, *Geophys. J. Int.*, *192*(3), 1000–1024, doi:10.1093/gji/ggs104.

Cosca, M., R. Arculus, J. Pearce, and J. Mitchell (1998), 40Ar/39Ar and K-Ar geochronological age constraints for the inception and early evolution of the Izu-Bonin-Mariana arc system, *Isl. Arc*, *7*(3), 579–595, doi:10.1111/j.1440-1738.1998.00211.x.

Cukur, D., S. Horozal, D. C. Kim, and H. C. Han (2011), Seismic stratigraphy and structural analysis of the northern East China Sea Shelf Basin interpreted from multi-channel seismic reflection data and cross-section restoration, *Mar. Pet. Geol.*, *28*(5), 1003–1022, doi:10.1016/j.marpetgeo.2011.01.002.

Cukur, D., S. Horozal, G. H. Lee, D. C. Kim, and H. C. Han (2012), Timing of trap formation and petroleum generation in the northern East China Sea Shelf Basin, *Mar. Pet. Geol.*, *36*(1), 154–163, doi:10.1016/j.marpetgeo.2012.04.009.

Cullen, A. B. (2010), Transverse segmentation of the Baram-Balabac Basin, NW Borneo: Refining the model of Borneo's tectonic evolution, *Pet. Geosci.*, *16*(1), 3–29, doi:10.1144/1354-079309-828.

DeBari, S. M., B. Taylor, K. Spencer, and K. Fujioka (1999), A trapped Philippine Sea plate origin for MORB from the inner slope of the Izu-Bonin trench, *Earth Planet. Sci. Lett.*, *174*(1–2), 183–197, doi:10.1016/S0012-821X(99)00252-6.

De Grave, J., E. De Pelsmaeker, F. I. Zhimulev, S. Glorie, M. M. Buslov, and P. Van den haute (2014), Meso-Cenozoic building of the northern Central Asian Orogenic Belt: Thermotectonic history of the Tuva region, *Tectonophysics*, *621*, 44–59, doi:10.1016/j.tecto.2014.01.039.

DeMets, C., R. G. Gordon, and D. F. Argus (2010), Geologically current plate motions, *Geophys. J. Int.*, *181*(1), 1–80, doi:10.1111/j.1365-246X.2009.04491.x.

Den, N., W. J. Ludwig, S. Murauchi, M. Ewing, H. Hotta, T. Asanuma, T. Yoshii, A. Kubotera, and K. Hagiwara (1971), Sediments and structure of the Eauripik-New Guinea Rise, *J. Geophys. Res.*, *76*, 4711–4723, doi:10.1029/JB076i020p04711.

Deschamps, A., and S. Lallemand (2002), The West Philippine Basin: An Eocene to early Oligocene back arc basin opened between two opposed subduction zones, *J. Geophys. Res.*, *107*(B12), 2322, doi:10.1029/2001JB001706.

Deschamps, A., S. Lallemand, and S. Dominguez (1999), The last spreading episode of the West Philippine Basin revisited, *Geophys. Res. Lett.*, *26*, 2073–2076, doi:10.1029/1999GL900448.

Deschamps, A., P. Monie, S. Lallemand, S. K. Hsu, and K. Y. Yeh (2000), Evidence for Early Cretaceous oceanic crust trapped in the Philippine Sea Plate, *Earth Planet. Sci. Lett.*, *179*(3-4), 503–516, doi:10.1016/s0012-821x(00)00136-9.

Deschamps, A., R. Shinjo, T. Matsumoto, C.-S. Lee, S. E. Lallemand, S. Wu, and Scientific party of KR03-04 and KR04-14 cruises (2008), Propagators and ridge jumps in a back-arc basin, the West Philippine Basin, *Terra Nova*, *20*(4), 327–332, doi:10.1111/j.1365-3121.2008.00824.x.

Deschamps, A. E., S. E. Lallemand, and J.-Y. Collot (1998), A detailed study of the Gagua Ridge: A fracture zone uplifted during a plate reorganisation in the Mid-Eocene, *Mar. Geophys. Res.*, *20*(5), 403–423, doi:10.1023/A:1004650323183.

Doo, W.-B., S.-K. Hsu, Y.-C. Yeh, C.-H. Tsai, and C.-M. Chang (2014), Age and tectonic evolution of the northwest corner of the West Philippine Basin, *Mar. Geophys. Res.*, *36*, 113–125, doi:10.1007/s11001-014-9234-8.

Dziewonski, A. M., and D. L. Anderson (1981), Preliminary reference Earth model, *Phys. Earth Planet. Inter.*, *25*(4), 297–356, doi:10.1016/0031-9201(81)90046-7.

Eakin, D. H., K. D. McIntosh, H. J. A. Van Avendonk, and L. Lavier (2015), New geophysical constraints on a failed subduction initiation: The structure and potential evolution of the Gagua Ridge and Huatung Basin, *Geochem. Geophys. Geosyst.*, *16*, 380–400, doi:10.1002/2014GC005548.

Engdahl, E. R., and A. Villaseñor (2002), Global seismicity: 1900–1999, in *International Handbook of Earthquake and Engineering Seismology, Part A*, edited by W. H. K. Lee et al., pp. 665–690, Academic Press, Cambridge.

Escartín, J., and J. P. Canales (2011), Detachments in oceanic lithosphere: Deformation, magmatism, fluid flow, and ecosystems, *Eos Trans. AGU*, *92*(4), 31–31, doi:10.1029/2011EO040003.
Faccenna, C., et al. (2014), Mantle dynamics in the Mediterranean, *Rev. Geophys.*, *52*, 283–332, doi:10.1002/2013RG000444.
Fischer, A. G., B. C. Heezen, R. E. Boyce, D. Bukry, R. G. Douglas, R. E. Garrison, S. A. Kling, V. Krasheninnikov, A. P. Lisitzin, and A. C. Pimm (1971), *Site 63 Shipboard Report*, pp. 449, 493, 539, U.S. Gov. Print. Off., Washington, D. C., doi:10.2973/dsdp.proc.6.1971.
Florendo, F. F. (1994), Tertiary arc rifting in northern Luzon, Philippines, *Tectonics*, *13*, 623–640, doi:10.1029/94TC00453.
Fornari, D. J., J. K. Weissel, M. R. Perfit, and R. N. Anderson (1979), Petrochemistry of the Sorol and Ayu Troughs: Implications for crustal accretion at the northern and western boundaries of the Caroline plate, *Earth Planet. Sci. Lett.*, *45*(1), 1–15, doi:10.1016/0012-821X(79)90102-X.
French, S. W., and B. Romanowicz (2015), Broad plumes rooted at the base of the Earth's mantle beneath major hotspots, *Nature*, *525*(7567), 95–99, doi:10.1038/nature14876.
Fujioka, K., K. Okino, T. Kanamatsu, Y. Ohara, O. Ishizuka, S. Haraguchi, and T. Ishii (1999), Enigmatic extinct spreading center in the West Philippine backarc basin unveiled, *Geology*, *27*(12), 1135–1138, doi:10.1130/0091-7613(1999)027<1135:EESCIT>2.3.CO;2.
Fujiwara, T., et al. (1995), Morphological studies of the Ayu trough, Philippine Sea-Caroline plate boundary, *Geophys. Res. Lett.*, *22*, 109–112, doi:10.1029/94GL02719.
Fukao, Y., M. Obayashi, H. Inoue, and M. Nenbai (1992), Subducting slabs stagnant in the mantle transition zone, *J. Geophys. Res.*, *97*, 4809–4822, doi:10.1029/91JB02749.
Fuller, M., R. McCabe, I. S. Williams, J. Almasco, R. Y. Encina, A. S. Zanoria, and J. A. Wolfe (1983), Paleomagnetism of Luzon, in *The Tectonic and Geologic Evolution of Southeast Asian Seas and Islands: Part 2*, edited by D. E. Hayes, pp. 79–94, AGU, Washington, D. C., doi:10.1029/GM027p0079.
Gaina, C., and D. Müller (2007), Cenozoic tectonic and depth/age evolution of the Indonesian gateway and associated back-arc basins, *Earth Sci. Rev.*, *83*(3–4), 177–203, doi:10.1016/j.earscirev.2007.04.004.
Gaina, C., W. R. Roest, and R. D. Müller (2002), Late Cretaceous-Cenozoic deformation of northeast Asia, *Earth Planet. Sci. Lett.*, *197*(3–4), 273–286, doi:10.1016/S0012-821X(02)00499-5.
Gibbons, A. D., J. M. Whittaker, and R. D. Müller (2013), The breakup of East Gondwana: Assimilating constraints from Cretaceous ocean basins around India into a best-fit tectonic model, *J. Geophys. Res. Solid Earth*, *118*, 808–822, doi:10.1002/jgrb.50079.
Goes, S., F. A. Capitanio, G. Morra, M. Seton, and D. Giardini (2011), Signatures of downgoing plate-buoyancy driven subduction in Cenozoic plate motions, *Phys. Earth Planet. Inter.*, *184*(1–2), 1–13, doi:10.1016/j.pepi.2010.10.007.
Govers, R., and M. J. R. Wortel (2005), Lithosphere tearing at STEP faults: Response to edges of subduction zones, *Earth Planet. Sci. Lett.*, *236*(1–2), 505–523, doi:10.1016/j.epsl.2005.03.022.
Grand, S. P. (2002), Mantle shear-wave tomography and the fate of subducted slabs, *Philos. Trans. R. Soc. London A*, *360*(1800), 2475–2491.
Gratier, J.-P., and B. Guillier (1993), Compatibility constraints on folded and faulted strata and calculation of total displacement using computational restoration (UNFOLD program), *J. Struct. Geol.*, *15*(3–5), 391–402, doi:10.1016/0191-8141(93)90135-W.
Gungor, A., G. H. Lee, H.-J. Kim, H.-C. Han, M.-H. Kang, J. Kim, and D. Sunwoo (2012), Structural characteristics of the northern Okinawa Trough and adjacent areas from regional seismic reflection data: Geologic and tectonic implications, *Tectonophysics*, *522–523*, 198–207, doi:10.1016/j.tecto.2011.11.027.
Gurnis, M., C. Hall, and L. Lavier (2004), Evolving force balance during incipient subduction, *Geochem. Geophys. Geosyst.*, *5*, Q07001, doi:10.1029/2003GC000681.
Hafkenscheid, E., M. J. R. Wortel, and W. Spakman (2006), Subduction history of the Tethyan region derived from seismic tomography and tectonic reconstructions, *J. Geophys. Res.*, *111*, B08401, doi:10.1029/2005JB003791.
Hall, R. (1987), Plate boundary evolution in the Halmahera region, Indonesia, *Tectonophysics*, *144*(4), 337–352, doi:10.1016/0040-1951(87)90301-5.
Hall, R. (2000), Neogene history of collision in the Halmahera Region, Indonesia, paper presented at Indonesian Petroleum Association 27th Annual Convention.
Hall, R. (2002), Cenozoic geological and plate tectonic evolution of SE Asia and the SW Pacific: Computer-based reconstructions, model and animations, *J. Asian Earth Sci.*, *20*(4), 353–431, doi:10.1016/S1367-9120(01)00069-4.
Hall, R. (2012), Late Jurassic-Cenozoic reconstructions of the Indonesian region and the Indian Ocean, *Tectonophysics*, *570–571*, 1–41, doi:10.1016/j.tecto.2012.04.021.
Hall, R. (2013), Contraction and extension in northern Borneo driven by subduction rollback, *J. Asian Earth Sci.*, *76*, 399–411, doi:10.1016/j.jseaes.2013.04.010.
Hall, R., and W. Spakman (2002), Subducted slabs beneath the eastern Indonesia-Tonga region: Insights from tomography, *Earth Planet. Sci. Lett.*, *201*(2), 321–336, doi:10.1016/S0012-821X(02)00705-7.
Hall, R., and W. Spakman (2015), Mantle structure and tectonic history of SE Asia, *Tectonophysics*, *658*, 14–45, doi:10.1016/j.tecto.2015.07.003.
Hall, R., M. G. Audley-Charles, F. T. Banner, S. Hidayat, and S. L. Tobing (1988), Basement rocks of the Halmahera region, eastern Indonesia: A Late Cretaceous-early Tertiary arc and fore-arc, *J. Geol. Soc.*, *145*(1), 65–84, doi:10.1144/gsjgs.145.1.0065.
Hall, R., J. R. Ali, and C. D. Anderson (1995a), Cenozoic motion of the Philippine Sea plate—Paleomagnetic evidence from eastern Indonesia, *Tectonics*, *14*, 1117–1132, doi:10.1029/95TC01694.
Hall, R., J. R. Ali, C. D. Anderson, and S. J. Baker (1995b), Origin and motion history of the Philippine Sea Plate, *Tectonophysics*, *251*(1-4), 229–250, doi:10.1016/0040-1951(95)00038-0.
Hall, R., M. Fuller, J. R. Ali, and C. D. Anderson (1995c), The Philippine Sea Plate: Magnetism and reconstructions, in *Active Margins and Marginal Basins of the Western Pacific*, edited by B. Taylor, and J. Natland, pp. 371–404, AGU, Washington, D. C., doi:10.1029/GM088p0371.
Harada, Y., and Y. Hamano (2000), Recent progress on the plate motion relative to hotspots, in *The History and Dynamics of Global Plate Motions*, edited by M. A. Richards, R. G. Gordon, and R. van der Hilst, pp. 327–338, AGU, Washington, D. C., doi:10.1029/GM121p0327.
Hasegawa, A., J. Nakajima, T. Yanada, N. Uchida, T. Okada, D. Zhao, T. Matsuzawa, and N. Umino (2013), Complex slab structure and arc magmatism beneath the Japanese Islands, *J. Asian Earth Sci.*, *78*, 277–290, doi:10.1016/j.jseaes.2012.12.031.
Haston, R. B., and M. Fuller (1991), Paleomagnetic data from the Philippine Sea plate and their tectonic significance, *J. Geophys. Res.*, *96*, 6073–6098, doi:10.1029/90JB02700.
Haston, R. B., L. B. Stokking, and J. Ali (1992), Paleomagnetic data from Holes 782A, 784A, and 786A, Leg 125, in *Proceedings of the Ocean Drilling Program, Bonin/Mariana Region; Covering Leg 125 of the Cruises of the Drilling Vessel JOIDES Resolution, Apra Harbor, Guam, to Tokyo, Japan, Sites 778-786, 15 February 1989-17 April 1989*, edited by P. Fryer et al., pp. 535–545, Tex. A & M Univ., Ocean Drill. Program, College Station, Tex.

Hayes, G. P., D. J. Wald, and R. L. Johnson (2012), Slab1.0: A three-dimensional model of global subduction zone geometries, *J. Geophys. Res.*, *117*, B01302, doi:10.1029/2011JB008524.
Hegarty, K. A., J. K. Weissel, and D. E. Hayes (1983), Convergence at the Caroline-Pacific plate boundary: Collision and subduction, in *The Tectonic and Geologic Evolution of Southeast Asian Seas and Islands: Part 2*, edited by D. E. Hayes, pp. 326–348, AGU, Washington, D. C., doi:10.1029/GM027p0326.
Heine, C., L. Quevedo, H. McKay, and D. Muller (2012), Plate tectonic consequences of competing models for the origin and history of the Banda Sea subducted oceanic lithosphere, paper presented at Eastern Australian Basin Symposium 4, Brisbane, Australia.
Hibbard, J. P., and D. E. Karig (1990), Alternative plate model for the early Miocene evolution of the southwest Japan margin, *Geology*, *18*(2), 170–174, doi:10.1130/0091-7613(1990)018<0170:apmfte>2.3.co;2.
Hickey-Vargas, R. (1998), Origin of the Indian Ocean-type isotopic signature in basalts from Philippine Sea plate spreading centers: An assessment of local versus large-scale processes, *J. Geophys. Res.*, *103*, 20,963–20,979, doi:10.1029/98JB02052.
Hilde, T. W. C., and C.-S. Lee (1984), Origin and evolution of the West Philippine Basin: A new interpretation, *Tectonophysics*, *102*(1–4), 85–104, doi:10.1016/0040-1951(84)90009-X.
Hilde, T. W. C., S. Uyeda, and L. Kroenke (1977), Evolution of the western pacific and its margin, *Tectonophysics*, *38*(1–2), 145–165, doi:10.1016/0040-1951(77)90205-0.
Hill, K. C., and R. Hall (2003), Mesozoic-Cenozoic evolution of Australia's New Guinea margin in a west Pacific context, *Geol. Soc. Am. Spec. Pap.*, *372*, 265–290.
Hollings, P., R. Wolfe, D. R. Cooke, and P. J. Waters (2011), Geochemistry of Tertiary igneous rocks of Northern Luzon, Philippines: Evidence for a back-arc setting for alkalic porphyry copper-gold deposits and a case for slab roll-back?, *Econ. Geol.*, *106*(8), 1257–1277, doi:10.2113/econgeo.106.8.1257.
Huang, T.-C., M.-P. Chen, and W.-R. Chi (1979), Calcareous nannofossils from the red shale of the ophiolite-mélange complex, eastern Taiwan, *Mem. Geol. Soc. China*, (3), 131–138.
Huang, Z., D. Zhao, A. Hasegawa, N. Umino, J.-H. Park, and I.-B. Kang (2013), Aseismic deep subduction of the Philippine Sea plate and slab window, *J. Asian Earth Sci.*, *75*, 82–94, doi:10.1016/j.jseaes.2013.07.002.
Hussong, D. M., and S. Uyeda (1982), Tectonic processes and the history of the Mariana Arc: A synthesis of the results of deep-sea drilling project Leg 60, in *Initial Reports of the Deep Sea Drilling Project Leg 60*, edited by M. Lee and R. Powell, pp. 909–929, Tex. A & M Univ., Ocean Drill. Program, College Station, Tex.
Iaffaldano, G. (2012), The strength of large-scale plate boundaries: Constraints from the dynamics of the Philippine Sea plate since ~5 Ma, *Earth Planet. Sci. Lett.*, *357–358*, 21–30, doi:10.1016/j.epsl.2012.09.018.
Ishizuka, O., R. N. Taylor, Y. Ohara, and M. Yuasa (2013), Upwelling, rifting, and age-progressive magmatism from the Oki-Daito mantle plume, *Geology*, *41*(9), 1011–1014, doi:10.1130/G34525.1.
Ishizuka, O., K. Tani, M. K. Reagan, K. Kanayama, S. Umino, Y. Harigane, I. Sakamoto, Y. Miyajima, M. Yuasa, and D. J. Dunkley (2011), The timescales of subduction initiation and subsequent evolution of an oceanic island arc, *Earth Planet. Sci. Lett.*, *306*(3–4), 229–240, doi:10.1016/j.epsl.2011.04.006.
Itoh, Y., K. Takemura, and H. Kamata (1998), History of basin formation and tectonic evolution at the termination of a large transcurrent fault system: Deformation mode of central Kyushu, Japan, *Tectonophysics*, *284*(1–2), 135–150, doi:10.1016/S0040-1951(97)00167-4.
Jacob, J., J. Dyment, and V. Yatheesh (2014), Revisiting the structure, age, and evolution of the Wharton Basin to better understand subduction under Indonesia, *J. Geophys. Res. Solid Earth*, *119*, 169–190, doi:10.1002/2013JB010285.
Jahn, B.-M. (1986), Mid-ocean ridge or marginal basin origin of the East Taiwan Ophiolite: Chemical and isotopic evidence, *Contrib. Mineral. Petrol.*, *92*(2), 194–206, doi:10.1007/BF00375293.
Jaxybulatov, K., I. Koulakov, and N. L. Dobretsov (2013), Segmentation of the Izu-Bonin and Mariana slabs based on the analysis of the Benioff seismicity distribution and regional tomography results, *Solid Earth*, *4*(1), 59–73, doi:10.5194/se-4-59-2013.
Johnson, R. W., I. E. M. Smith, and S. R. Taylor (1978), Hot-spot volcanism in St Andrew Strait, Papua New Guinea: Geochemistry of a Quaternary bimodal rock suite, *BMR J. Aust. Geol. Geophys.*, *3*(1), 55–69.
Jolivet, L., P. Huchon, and C. Rangin (1989), Tectonic setting of Western Pacific marginal basins, *Tectonophysics*, *160*(1–4), 23–47, doi:10.1016/0040-1951(89)90382-X.
Judge, P. A., and R. W. Allmendinger (2011), Assessing uncertainties in balanced cross sections, *J. Struct. Geol.*, *33*(4), 458–467, doi:10.1016/j.jsg.2011.01.006.
Karig, D., et al. (1973), Origin of the West Philippine Basin, *Nature*, *246*(5434), 458–461, doi:10.1038/246458a0.
Keating, B. H. (1980), Paleomagnetic study of sediments from Deep Sea Drilling Project Leg 59, in *Leg 59 of the Cruises of the Drilling Vessel Glomar Challenger, Naha, Okinawa to Apra, Guam; February–March 1978*, edited by L. S. Kroenke et al., pp. 523–532, Texas A & M Univ., Ocean Drilling Program, College Station, Tex.
Keating, B. H., and E. Herrero (1980), Paleomagnetic studies of basalts and andesites from Deep Sea Drilling Project Leg 59, in *Leg 59 of the Cruises of the Drilling Vessel Glomar Challenger, Naha, Okinawa to Apra, Guam; February-March 1978*, edited by L. S. Kroenke et al., pp. 533–543, Texas A & M Univ., Ocean Drilling Program, College Station, Tex.
Keating, B. H., and C. E. Helsley (1985), Implications of island arc rotations to the studies of marginal terranes, *J. Geodyn.*, *2*(2–3), 159–181, doi:10.1016/0264-3707(85)90008-0.
Keating, B. H., D. P. Mattey, C. E. Helsley, J. J. Naughton, D. Epp, A. Lazarewicz, and D. Schwank (1984), Evidence for a hot spot origin of the Caroline Islands, *J. Geophys. Res.*, *89*, 9937–9948, doi:10.1029/JB089iB12p09937.
Kimura, G., Y. Hashimoto, Y. Kitamura, A. Yamaguchi, and H. Koge (2014), Middle Miocene swift migration of the TTT triple junction and rapid crustal growth in southwest Japan: A review, *Tectonics*, *33*, 1219–1238, doi:10.1002/2014TC003531.
Kimura, J.-I., R. J. Stern, and T. Yoshida (2005), Reinitiation of subduction and magmatic responses in SW Japan during Neogene time, *Geol. Soc. Am. Bull.*, *117*(7-8), 969–986, doi:10.1130/B25565.1.
Kinoshita, H. (1980), Paleomagnetism of sediment cores from Deep Sea Drilling Project Leg 58, Philippine Sea, in *Leg 58 of the Cruises of the Drilling Vessel Glomar Challenger; Yokahama, Japan to Okinawa, Japan; December, 1977-January, 1978*, edited by G. d. V. et al., pp. 765–768, Texas A & M Univ., Ocean Drilling Program, College Station, Tex.
Klaus, A., and B. Taylor (1991), Submarine canyon development in the Izu-Bonin forearc: A SeaMARC II and seismic survey of Aoga Shima Canyon, *Mar. Geophys. Res.*, *13*(2), 131–152, doi:10.1007/BF00286285.
Kobayashi, K., and M. Nakada (1978), Magnetic anomalies and tectonic evolution of the Shikoku inter-arc basin, *J. Phys. Earth*, *26*(Supplement), S391–S402, doi:10.4294/jpe1952.26.Supplement_S391.
Kodama, K., B. H. Keating, and C. E. Helsley (1983), Paleomagnetism of the Bonin Islands and its tectonic significance, *Tectonophysics*, *95*(1–2), 25–42, doi:10.1016/0040-1951(83)90257-3.

Koulakov, I., Y.-M. Wu, H.-H. Huang, N. Dobretsov, A. Jakovlev, I. Zabelina, K. Jaxybulatov, and V. Chervov (2014), Slab interactions in the Taiwan region based on the P- and S-velocity distributions in the upper mantle, *J. Asian Earth Sci.*, *79*(Part A), 53–64, doi:10.1016/j.jseaes.2013.09.026.

Koyama, M., S. M. Cisowski, and P. A. Pezard (1992), Paleomagnetic evidence for northward drift and clockwise rotation of the Izu-Bonin Forearc since the early Oligocene, in *Proceedings of the Ocean Drilling Program, Bonin Arc-Trench System; Covering Leg 126 of the Cruises of the Drilling Vessel JOIDES Resolution, Tokyo, Japan to Tokyo, Japan, Sites 787–793, 18 April 1989–19 June 1989*, edited by E. M. Barbu and A. P. Julson, pp. 353–370, Tex. A & M Univ., Ocean Drill. Program, College Station, Tex.

Kumagai, H., I. Kaneoka, and T. Ishii (1996), The active period of the Ayu Trough estimated from K-Ar ages: The southeastern spreading center of Philippine Sea Plate, *Geochem. J.*, *30*(2), 81–87, doi:10.2343/geochemj.30.81.

Kuo, B.-Y., W.-C. Chi, C.-R. Lin, E. T.-Y. Chang, J. Collins, and C.-S. Liu (2009), Two-station measurement of Rayleigh-wave phase velocities for the Huatung basin, the westernmost Philippine Sea, with OBS: Implications for regional tectonics, *Geophys. J. Int.*, *179*(3), 1859–1869, doi:10.1111/j.1365-246X.2009.04391.x.

Lallemand, S., Y. Font, H. Bijwaard, and H. Kao (2001), New insights on 3-D plates interaction near Taiwan from tomography and tectonic implications, *Tectonophysics*, *335*(3–4), 229–253, doi:10.1016/S0040-1951(01)00071-3.

Lallemand, S. E., M. Popoff, J.-P. Cadet, A.-G. Bader, M. Pubellier, C. Rangin, and B. Deffontaines (1998), Genetic relations between the central and southern Philippine Trench and the Sangihe Trench, *J. Geophys. Res.*, *103*, 933–950, doi:10.1029/97JB02620.

Lee, S.-M., and S.-S. Kim (2004), Vector magnetic analysis within the southern Ayu Trough, equatorial western Pacific, *Geophys. J. Int.*, *156*(2), 213–221, doi:10.1111/j.1365-246X.2003.02125.x.

Lee, T.-Q., C. Kissel, E. Barrier, C. Laj, and W.-R. Chi (1991), Paleomagnetic evidence for a diachronic clockwise rotation of the Coastal Range, eastern Taiwan, *Earth Planet. Sci. Lett.*, *104*(2–4), 245–257, doi:10.1016/0012-821X(91)90207-X.

Legendre, C. P., Q. F. Chen, and L. Zhao (2014), Lithospheric structure beneath the East China Sea revealed by Rayleigh-wave phase velocities, *J. Asian Earth Sci.*, *96*, 213–225, doi:10.1016/j.jseaes.2014.08.037.

Leng, W., and M. Gurnis (2011), Dynamics of subduction initiation with different evolutionary pathways, *Geochem. Geophys. Geosyst.*, *12*, Q12018, doi:10.1029/2011GC003877.

Letouzey, J., and M. Kimura (1985), Okinawa Trough genesis: Structure and evolution of a backarc basin developed in a continent, *Mar. Pet. Geol.*, *2*(2), 111–130, doi:10.1016/0264-8172(85)90002-9.

Li, C., and R. D. van der Hilst (2010), Structure of the upper mantle and transition zone beneath Southeast Asia from traveltime tomography, *J. Geophys. Res.*, *115*, B07308, doi:10.1029/2009JB006882.

Li, C., R. D. van der Hilst, E. R. Engdahl, and S. Burdick (2008), A new global model for P wave speed variations in Earth's mantle, *Geochem. Geophys. Geosyst.*, *9*, Q05018, doi:10.1029/2007GC001806.

Li, Z., J.-S. Qiu, and X.-M. Yang (2014), A review of the geochronology and geochemistry of Late Yanshanian (Cretaceous) plutons along the Fujian coastal area of southeastern China: Implications for magma evolution related to slab break-off and rollback in the Cretaceous, *Earth Sci. Rev.*, *128*, 232–248, doi:10.1016/j.earscirev.2013.09.007.

Lister, G. S., L. T. White, S. Hart, and M. A. Forster (2012), Ripping and tearing the rolling-back New Hebrides slab, *Aust. J. Earth Sci.*, *59*(6), 899–911, doi:10.1080/08120099.2012.686454.

Liu, L., X. Xu, and Y. Xia (2014), Cretaceous Pacific plate movement beneath SE China: Evidence from episodic volcanism and related intrusions, *Tectonophysics*, *614*, 170–184, doi:10.1016/j.tecto.2013.12.007.

Louden, K. E. (1977), Paleomagnetism of DSDP sediments, phase shifting of magnetic anomalies, and rotations of the West Philippine Basin, *J. Geophys. Res.*, *82*, 2989–3002, doi:10.1029/JB082i020p02989.

Macpherson, C., and R. Hall (2001), Tectonic setting of Eocene boninite magmatism in the Izu-Bonin-Mariana forearc, *Earth Planet. Sci. Lett.*, *186*(2), 215–230, doi:10.1016/S0012-821X(01)00248-5.

Macpherson, C. G., D. R. Hilton, J. M. Sinton, R. J. Poreda, and H. Craig (1998), High $^{3}He/^{4}He$ ratios in the Manus backarc basin: Implications for mantle mixing and the origin of plumes in the western Pacific Ocean, *Geology*, *26*(11), 1007–1010, doi:10.1130/0091-7613(1998)026<1007:HHHRIT>2.3.CO;2.

Mallet, J. (2002), *Geomodeling*, Oxford Univ. Press, New York.

Maus, S., et al. (2009), EMAG2: A 2-arc min resolution Earth Magnetic Anomaly Grid compiled from satellite, airborne, and marine magnetic measurements, *Geochem. Geophys. Geosyst.*, *10*(8), doi:10.1029/2009GC002471.

McCabe, R., and S. Uyeda (1983), Hypothetical model for the bending of the Mariana Arc, in *The Tectonic and Geologic Evolution of Southeast Asian Seas and Islands: Part 2*, edited by D. E. Hayes, pp. 281–293, AGU, Washington, D. C., doi:10.1029/GM027p0281.

McCabe, R., E. Kikawa, J. T. Cole, A. J. Malicse, P. E. Baldauf, J. Yumul, and J. Almasco (1987), Paleomagnetic results from Luzon and the central Philippines, *J. Geophys. Res.*, *92*, 555–580, doi:10.1029/JB092iB01p00555.

McCourt, W. J., M. J. Crow, E. J. Cobbing, and T. C. Amin (1996), Mesozoic and Cenozoic plutonic evolution of SE Asia: Evidence from Sumatra, Indonesia, *Geol. Soc. London Spec. Publ.*, *106*(1), 321–335.

Meffre, S., T. J. Falloon, T. J. Crawford, K. Hoernle, F. Hauff, R. A. Duncan, S. H. Bloomer, and D. J. Wright (2012), Basalts erupted along the Tongan fore arc during subduction initiation: Evidence from geochronology of dredged rocks from the Tonga fore arc and trench, *Geochem. Geophys. Geosyst.*, *13*, Q12003, doi:10.1029/2012GC004335.

Meijer, A., M. Reagan, H. Ellis, M. Shafiqullah, J. Sutter, P. Damon, and S. Kling (1983), Chronology of volcanic events in the Eastern Philippine Sea, in *The Tectonic and Geologic Evolution of Southeast Asian Seas and Islands: Part 2*, edited by D. E. Hayes, pp. 349–359, AGU, Washington, D. C., doi:10.1029/GM027p0349.

Miller, M. S., B. L. N. Kennett, and V. G. Toy (2006), Spatial and temporal evolution of the subducting Pacific plate structure along the western Pacific margin, *J. Geophys. Res.*, *111*, B02401, doi:10.1029/2005JB003705.

Molnar, P., and P. Tapponnier (1975), Cenozoic tectonics of Asia: Effects of a continental collision: Features of recent continental tectonics in Asia can be interpreted as results of the India-Eurasia collision, *Science*, *189*(4201), 419–426, doi:10.1126/science.189.4201.419.

Mrozowski, C. L., and D. E. Hayes (1979), Evolution of the Parece Vela basin, eastern Philippine Sea, *Earth Planet. Sci. Lett.*, *46*(1), 49–67, doi:10.1016/0012-821x(79)90065-7.

Müller, R. D., M. Sdrolias, C. Gaina, and W. R. Roest (2008), Age, spreading rates, and spreading asymmetry of the world's ocean crust, *Geochem. Geophys. Geosyst.*, *9*, Q04006, doi:10.1029/2007GC001743.

Nakamura, K., et al. (1987), Oblique and near collision subduction, Sagami and Suruga Troughs—Preliminary results of the French-Japanese 1984 Kaiko cruise, Leg 2, *Earth Planet. Sci. Lett.*, *83*(1), 229–242, doi:10.1016/0012-821X(87)90068-9.

Okino, K., Y. Shimakawa, and S. Nagaoka (1994), Evolution of the Shikoku Basin, *J. Geomagn. Geoelectr.*, *46*(6), 463–479, doi:10.5636/jgg.46.463.

Okino, K., Y. Ohara, S. Kasuga, and Y. Kato (1999), The Philippine Sea: New survey results reveal the structure and the history of the marginal basins, *Geophys. Res. Lett.*, *26*, 2287–2290, doi:10.1029/1999GL900537.

O'Neill, C., D. Müller, and B. Steinberger (2005), On the uncertainties in hot spot reconstructions and the significance of moving hot spot reference frames, *Geochem. Geophys. Geosyst.*, *6*, Q04003, doi:10.1029/2004GC000784.
Otofuji, Y.-I., T. Matsuda, and S. Nohda (1985), Opening mode of the Japan Sea inferred from the palaeomagnetism of the Japan Arc, *Nature*, *317*(6038), 603–604, doi:10.1038/317603a0.
Park, S.-H., S.-M. Lee, and R. J. Arculus (2006), Geochemistry of basalt from the Ayu Trough, equatorial western Pacific, *Earth Planet. Sci. Lett.*, *248*(3–4), 700–714, doi:10.1016/j.epsl.2006.06.021.
Parker, R. L., and D. W. Oldenburg (1973), Thermal model of ocean ridges, *Nat. Phys. Sci.*, *242*, 137–139, doi:10.1038/physci242137a0.
Pickering, K. T., M. B. Underwood, S. Saito, H. Naruse, S. Kutterolf, R. Scudder, J.-O. Park, G. F. Moore, and A. Slagle (2013), Depositional architecture, provenance, and tectonic/eustatic modulation of Miocene submarine fans in the Shikoku Basin: Results from Nankai Trough Seismogenic Zone Experiment, *Geochem. Geophys. Geosyst.*, *14*, 1722–1739, doi:10.1002/ggge.20107.
Pubellier, M., A. G. Bader, C. Rangin, B. Deffontaines, and R. Quebral (1999), Upper plate deformation induced by subduction of a volcanic arc: The Snellius Plateau (Molucca Sea, Indonesia and Mindanao, Philippines), *Tectonophysics*, *304*(4), 345–368, doi:10.1016/S0040-1951(98)00300-X.
Pubellier, M., F. Ego, N. Chamot-Rooke, and C. Rangin (2003), The building of pericratonic mountain ranges: Structural and kinematic constraints applied to GIS-based reconstructions of SE Asia, *Bull. Soc. Geol. Fr.*, *174*, 561–584, doi:10.2113/174.6.561.
Queano, K. L., J. R. Ali, J. Milsom, J. C. Aitchison, and M. Pubellier (2007), North Luzon and the Philippine Sea Plate motion model: Insights following paleomagnetic, structural, and age-dating investigations, *J. Geophys. Res.*, *112*, B05101, doi:10.1029/2006JB004506.
Raimbourg, H., R. Augier, V. Famin, L. Gadenne, G. Palazzin, A. Yamaguchi, and G. Kimura (2014), Long-term evolution of an accretionary prism: The case study of the Shimanto Belt, Kyushu, Japan, *Tectonics*, *33*, 936–959, doi:10.1002/2013TC003412.
Rangin, C., W. Spakman, M. Pubellier, and H. Bijwaard (1999), Tomographic and geological constraints on subduction along the eastern Sundaland continental margin (South-East Asia), *Bull. Soc. Geol. Fr.*, *170*(6), 775–788.
Reagan, M. K., et al. (2010), Fore-arc basalts and subduction initiation in the Izu-Bonin-Mariana system, *Geochem. Geophys. Geosyst.*, *11*, Q03X12, doi:10.1029/2009GC002871.
Rehman, H. U., H. Nakaya, and K. Kawai (2013), Geological origin of the volcanic islands of the Caroline Group in the Federated States of Micronesia, Western Pacific, *South Pac. Stud.*, *33*(2), 101–118.
Ren, J., K. Tamaki, S. Li, and Z. Junxia (2002), Late Mesozoic and Cenozoic rifting and its dynamic setting in Eastern China and adjacent areas, *Tectonophysics*, *344*(3–4), 175–205, doi:10.1016/S0040-1951(01)00271-2.
Replumaz, A., and P. Tapponnier (2003), Reconstruction of the deformed collision zone Between India and Asia by backward motion of lithospheric blocks, *J. Geophys. Res.*, *108*(B6), 2285, doi:10.1029/2001JB000661.
Richards, S., G. Lister, and B. Kennett (2007), A slab in depth: Three-dimensional geometry and evolution of the Indo-Australian plate, *Geochem. Geophys. Geosyst.*, *8*, Q12003, doi:10.1029/2007GC001657.
Richter, C., and J. R. Ali (2015), Philippine Sea Plate motion history: Eocene-Recent record from ODP Site 1201, central West Philippine Basin, *Earth Planet. Sci. Lett.*, *410*, 165–173, doi:10.1016/j.epsl.2014.11.032.
Rouby, D., H. Xiao, and J. Suppe (2000), 3-D restoration of complexly folded and faulted surfaces using multiple unfolding mechanisms, *AAPG Bull.*, *84*(6), 805–829, doi:10.1306/A9673400-1738-11D7-8645000102C1865D.
Sasaki, T., T. Yamazaki, and O. Ishizuka (2014), A revised spreading model of the West Philippine Basin, *Earth Planets Space*, *66*(1), 1–9, doi:10.1186/1880-5981-66-83.
Schellart, W. P., and W. Spakman (2015), Australian plate motion and topography linked to fossil New Guinea slab below Lake Eyre, *Earth Planet. Sci. Lett.*, *421*, 107–116, doi:10.1016/j.epsl.2015.03.036.
Sdrolias, M., and R. D. Müller (2006), Controls on back-arc basin formation, *Geochem. Geophys. Geosyst.*, *7*, Q04016, doi:10.1029/2005GC001090.
Sdrolias, M., W. R. Roest, and R. D. Muller (2004), An expression of Philippine Sea plate rotation: The Parece Vela and Shikoku Basins, *Tectonophysics*, *394*(1-2), 69–86, doi:10.1016/j.tecto.2004.07.061.
Seno, T., and S. Maruyama (1984), Paleogeographic reconstruction and origin of the Philippine Sea, *Tectonophysics*, *102*(1–4), 53–84, doi:10.1016/0040-1951(84)90008-8.
Seton, M., et al. (2012), Global continental and ocean basin reconstructions since 200 Ma, *Earth Sci. Rev.*, *113*(3–4), 212–270, doi:10.1016/j.earscirev.2012.03.002.
Shephard, G. E., H. P. Bunge, B. S. A. Schuberth, R. D. Müller, A. S. Talsma, C. Moder, and T. C. W. Landgrebe (2012), Testing absolute plate reference frames and the implications for the generation of geodynamic mantle heterogeneity structure, *Earth Planet. Sci. Lett.*, *317–318*, 204–217, doi:10.1016/j.epsl.2011.11.027.
Shi, H., and C.-F. Li (2012), Mesozoic and early Cenozoic tectonic convergence-to-rifting transition prior to opening of the South China Sea, *Int. Geol. Rev.*, *54*(15), 1801–1828, doi:10.1080/00206814.2012.677136.
Sibuet, J.-C., et al. (1987), Back arc extension in the Okinawa Trough, *J. Geophys. Res.*, *92*, 14,041–14,063, doi:10.1029/JB092iB13p14041.
Sibuet, J.-C., S.-K. Hsu, X. Le Pichon, J.-P. Le Formal, D. Reed, G. Moore, and C.-S. Liu (2002), East Asia plate tectonics since 15 Ma: Constraints from the Taiwan region, *Tectonophysics*, *344*(1–2), 103–134, doi:10.1016/S0040-1951(01)00202-5.
Sibuet, J.-C., S.-K. Hsu, and E. Debayle (2004), Geodynamic context of the Taiwan orogen, in *Continent-Ocean Interactions Within East Asian Marginal Seas*, edited by P. D. Clift, et al., pp. 127–158, AGU, Washington, D. C., doi:10.1029/149GM08.
Sibuet, J.-C., Y.-C. Yeh, and C.-S. Lee (2016), Geodynamics of the South China Sea, *Tectonophysics*, doi:10.1016/j.tecto.2016.02.022, in press.
Sigloch, K., and M. G. Mihalynuk (2013), Intra-oceanic subduction shaped the assembly of Cordilleran North America, *Nature*, *496*(7443), 50–56, doi:10.1038/nature12019.
Simmons, N. A., S. C. Myers, G. Johannesson, and E. Matzel (2012), LLNL-G3Dv3: Global P wave tomography model for improved regional and teleseismic travel time prediction, *J. Geophys. Res.*, *117*, B10302, doi:10.1029/2012JB009525.
Steinberger, B., T. H. Torsvik, and T. W. Becker (2012), Subduction to the lower mantle—A comparison between geodynamic and tomographic models, *Solid Earth*, *3*(2), 415–432, doi:10.5194/se-3-415-2012.
Stern, R. J., M. J. Fouch, and S. L. Klemperer (2004), An overview of the Izu-Bonin-Mariana subduction factory, in *Inside the Subduction Factory*, edited by J. Eller, pp. 175–222, AGU, Washington, D. C., doi:10.1029/138GM10.
Su, J., W. Zhu, J. Chen, R. Ge, B. Zheng, and B. Min (2014), Cenozoic inversion of the East China Sea Shelf Basin: Implications for reconstructing Cenozoic tectonics of eastern China, *Int. Geol. Rev.*, *56*(12), 1541–1555, doi:10.1080/00206814.2014.951004.
Suppe, J., J. G. Liou, and W. G. Ernst (1981), Paleogeographic origins of the Miocene East Taiwan Ophiolite, *Am. J. Sci.*, *281*(3), 228–246, doi:10.2475/ajs.281.3.228.
Takahashi, M., and K. Saito (1997), Miocene intra-arc bending at an arc-arc collision zone, central Japan, *Isl. Arc*, *6*(2), 168–182, doi:10.1111/j.1440-1738.1997.tb00168.x.

Tamura, Y., et al. (2010), Missing Oligocene Crust of the Izu-Bonin Arc: Consumed or Rejuvenated During Collision?, *J. Petrol.*, *51*(4), 823–846, doi:10.1093/petrology/egq002.
Tani, K., D. J. Dunkley, and Y. Ohara (2011), Termination of backarc spreading: Zircon dating of a giant oceanic core complex, *Geology*, *39*(1), 47–50, doi:10.1130/G31322.1.
Tani, K., et al. (2015), Temporal constraints for the tectonic development of the Philippine ophiolite belts from new zircon U-Pb ages, paper presented at Japan Geoscience Union Meeting 2015, Tokyo, Japan.
Taylor, B., and D. E. Hayes (1983), Origin and history of the South China Sea Basin, in *The Tectonic and Geologic Evolution of Southeast Asian Seas and Islands: Part 2*, edited by D. E. Hayes, pp. 23–56, AGU, Washington, D. C., doi:10.1029/GM027p0023.
Torsvik, T. H., R. D. Müller, R. Van der Voo, B. Steinberger, and C. Gaina (2008), Global plate motion frames: Toward a unified model, *Rev. Geophys.*, *46*, RG3004, doi:10.1029/2007RG000227.
Ueda, Y. (2004), Paleomagnetism of seamounts in the West Philippine Sea as inferred from correlation analysis of magnetic anomalies, *Earth Planet Space*, *56*(10), 967–977, doi:10.1186/BF03351794.
Uyeda, S., and Z. Ben-Avraham (1972), Origin and development of the Philippine Sea, *Nat. Phys. Sci.*, *240*(104), 176–178, doi:10.1038/physci240176a0.
van der Hilst, R., and T. Seno (1993), Effects of relative plate motion on the deep structure and penetration depth of slabs below the Izu-Bonin and Mariana island arcs, *Earth Planet. Sci. Lett.*, *120*(3–4), 395–407, doi:10.1016/0012-821X(93)90253-6.
van der Hilst, R. D., E. R. Engdahl, and W. Spakman (1993), Tomographic inversion of *P* and *pP* data for aspherical mantle structure below the northwest Pacific region, *Geophys. J. Int.*, *115*(1), 264–302, doi:10.1111/j.1365-246X.1993.tb05603.x.
van der Meer, D. G., W. Spakman, D. J. J. van Hinsbergen, M. L. Amaru, and T. H. Torsvik (2010), Towards absolute plate motions constrained by lower-mantle slab remnants, *Nat. Geosci.*, *3*(1), 36–40, doi:10.1038/ngeo708.
van der Meer, D. G., T. H. Torsvik, W. Spakman, D. J. J. van Hinsbergen, and M. L. Amaru (2012), Intra-Panthalassa Ocean subduction zones revealed by fossil arcs and mantle structure, *Nat. Geosci.*, *5*(3), 215–219, doi:10.1038/ngeo1401.
Wang, Z., R. Huang, J. Huang, and Z. He (2008), *P*-wave velocity and gradient images beneath the Okinawa Trough, *Tectonophysics*, *455*(1–4), 1–13, doi:10.1016/j.tecto.2008.03.004.
Watts, A. B., and J. K. Weissel (1975), Tectonic history of the Shikoku marginal basin, *Earth and Planetary Science Letters*, *25*(3), 239–250, doi:10.1016/0012-821X(75)90238-1.
Wei, W., J. Xu, D. Zhao, and Y. Shi (2012), East Asia mantle tomography: New insight into plate subduction and intraplate volcanism, *J. Asian Earth Sci.*, *60*, 88–103, doi:10.1016/j.jseaes.2012.08.001.
Weiler, P. D., and R. S. Coe (1997), Paleomagnetic evidence for rapid vertical-axis rotations during thrusting in an active collision zone, northeastern Papua New Guinea, *Tectonics*, *16*, 537–550, doi:10.1029/97TC00493.
Weiler, P. D., and R. S. Coe (2000), Rotations in the actively colliding Finisterre Arc Terrane: Paleomagnetic constraints on Plio-Pleistocene evolution of the South Bismarck microplate, northeastern Papua New Guinea, *Tectonophysics*, *316*(3–4), 297–325, doi:10.1016/S0040-1951(99)00259-0.
Weissel, J. K., and R. N. Anderson (1978), Is there a Caroline plate?, *Earth Planet. Sci. Lett.*, *41*(2), 143–158, doi:10.1016/0012-821X(78)90004-3.
Wessel, P., and L. W. Kroenke (2008), Pacific absolute plate motion since 145 Ma: An assessment of the fixed hot spot hypothesis, *J. Geophys. Res.*, *113*, B06101, doi:10.1029/2007JB005499.
Wessel, P., and R. D. Müller (2015), Plate tectonics, in *Treatise on Geophysics*, 2nd ed., edited by G. Schubert, chap. 6.02, pp. 45–93, Elsevier, Oxford, U. K., doi:10.1016/B978-0-444-53802-4.00111-1.
Whittaker, J. M., R. D. Müller, G. Leitchenkov, H. Stagg, M. Sdrolias, C. Gaina, and A. Goncharov (2007), Major Australian-Antarctic Plate reorganization at Hawaiian-Emperor bend time, *Science*, *318*(5847), 83–86, doi:10.1126/science.1143769.
Whittaker, J. M., J. C. Afonso, S. Masterton, R. D. Muller, P. Wessel, S. E. Williams, and M. Seton (2015), Long-term interaction between mid-ocean ridges and mantle plumes, *Nat. Geosci.*, *8*(6), 479–483, doi:10.1038/ngeo2437.
Widiyantoro, S., and R. van der Hilst (1997), Mantle structure beneath Indonesia inferred from high-resolution tomographic imaging, *Geophys. J. Int.*, *130*(1), 167–182, doi:10.1111/j.1365-246X.1997.tb00996.x.
Winterer, E. L., W. R. Riedel, R. M. Moberly Jr., J. M. Resig, L. W. Kroenke, E. L. Gealy, G. R. Heath, P. Bronnimann, E. Martini, and T. R. Worsley (1971), *Site 63 Shipboard Report*, pp. 323–340, U.S. Gov. Print. Off., Washington, D. C., doi:10.2973/dsdp.proc.7.1971.
Xu, J., Z. Ben-Avraham, T. Kelty, and H.-S. Yu (2014), Origin of marginal basins of the NW Pacific and their plate tectonic reconstructions, *Earth Sci. Rev.*, *130*, 154–196, doi:10.1016/j.earscirev.2013.10.002.
Yamaji, A. (2000), The multiple inverse method applied to meso-scale faults in mid-Quaternary fore-arc sediments near the triple trench junction off central Japan, *J. Struct. Geol.*, *22*(4), 429–440, doi:10.1016/S0191-8141(99)00162-5.
Yamazaki, T., N. Seama, K. Okino, K. Kitada, M. Joshima, H. Oda, and J. Naka (2003), Spreading process of the northern Mariana Trough: Rifting-spreading transition at 22°N, *Geochem. Geophys. Geosyst.*, *4*(9), 1075, doi:10.1029/2002GC000492.
Yamazaki, T., M. Takahashi, Y. Iryu, T. Sato, M. Oda, H. Takayanagi, S. Chiyonobu, A. Nishimura, T. Nakazawa, and T. Ooka (2010), Philippine Sea Plate motion since the Eocene estimated from paleomagnetism of seafloor drill cores and gravity cores, *Earth Planets Space*, *62*(6), 495–502, doi:10.5047/eps.2010.04.001.
Yan, C., and L. Kroenke (1993), A plate tectonic reconstruction of the Southwest Pacific 0-100 Ma, in *Proceedings of the Ocean Drilling Program, Sci. Results*, edited by W. H. Berger, L. Kroenke, and L. A. Mayer, pp. 697–709, Ocean Drill. Program, College Station, Tex.
Yen, H. Y., Y. T. Lo, Y. L. Yeh, H. H. Hsieh, W. Y. Chang, C. H. Chen, C. R. Chen, and M. H. Shih (2015), The crustal thickness of the Philippine Sea plate derived from gravity data, *Terr. Atmos. Oceanic Sci.*, *26*(3), 7.
Yumul, G. P. (2007), Westward younging disposition of Philippine ophiolites and its implication for arc evolution, *Isl. Arc*, *16*(2), 306–317, doi:10.1111/j.1440-1738.2007.00573.x.
Zahirovic, S., M. Seton, and R. D. Müller (2014), The Cretaceous and Cenozoic tectonic evolution of Southeast Asia, *Solid Earth*, *5*(1), 227–273, doi:10.5194/se-5-227-2014.
Zhao, D. (2015), The 2011 Tohoku earthquake (M_w 9.0) sequence and subduction dynamics in Western Pacific and East Asia, *J. Asian Earth Sci.*, *98*, 26–49, doi:10.1016/j.jseaes.2014.10.022.
Zhao, D., T. Yanada, A. Hasegawa, N. Umino, and W. Wei (2012), Imaging the subducting slabs and mantle upwelling under the Japan Islands, *Geophys. J. Int.*, *190*(2), 816–828, doi:10.1111/j.1365-246X.2012.05550.x.
Zhou, X. M., and W. X. Li (2000), Origin of Late Mesozoic igneous rocks in Southeastern China: Implications for lithosphere subduction and underplating of mafic magmas, *Tectonophysics*, *326*(3–4), 269–287, doi:10.1016/S0040-1951(00)00120-7.